Characterization of Transient Behaviors & Operability study of a novel small scale Methanol Synthesis Reactor

Working on feed recycle by Natural Convection

Shashish Mishra

Master's Thesis
May, 2020

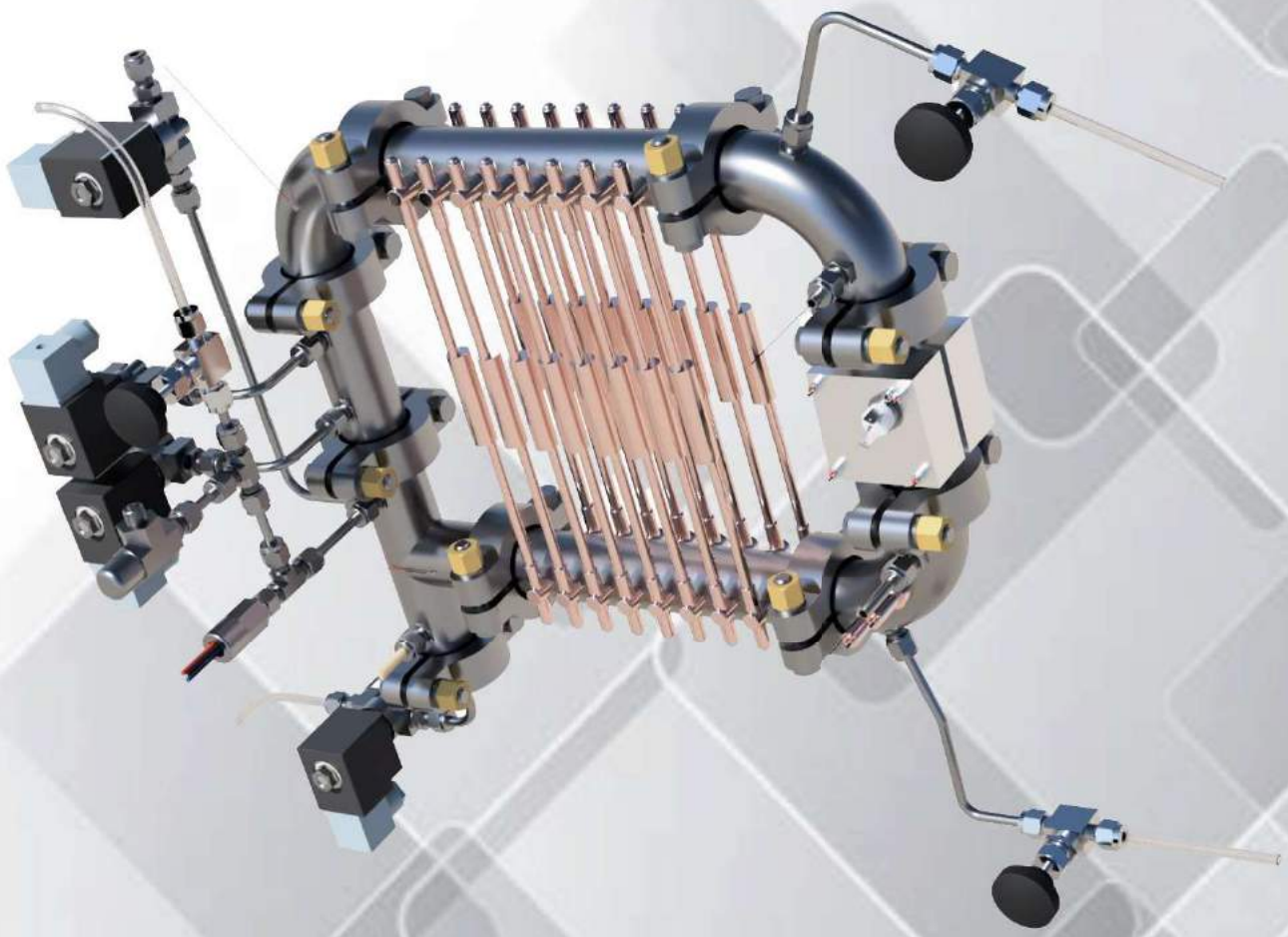

Technische Universiteit Delft

TU Delft Delft University of Technology

ZEF

Challenge the future

CHARACTERIZATION OF TRANSIENT BEHAVIORS & OPERABILITY STUDY OF A NOVEL METHANOL SYNTHESIS REACTOR

WORKING ON FEED RECYCLE BY NATURAL CONVECTION

Dissertation by

SHASHISH MISHRA

towards partial fulfillment for the degree of

MASTER OF SCIENCE

in Mechanical Engineering

Track - Energy & Process Technology

at the department of Mechanical, Maritime & Materials Engineering,

Delft University of Technology

to be defended publicly on Friday May 29, 2019 at 11:00 AM.

Student number	:	4732197	
Project duration	:	April 17, 2019 – May 29, 2020	
Daily supervisor	:	Ir. J. van Kranendonk,	ZEF BV
Thesis committee	:	Prof. dr. ir. W. de Jong	TU Delft (Chair)
		Prof. dr. ir. E. Goetheer	TU Delft
		Dr. ir. H. B. Eral,	TU Delft

This thesis is confidential and cannot be made public until December 31, 2022.

An electronic version of this thesis is available at http://repository.tudelft.nl/.

TU Delft Delft University of Technology

ZEF

कर्मण्येवाधिकारस्ते मा फलेषु कदाचन ।
मा कर्मफलहेतुर्भूर्मा ते सङ्गोऽस्त्वकर्मणि ॥

“As a man you only have the power to take action, not to determine its outcome. So perform all your duties with diligence and integrity without any fear of failure. Never let the fruits become the motive for acting, nor get attached to inaction.”

Bhagavad Gita, Verse 47

ACKNOWLEDGEMENTS

First and foremost, I would like to thank my parents for the support they have given to me. Without their blessings, I wouldn't even have the means to come here at TU Delft in the first place. Heartfelt thanks to my brother **Ashish** and **Ruchi** for being the pillars of my confidence through this masters journey.

Special Thanks to **Prof. dr. ir. W. de Jong** for being my thesis supervisor. Your guidance and inputs from time to time have been monumental towards the work I have been able to do in this thesis. **Prof. dr. ir. E. Goetheer** and **Dr. ir. H. B. Eral** for giving me the privilege of having you on board in my thesis committee.

This Graduation Dissertation would not have been possible without the exemplary leadership of Zero Emission Fuels. I would start by thanking **Ulrich**, for being calm and understanding towards me in every situation, especially when I had a lot on my plate, and was juggling too many problems. Thank you for your discussions and motivation, and empathizing with me even on personal matters. I thank **Jan** for all the "Spaghetti on the wall" sessions. You acknowledged my work several times and lifted my spirits to work even harder. I have always walked out with a positive attitude after having any conversation with you about setup issues. Thank you for being such an inspirational leader. I am grateful to **Hessel** for believing in me and making me feel welcomed at ZEF. Thank you for your stories about surfing and for inducing your enthusiasm in me.

I thank all my team members from MSR team. **Rowan** for imparting his knowledge about the reactor operation and bringing me up to speed. **Martijn** for sharing the load of experimental work with me. **Stefan** for helping me develop tools for better data acquisition. **Amogh** and **Mrigank** for helping me organize my report. I also extend my gratitude to **Mr. Michel van de Brink** and **Mr. Jaap van Raampt**, for helping me out in the chemistry lab whenever needed.

Special mention to **Peggy** & **Mijntje** for helping me deal with my emotional problems and getting me back up. Deepest gratitude for **Arya**, **Anurag**, **Samruddhi** & **Varun Advani** for the love and care you have given to me. I could not have done it without you all. And finally, heartfelt thanks to **Siddharth**, **Marlinda**, **Vandana**, **Lyke**, **Maaike**, **Uddhav**, **Varun Kothari** and **Nishant** for the immense support they have given by being there for me through thick and thin.

Shashish Mishra

May 24, 2020

ABSTRACT

The dwindling of natural resources, mainly fossil fuels, and the alarming increase in the global average temperatures, are the biggest concerns of the engineering and scientific community of 21st century. Studies have found that known reserves of oil and natural gas will last another 50 years. Coal will last another 110 years, which points towards dire consequences. The experience will not be that of a car slowly running out of gas, but rather like driving off a cliff, since we innately depend on these resources. The realization of these concerns have lead to a rise in the investments all over the globe for Sustainability. The right questions are now being asked. How can we fulfill our demands without compromising the demands of our future generations? One of the keen areas of interest is the conversion of power into fuel. Synthesis of hydrocarbons from sequestrated carbon can produce carbon neutral fuels that can replace some of the conventional fossil fuels. Methanol has been actively wiping the floor with the research community due to its simplicity of production and less toxic nature. While there are quite a lot of ways of producing methanol, very few of them are carbon neutral.

Zero Emission Fuels B.V. has embarked on a venture to produce methanol by a totally carbon neutral process. They begin by capturing carbon dioxide and water from air and splitting the water into hydrogen and oxygen using solar power. Carbon dioxide and hydrogen are then combined in a reactor to form methanol, making a truly carbon neutral process. They aim to make fuel consumption, a completely circular process while keeping it economic.

An experimental characterization of ZEF's methanol reactor under varying pressures and H_2/CO_2 compositions was done. The new reactor design focuses on heating the feed gases before catalyst bed, more heat integration, reliable sensor data, and the ability to mix gases in desired compositions. Methanol yield, quality, energy efficiency, reactor inlet and outlet temperatures, power requirements were experimentally determined in a transient analysis.

It was seen that the reactor produces 4.84 mmol/g_{cat}/hr of methanol at 50 Bar and reactor wall temperature of 250°C with $H_2 : CO_2$ = 3:1 mol% feed gas. The catalyst exhibited partial deactivation during night after shutdown. Contrary to expectation, the reactor produced more methanol at lower pressure. The production was reported at 5.96 mmol/g_{cat}/hr at 35 Bar. Although, only 4.36 mmol/g_{cat}/hr at 25 Bar. Moreover, the pressure reduction caused the natural circulation to slow down, and increase the inlet temperature from 208°C at 50 Bar to 234°C at 35 Bar, which is the reason for the observed increase in yield. It can be concluded that the reactor yield under these conditions is limited by kinetics and not thermodynamics. The reduced mass flow rate allowed the reactor to consume less power and show higher energy efficiency. It increased from 34.7% at 50 Bar to 43.2% at 35 Bar.

The rate of pressure decline in the reactor was correlated with the methanol yield using gas law by accounting for non-ideality with compressibility factor. The predicted yield was seen to be in good agreement with experimentally determined. The methanol yield of the reactor with variable feed gas composition was obtained for 50 Bar and 250°C reactor wall temperature and seen to decrease on either side of the ideal composition. It was concluded that the yield becomes both stochiometrically and kinetically limited.

It is recommended that similar experiments be done at increasing temperatures and equilibrium yield be determined experimentally. Additionally, the reactor needs to be operated with varying compositions and higher reactor wall temperatures at constant pressure, to obtain the operating line for maximum production of reactor.

Contents

List of Figures

List of Tables

NOMENCLATURE

ABBREVIATIONS

BASF	Badische Anilin & Soda Fabrik
CAS	Chemical Abstract Services
CCS	Carbon Capture and Sequestration
DEA	diethanolamine
DME	di-methyl ether
DMFC	Direct oxidation Methanol Fuel Cells
EXAFS	Extended X-Ray Absorption Fine Structure
FBR	Fluidized Bed Reactor
FFV	Flexible Fuel Vehicles
FID	Flame Ionization Detector
GC	Gas Chromatograph
HHV	Higher Heating Value
HPLC	High Performance Liquid Chromatography
ICE	Internal Combustion Engine
ICI	Imperial Chemical Industries
IPCC	Intergovernmental Panel for Climate Change
JPL	Jet Propulsion Laboratory
LHV	Lower Heating Value
LOGIC	Liquid Out Gas In Concept
MBR	Modified Brilman Reactor
MEA	monoethanolamine
MON	Motor Octane Number
MSR	Methanol Synthesis reactor
MTBE	methyl tert-butyl ether
NTC	Negative Temperature Coefficient
PBR	Packed Bed Reactor
PEEK	Polyether ether ketone
PEI	polyethyleneimine
PID	Proportional Integral Derivative
PTFE	Polytetrafluoroethylene
RFC	Reactive Frontal Chromatography
RON	Research Octane Number
RWGS	Reverse Water Gas Shift
SOP	Standard operating Procedure
STY	Space Time Yield
TCD	Thermal Conductivity Detector
TEGDME	tetraethylene glycol dimethyl ether
TEPA	tetraethylenepentamine
TPD	Temperature Programmed Desorption
ZEF	Zero Emission Fuels

SYMBOLS

d_t	Diameter of the reactor pipe	mm
d_p	Diameter of the catalyst pellets	mm
h_p	Height of the catalyst pellets	mm
ϵ	Catalyst bed void fraction [V_{bed}/V_{cat}]	-
SV	Space velocity [$V_{gas}/V_{catalyst}$/hr]	h^{-1}
STY	Space time yield	mmol/g_{cat}/hr
A_{cross}	Cross sectional area of the reactor Tri-Clamp pipe	m^2
g_{cat}	Weight of the catalyst used in the reactor	g
$V_{reactor}$	Approximate volume of the reactor	m^3
ρ_{gas}	Density of gas mixture inside the reactor	Kg/m^3
$\dot{m}_{top}$	Mass flow rate through the top heat exchanger section	g/s
$\dot{m}_{bottom}$	Mass flow rate through the bottom heat exchanger section	g/s
$\dot{m}_{bed}$	Mass flow rate through the catalyst bed	g/s
$\dot{m}_{1,HP}$	Mass flow rate through the bed using only heat pipe 1	g/s
$\dot{m}_{2,HP}$	Mass flow rate through the bed using only heat pipe 2	g/s
c_p	Specific heat capacity of the gas mixture inside the reactor	J/kg/K
$T_{top,1}$	Temperature of top heat pipe number 1	°C
T_{gasIN}	Temperature of gas at reactor inlet	°C
T_{gasOUT}	Temperature of gas at reactor outlet	°C
$T_{bottom,1}$	Temperature of bottom heat pipe number 1	°C
$\dot{Q}_{reaction}$	Heat production rate through the reaction	W
$\dot{Q}_{HP}$	Heat pipe duty	W
P_{bed}	Catalyst bed heater duty	W
P_{corner}	Corner heater duty	W
P_{total}	Total heater duty	W
η_{energy}	Overall energy efficiency	-
ξ_{HP}	Heat exchanger efficiency	-
dP/dt	Rate of pressure decline inside the reactor	Bar/min
Z	Compressibility factor of the gas mixture inside the reactor	-
R	Universal gas constant	J/mol/K

1

INTRODUCTION

"The greatest threat to our planet is the misplaced belief that someone else will save it."
-Robert Swan-

The world still relies on fossil fuels to cater to almost 80% of its energy needs [3] and to produce a vast multitude of derived fuels and necessary products. The availability of such fossil fuels is however, limited and is depleting at an alarming rate. The dwindling of fossil fuel reserves (oil, natural gas, coal, tar sands) has raised serious questions about the exhaustible and unsustainable nature of their use. Only sufficient geological time can allow the formation of new fossil fuel, which hopelessly outmatches human time scale itself. This chapter very briefly glances the problem at hand and delineates certain important global trends that have incited the current research topic of this thesis.

1.1. IMPORTANT GLOBAL TRENDS: THE PROBLEM

Fossil fuels have played an integral role in the industrial revolution, and have been the prime mover of global change so far, which reflects from their increased consumption (figure-1.1). Coal started off as the main candidate but has been replaced by oil and natural gas recently due to rise of transport and district heating sector [1].

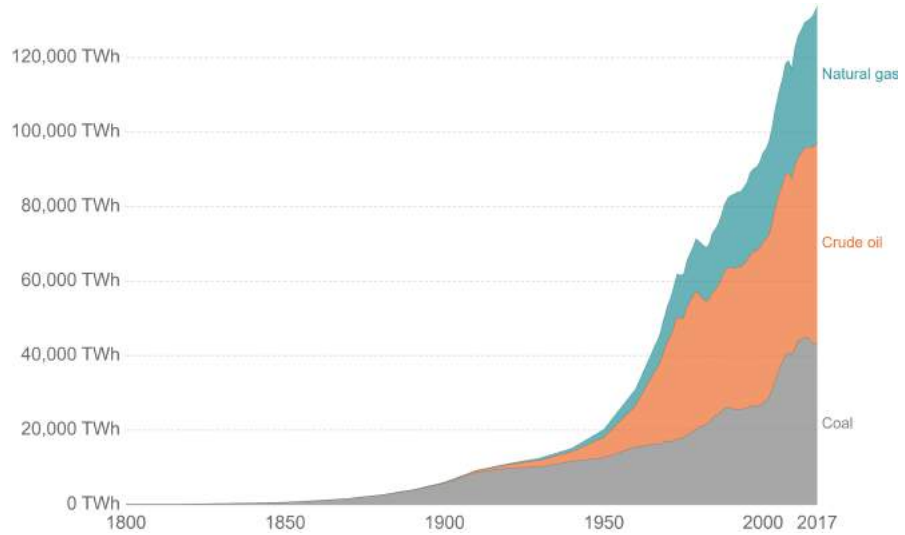

Figure 1.1: Global fossil fuel consumption.[1]

Nevertheless, it is still used in many nations (China, India etc) as a source for generating electricity. It can be seen that the consumption has nearly exploded in the past 6 decades. Even though the production rates are going up exponentially, we must not lose sight of the fact that total reserves are limited and will vanish one day. Figure-1.2a shows the estimated exhaustion time of the fossil fuels based on the current production capacity and the quantity of known reserves (also known as the R/P ratio). It can be seen that oil and natural gas which forms the basis of the transport and domestic heating sector will vanish in the upcoming 50 years. Although, coal reserves are estimated to be more, they will perish too in the next 114 years.

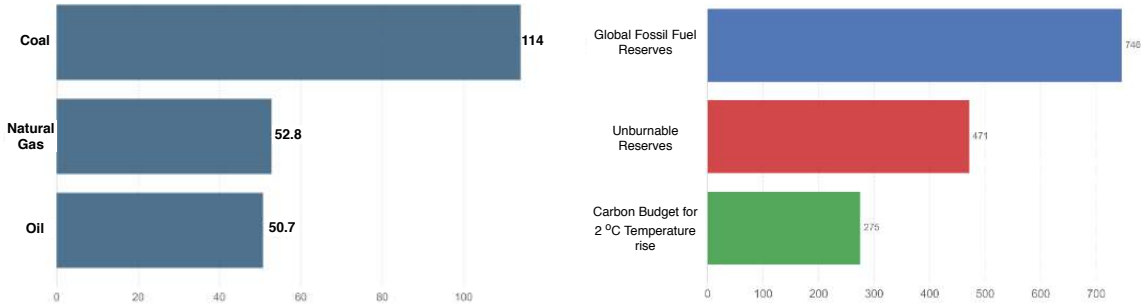

(a) *Years of fossil fuel reserves left as per the known reserves and production rate data of 2015 (R/P ratio [years]).*

(b) *Unburnable and burnable fossil fuel reserves for a 50% chance to limit global temperature rise below the target.*

Figure 1.2: Comparison of available reserves and usable reserves.[1]

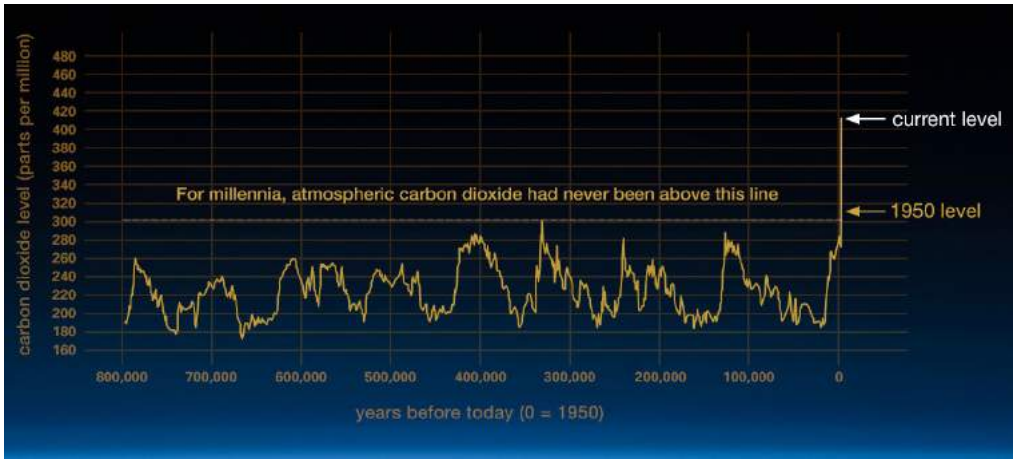

Figure 1.3: Global rise in the CO_2 concentration in the atmosphere over large timescales.

Moreover, it is not just the fossil fuel depletion that poses dire consequences. The use of such fossil fuel reserves have spurred an increase in the CO_2 concentration all across the globe (Figure[1]-1.3). The carbon that was naturally captured via photosynthesis and sequestrated in the earth for millions of years has been released into the atmosphere in a matter of hundred years due to human actions [19]. As CO_2 is a green house gas[2] (unlike oxygen or nitrogen), it has lead to a steady increase in global average temperature due to the green house effect [20]. Notwithstanding the fact that without green house effect the average global temperature would be below freezing point, but its excess has tipped the scales of energy balance on the other side. Some experts even point out that we live in a new geologic era, which they call "Anthropocene", where the climate is very different from the one that our ancestors knew [21]. The UN Paris agreement also mandated that the global

[1] source: NASA- Global climate change (www.climate.nasa.gov)
[2] Gases that absorb and radiate heat gradually

average temperature rise must be limited to 2 °C in the first half of this century [22].

This gives us the ability to calculate the amount of CO_2 emissions that we can afford to release in the atmosphere (also known as Carbon Budget), while maintaining a certain probability of remaining below the target temperature. In the latest Intergovernmental Panel for Climate Change (IPCC) of 2013, the carbon budget for a 50% chance of remaining below 2 °C temperature rise was estimated to be 275 billion tonnes of carbon [23]. Therefore, we can now estimate the unburnable reserves (figure-1.2b) considering no use of any Carbon Capture and Sequestration (CCS) technology or other known green house gases that are even more potent than CO_2. This has far more reaching consequences for the industry than meets the eye. It means that we must leave 67% of the fossil fuel reserves in the ground in order to meet the global climate targets. The capital investment on carbon-emitting assets is still on the rise. According to an estimate, 6.74 trillion US$ (Twice the GDP of Germany as of 2016) will become what is referred to as Stranded assets due to unburnable reserves [24].

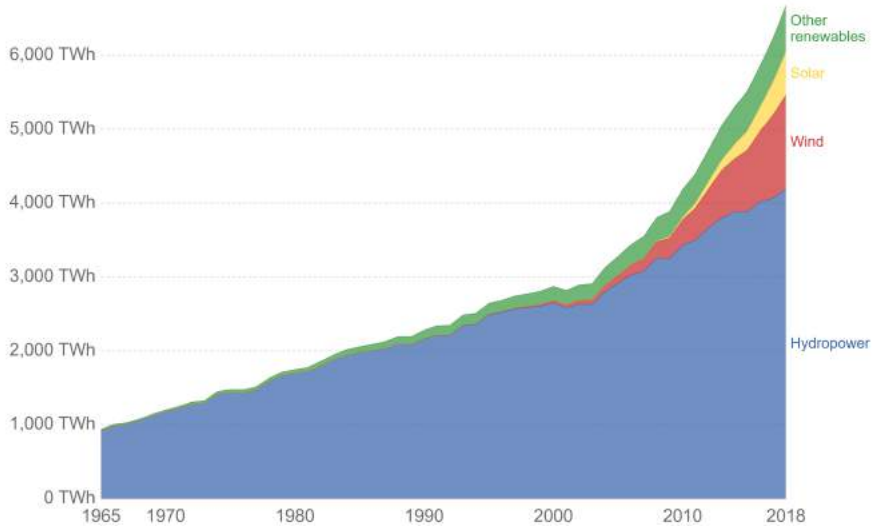

Figure 1.4: Growth of modern renewable energy sector.[2]

There is also a positive trend that is the apparent growth of the modern renewable[3] energy sector (see figure-1.4). The overall clean energy production from these sources such as wind, solar, hydro, geothermal, biofuels has increased 6 folds since 1960s [24]. Hydroelectric power remains a dominant contributor because the technology was developed very early. But other sources such as wind, solar and ocean energy have seen a massive increase in the capital investment and hence, are moving towards technological maturity. As a result, hydroelectric power has seen a decline in favor of other sources.

KEY TAKEAWAY:

All the trends that were presented above can be simplified to pose the following hard hitting problems:

- What can we do to find alternatives to fossil fuels which we currently rely on and which will definitely be non existent in the future?
- Even if we find an inexhaustible fuel source, is it wise to keep burning it? How can we develop a fuel source that does not contribute to climate change?
- How can we convert the clean energy from the renewable energy source into clean fuel?

[3] Renewables except traditional biomass

1.2. Methanol Economy: The solution

All renewable sources are highly touted as the solution to the energy crisis that approaches our society. Sources such as wind, hydro & solar energy are infact renewable, cost effective, well studied, pollution free as well as CO_2 emission free. But these sources provide clean electricity and not clean liquid fuel that is needed for transportation industry which is yet to make its transition to electric power [20]. Moreover, a sudden transition to electric power drive will create trillions of euros worth of locked assets which will all be rendered useless. Vast majority of these sources are also, geographically located away from the main land electricity grids [25]. Therefore, it becomes logical to invest and develop technologies that convert renewable electricity to renewable fuels that can be seamlessly integrated to the current infrastructure.

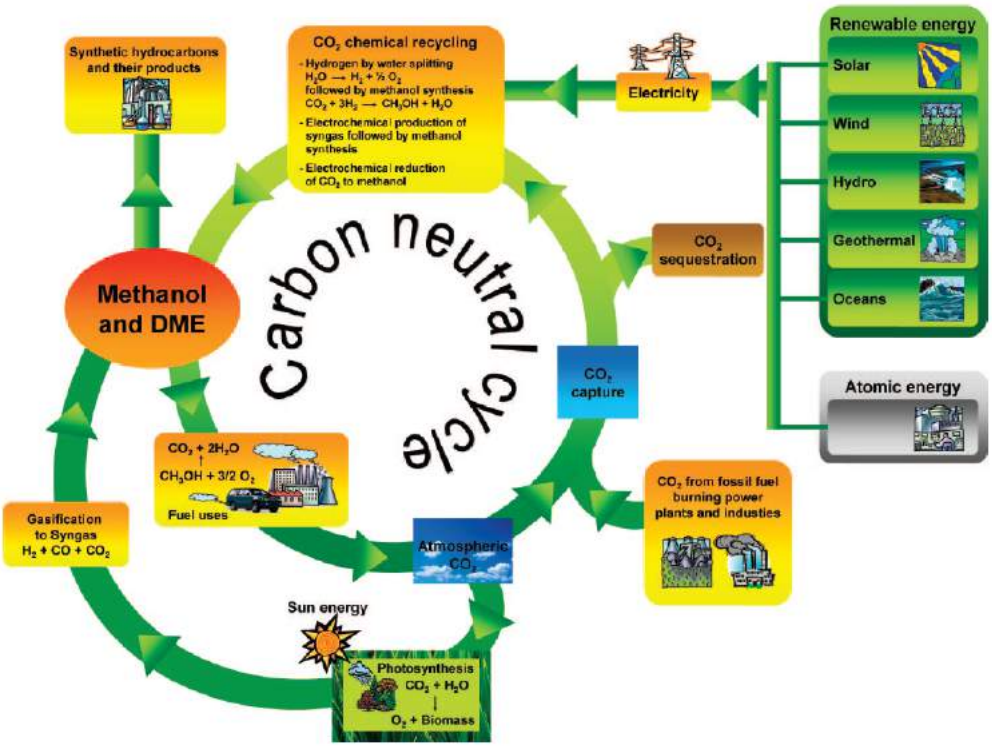

Figure 1.5: Recycling of carbon dioxide in a Methanol Economy.[3]

Nowadays, methanol [CAS 67-56-1] has taken its place as the starting point for many innovative applications, because it can be produced from many different sources such as: natural gas, oil shale, tar sands, coal, biomass, landfill gas power plant or industrial emissions. Practically any derived hydrocarbon product can be formed with methanol as starting point [26] [27]. It is one of the most promising potential storage media, which can store other forms of energy into chemical energy as an easily transportable liquid fuel which is safer than gasoline[28]. It has also polarized a lot of attention from automotive industry as a fuel for Internal Combustion Engine (ICE) since it has a higher octane number of 100 (which is the average of Research Octane Number (RON) that is 107 and Motor Octane Number (MON) that is 92) [29]. This is the reason why it is the fuel of choice for race cars. Even gasoline powered vehicles can be easily modified to run on methanol to make so-called Flexible Fuel Vehicles (FFV). Other factors include, the ability to act as a reagent for some common transesterification reactions that not only produce bio-diesel and methyl tert-butyl ether (MTBE), but also di-methyl ether (DME) which is the diesel counterpart of methanol. Since, methanol has a lower cetane number, it is not an effective fuel for diesel engines. DME, on the other hand, formed by bimolecular dehydration (equation-1.1) of methanol has a cetane number of 55-

60, which is considerably higher than diesel (40-55) [30]. Even for those markets that explore fuel cells for automotive power, methanol can be be a very good hydrogen carrier in Direct oxidation Methanol Fuel Cells (DMFC) as demonstrated by Jet Propulsion Laboratory (JPL) in Caltech [31].

$$2\,CH_3OH \rightleftharpoons CH_3OCH_3 + H_2O \quad \Delta H_{298K} = -24.04\,kJ/mol \tag{1.1}$$

From an environmental perspective, methanol is found to be cleaner than most energy sources [20]. This is due to its molecular structure, which is replete with hydrogen and has no carbon-to-carbon chemical bonds. Methanol also gets spontaneously released into the environment due to a lot of natural sources too. Such as volcanoes,vegetation, microbes, insects & decomposing organic matter. Although such a release contaminates the ground and water, it is not particularly hazardous because it can be rapidly degraded by photo-oxidation and bio degradation processes, which can be both aerobic and anaerobic [6]. Some microbes even use it as nutrition. Due to this there is no such evidence of accumulation and it has low toxicity to terrestrial and aquatic organism. As such an accidental methanol spill has lower impact than a corresponding oil spill. Methanol is toxic when ingested in quantities above 30 mL, where it can cause blindness or death. It is a large-volume product that is in big demand due to easy storage and transportation.

Nobel Laureate George Olah and his group of researchers [3] have very carefully assessed the viability of CO_2 recycling from the atmosphere. They concluded that chemical recycling of carbon dioxide to methanol, DME and derived hydrocarbons can give us a renewable, carbon-neutral and inexhaustible source of transportation fuels, essentially replacing petroleum oil and natural gas. This solution becomes even more promising when we consider the possibility of arresting or even lowering the CO_2 concentration in the atmosphere, thus mitigating the green house effect and global warming. An overview of the Methanol Economy that they posited is shown in figure-1.5.

1.3. The Approach taken by ZEF BV: Technical Photosynthesis

More than half of the anthropogenic CO_2 emissions happen from sporadic burning of fossil fuel such as home and office heating, cooking, transport etc. These sources produce CO_2 that is highly dispersed in the atmosphere making it highly impractical to setup carbon capture units at each of these billions of sources. Given that the concentration of CO_2 is in equilibrium all around the world, a method can be developed to mimic the nature's photosynthesis (where plants capture the CO_2 from the atmosphere to produce organic compounds and release oxygen). Methanol is increasingly being viewed as an alternative to H_2 as the fuel of choice for the future as it has almost 7 times more energy per unit volume than the latter. The fact that it can be transported using the existing fuel infrastructure, only adds to its advantage. However, high capital costs currently limit the production of cheap synthetic fuels.

Zero Emission Fuels (ZEF) B.V. is a start-up company in the Netherlands which has a power-to-chemicals approach for methanol production. The ZEF system is a micro-plant for methanol synthesis, that is powered purely by Solar panels. Thus, the ZEF system can contribute towards two important aspects of a sustainable future, viz. energy storage for renewable energy via synthetic fuels and sustainable feedstocks for the chemical industry. ZEF's entire process is carbon neutral. The system captures carbon dioxide (CO_2) and water vapor from the atmosphere, and produces methanol using power from a single solar cell. ZEF envisions solar farms with one such micro-plant attached to each solar panel. This vision takes advantage of economics of scale by producing a large number of micro-systems rather than one large system. The small size makes the system more immune to dynamic operations, which is essential because solar power is fluctuating in nature. The size also makes it easier to manufacture prototypes and thus develop many iterations in shorter time intervals, making it possible to have a steep learning curve, compared to large scale systems, where it takes several years (or decades) to design and build one iteration. The system consists of many subsystems. The Direct Air Capture (DAC) unit captures CO_2 and water from air using polyethylen-

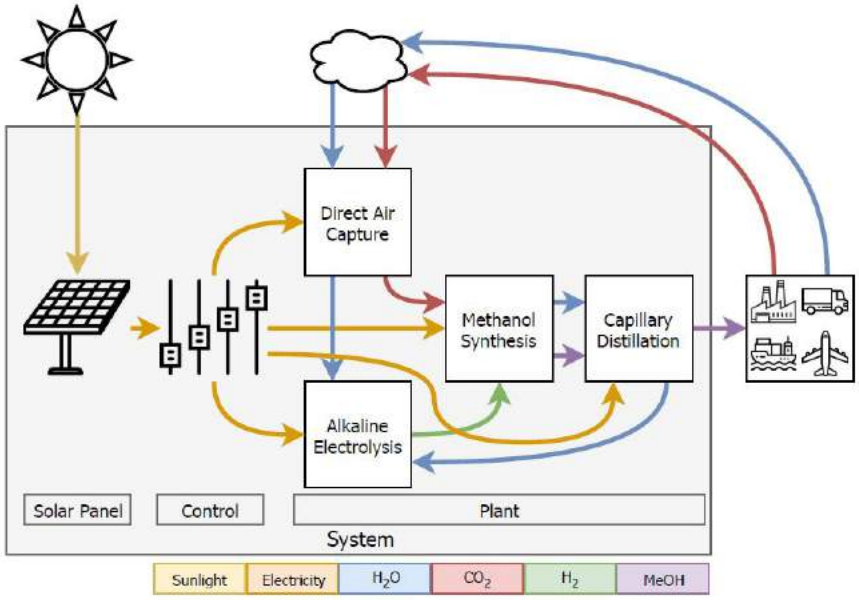

Figure 1.6: An Overview of the ZEF's process

imine (PEI). The CO_2 and water desorbed from the PEI are compressed in the Compressor unit to 60 bar. At this pressure, the water condenses and can be easily separated from most of the CO_2. The condensed water then goes into a Degasser unit, which removes the CO_2 dissolved in the water. This "clean" water then goes into Alkaline Electrolysis Cell (AEC), where it is electrochemically split into hydrogen and oxygen. The oxygen is vented out, and the hydrogen goes to the Methanol Synthesis Reactor (MSR), where it reacts with the CO_2 to produce a mixture of methanol and water. This mixture is then separated in a Distillation system to get grade AA (99.8%) methanol.

1.4. Broad Research Goals

Basarkar[16] built the first reactor for ZEF that produced methanol. Proof of concept was given for methanol production in a small scale plant working on feed recycle by natural convection. The reactor was designed and completely built in-house with Aluminium blocks. The work was followed up by van Laake[17] who re scaled the reactor to incorporate reactor part modularity, larger catalyst bed and heat integration. The reactor was built using standard high pressure rated equipments due to which its size and design was changed. In both these works feed gas at stochiometric composition ($H_2 : CO_2 = 3 : 1$) was used at optimized reaction temperature to produce methanol and establish base cases in two different, yet similar reactor designs. Characterization of transient behaviors in the reactor during operation is important and still remains unanswered. Such a study is important due to following reasons:

1. How can the reactor output be maximized at varying input parameters?

    - **Fluctuating Power:** The entire ZEF plant is dependent on solar panels to fulfil their power requirements for operation. But its availability is contingent on intermittent and often unpredictable weather conditions. Since, the reactor is the most taxing energy system in the whole ZEF plant, the knowledge about its behaviour in times of inadequate power supply becomes important. Inadequate power supply implies that the reactor catalyst bed might not be able to run at the optimum temperature. Therefore, How can the reactor control parameters be changed to maximize production at lower temperatures?

- **Fluctuating reactant availability:** Inadequate power supply or changes in environmental conditions can lead to offsets in the supply of either of the reactants, H_2 or CO_2. In such an event the reactor might need to be operated at lower pressures or gas compositions, different from what is stochiometrically needed for production. Therefore, How can the reactor control parameters be changed to maximize production at lower pressures or different compositions.

2. Experimental data requirement for future modelling purposes.

1.5. Thesis Research Focus

In order to answer some questions from the broad research objectives of ZEF, some questions were posed for this thesis, that contribute towards answering them:

1. What is the reactor performance with the current enhancements at constant pressure, temperature and composition, optimized in earlier works?
   - **Experimental conditions:** Pressure = 50 Bar; Gas used: $H_2 : CO_2$ = 75 : 25 vol%; Heater set point = 250 °C; Catalyst: $Cu/ZnO/Al_2O_3$.
   - **Performance criteria:** Space Time Yield (STY) [mmol/g_{cat}/hr]; Mass flow rate [g/s]; Reactor inlet and outlet gas temperatures [K]; heater input power [W]; energy efficiency; heat exchanger duty [W], heat exchanger efficiency; Carbon conversion efficiency, quality of methanol produced.
2. What is the effect of lowering the pressure on reactor performance with premixed gas cylinder?
   - **Experimental conditions:** Pressure = 50 Bar to 25 Bar; Gas used: $H_2 : CO_2$=75 : 25 vol%; Heater set point = 250 °C; Catalyst- $Cu/ZnO/Al_2O_3$.
   - **Performance criteria:** STY [mmol/g_{cat}/hr]; Mass flow rate [g/s]; Reactor inlet and outlet gas temperatures [K]; heater input power [W]; energy efficiency; heat exchanger duty [W], heat exchanger efficiency.
3. What is the effect of varying feed compositions on reactor performance at constant pressure and temperature?
   (a) What is the best way to feed gases in desired compositions, in the absence of a premixed cylinder?
   (b) Does the rate of pressure decline be correlated to the rate of methanol synthesis?
   - **Experimental conditions:** Pressure = 50 Bar; Gas used:$H_2 : CO_2$ = 80 : 20 vol% to $H_2 : CO_2$ = 20 : 80 vol%; Heater set point = 250 °C; Catalyst: $Cu/ZnO/Al_2O_3$.
   - **Performance criteria:** STY [mmol/g_{cat}/hr]; Mass flow rate [g/s]; Reactor inlet and outlet gas temperatures [K]; heater input power [W]; energy efficiency; heat exchanger duty [W].

Approach:

- Use the new valve control system to monitor and regulate varying pressures inside the reactor [50, 45, 40, 35, 30, 25 Bar].
- Use improved gas flow temperatures instead of wall temperature measurements to characterize the actual gas inlet and outlet temperatures. This data is important for future modelling exercises too.

- Use the temperature data and improved heater duty quantifications, to estimate the internal mass flow inside the reactor. Find and test ways to estimate this mass flow and cross check.
- Use new level sensor to account for exact time and volume of sluiced liquid. Use density measurements to determine methanol production and quantify STY.
- Use temperature measurements and heat correlation to estimate the heat exchanger duty.
- Use the pressure response of the reactor in operation to find correlation with experimentally observed yield. Cross check the predictions with multiple experimental measurements.

1.6. Research Scope

Apart from answering the research questions, this thesis attempts to improve the data acquisition system of the reactor. The sensor data in earlier works was only used for calculations. But in this thesis, the data is seen not just as numbers, but as patterns. As such, changes in the patterns of the observed data has been linked with physical log of events while operating the reactor. This gave insights into the functioning of reactor in a transitory manner. However, this thesis does not delve into the following:

- This thesis does not try to go in depth in to estimating the heat losses and their bifurcations in the reactor while in transient operation. Such a study, would have affected the design of experiments. For example- overall heat losses have been estimated but not their distribution to individual elements of the reactor.
- This thesis does not try to create or validate any virtual reactor model. It is aimed at collecting real experimental data that can later be used to create a sound model.

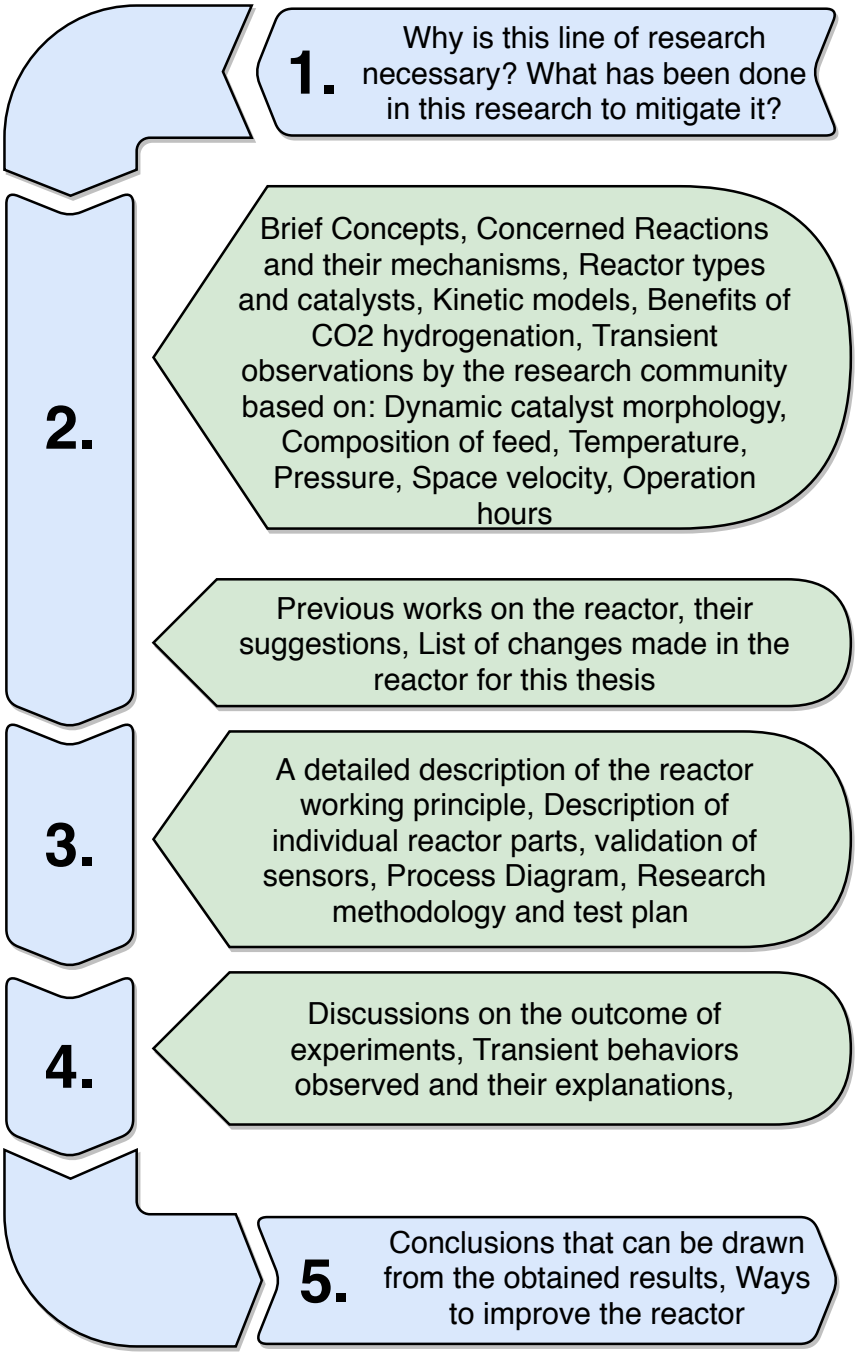

Figure 1.7: An Overview of structure of this thesis Report

2

From theory to State of the Art Methanol Synthesis: A comprehensive Literature review

"The measure of whether or not you learn something is not contingent on whether it was obvious to you upon first glance."
-Mark Twain-

2.1. Brief History of Conventional Methanol Synthesis

Methanol, also known as Carbinol was first produced by destructive distillation of wood in 17^{th} century by Robert Boyle, thereby getting its moniker as wood alcohol [6]. Unfortunately, it could not get much traction as the fuel of choice due to other cheaper fuels such as kerosene. The current state of fossil fuels on the precipice of depletion, has put methanol back into the limelight as fuel of sustainable future. There are several ways to produce methanol from CO/CO_2 that have been studied in the literature and pursued, as depicted in figure-2.1.

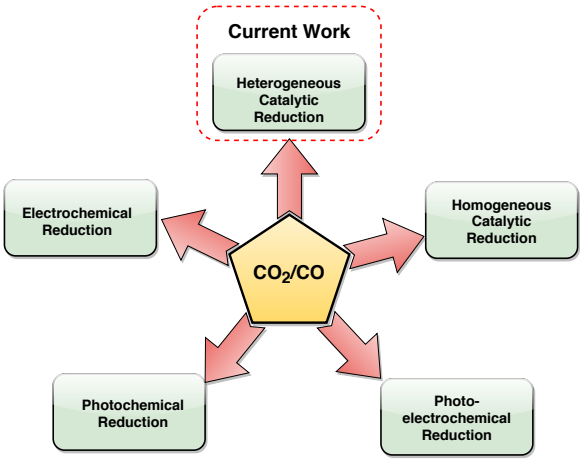

Figure 2.1: Different methods to convert CO_2 /CO to Methanol.

This thesis is focused towards methanol synthesis over heterogeneous catalysts. Contrary to homogeneous catalysis, heterogeneous catalysis uses a catalyst that is not in the same phase as the reactants. In some cases it can even be two liquids that are immiscible, as such, the presence of an

interface being the distinguishing criteria [32]. Heterogeneous catalysis is the most used method to convert CO/CO_2 into methanol. This is attributed to the easy separation of the liquids from solid catalyst, convenience in handling different type of reactors(fixed bed, fluidized bed or moving bed) and the possibility for catalyst regeneration [33].

Methanol is produced largely from syngas (mixture of CO, CO_2 & H_2) and was commercially produced first in 1920s by Badische Anilin & Soda Fabrik (BASF) [7], using syngas from coal gasification. The synthesis reaction happened at 300-400 °C and 300 Bar with zinc chromite catalyst ($ZnO-Cr_3O_3$). The source of syngas can be varied though; Coal, natural gas, biomass gasification, petroleum, heavy oils, that lead to different content of gases in it which is characterized by its stochiometric number S (equation-4.3). Syngas produced from coal gasification (Partial oxidation followed by steam reforming, equation- 2.2, 2.3) is deficient in H_2 due to low H/C ratio in coal and steam being the only source of H_2. Impurities such as sulfur and halogenated compounds, limited the catalyst activity in those times [34].

$$S = \frac{moles\,H_2 - moles\,CO_2}{moles\,CO_2 + moles\,CO} \tag{2.1}$$

The most disruptive of the advancements was brought about by Imperial Chemical Industries (ICI), UK in 1963. The ICI process operated between 30-120 bar and 200-300 °C while using $Cu/ZnO/Cr_2O_3$ catalyst. This was made possible due to the advancements in syngas purification and use of natural gas for making syngas, which already had low impurities. Selectivities as high as 99.5 % were achieved due to this development. After 1966, no plant was setup anywhere that used high pressure methanol synthesis [7].

$$3\,C + O_2 + H_2O \rightleftharpoons 3\,CO + H_2 \qquad \Delta H_{298K} = -91\,kJ/mol \qquad \text{(Coal Gasification)} \tag{2.2}$$

$$CO + H_2O \rightleftharpoons CO_2 + H_2 \qquad \Delta H_{298K} = -41\,kJ/mol \tag{2.3}$$

$$CH_4 + H_2O \rightleftharpoons CO + 3\,H_2 \qquad \Delta H_{298K} = 206\,kJ/mol \qquad \text{(Steam reforming)} \tag{2.4}$$

$$CH_4 + 2\,H_2O \rightleftharpoons CO_2 + 4\,H_2 \qquad \Delta H_{298K} = 165\,kJ/mol \tag{2.5}$$

$$CH_4 + \frac{1}{2}O_2 \rightleftharpoons CO + 2\,H_2 \qquad \Delta H_{298K} = -36\,kJ/mol \qquad \text{(Autothermal reforming)} \tag{2.6}$$

$$CH_4 + CO_2 \rightleftharpoons 2\,CO + 2\,H_2 \qquad \Delta H_{298K} = 247\,kJ/mol \qquad \text{(Dry reforming)} \tag{2.7}$$

$$3\,CH_4 + 2\,H_2O + CO_2 \rightleftharpoons 4\,CO + 8\,H_2 \qquad \Delta H_{298K} = 247\,kJ/mol \qquad \text{(Bi-reforming)} \tag{2.8}$$

$$CO_2 + C \rightleftharpoons 2\,CO \qquad \Delta H_{298K} = 170.7\,kJ/mol \qquad \text{(Boudouard reaction)} \tag{2.9}$$

Currently, syngas is mainly obtained from natural gas via methane steam reforming (equation-2.4, 2.5) [35], which is then converted into methanol at a temperature between 250-300°C and pressure between 50-100 bar using Cu/ZnO based catalysts [36]. The conversion is thermodynamically limited to 0.3-0.7, from syngas, which leads to large recycle of non-converted gases[37]. Since, the feed gas is never entirely pure and contains traces of methane and nitrogen, some fraction of the gas has to be purged to prevent accumulation in the system. For any natural gas based methanol plant, the steam reformer is the most taxing unit and has the highest carbon footprint [35]. This problem is often circumvented using partial oxidation in a process called autothermal reforming in which a stream of oxygen is injected into the partially reformed natural gas with the idea of igniting some of the hydrogen that provides the necessary heat for further reforming (equation-2.6). Steam reforming can also be coupled with autothermal reforming in what is referred as parallel reforming. There is another process called dry reforming (equation-2.7) which produces syngas without using steam, but it is highly endothermic and the ratio of H_2/CO=1:1 in the syngas is also not suitable for methanol production. It is still pursued because some natural gas sources contain higher CO_2 concentration [38]. For methanol production this ratio must be 2:1 in what is also called sometimes, metgas [6].

2.2. Reactions Involved with Methanol Synthesis

"**The methanol synthesis reactions and reverse water gas shift reaction runs parallelly. Lower temperatures and higher pressures drive the methanol yield. Both CO and H_2O formation has an inhibitory effect on methanol synthesis, effect of H_2O being higher. All considered, direct CO_2 hydrogenation is a promising route.**"

The equations- 2.10, 2.11 represent the hydrogenation of CO & CO_2, and are referred to as the methanol synthesis reactions. Equation- 2.12 is the Reverse Water Gas Shift (RWGS) reaction and it offers a way for inter conversion of CO & CO_2. Due to the exothermic nature of the methanol synthesis reactions and the endothermic nature of the RWGS reaction it is advantageous to operate at lower temperature. Otherwise, the reactor yield shifts to a CO rich mixture [6]. The methanol synthesis reactions also proceed by decrease in the number of moles, which means higher pressures drive the equilibrium forward by Le Chatelier's principle. Although, it has been seen that equilibrium yield is a stronger function of temperature than the pressure [5]. It is also worthwhile to note that CO_2 hydrogenation is less exothermic as compared to CO hydrogenation, thereby helping in better control over the reactor temperature. The conversion per pass through a reactor is low due to the thermodynamic and equilibrium considerations [10].

$$CO + 2H_2 \rightleftharpoons CH_3OH \qquad \Delta H_{298K} = -90.8\,kJ/mol \tag{2.10}$$

$$CO_2 + 3H_2 \rightleftharpoons CH_3OH + H_2O \qquad \Delta H_{298K} = -49.2\,kJ/mol \tag{2.11}$$

$$CO_2 + H_2 \rightleftharpoons CO + H_2O \qquad \Delta H_{298K} = 41.6\,kJ/mol \tag{2.12}$$

The methanol synthesis over Cu/ZnO based catalysts is inhibited by both CO and water formation;

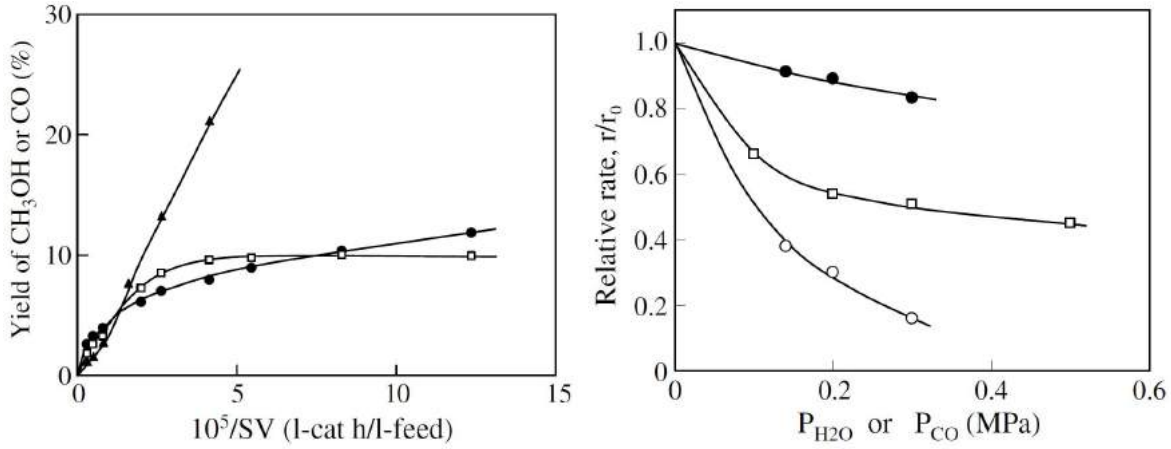

(a) *Yields of MeOH and CO over Cu/ZnO/ZrO_2 catalyst at 523 K and 50 bar.*
□*: CO yield-CO_2(25);H_2(75)*
•*: MeOH yield-CO_2(25);H_2(75)*
▲*: MeOH yield-CO_2(6);H_2(69);CO(25).*

(b) *Effect of CO and water addition on rate of methanol synthesis over Cu/ZnO/ZrO_2 catalyst at 523 K, SV = 180,000 h^{-1}.*
□*: MeOH yield- CO addition;CO_2(25);H_2(75)*
•*: CO yield- H_2O addition;CO_2(25);H_2(75)*
○*: MeOH yield- H_2O addition;CO_2(25);H_2(75).*

Figure 2.2: The inhibitory effects of CO and water on methanol synthesis. [4]

the effect of water being stronger than CO [39]. Saito et al. [4] did an experimental study to demonstrate the same. Figure-2.2a shows that the CO yield (shown by □) increases with reciprocal space velocity ($V_{reactor}/V_{gas}$/hr) and reaches a maximum when reaction-2.12 reaches equilibrium using a feed of $H_2 : CO_2$ = 3:1. The yield of methanol (•) is also shown for the same feed. In figure-2.2b, $r_\circ$ and r are the rates of methanol synthesis without and with the addition of CO or H_2O. The decrease in methanol yield is greater for H_2O addition (shown by ○) than CO addition (shown by □). This is because water does not desorb quickly and keeps the reaction sites inactive for synthesis. It must also be noted that as more water is added, the CO formation is also limited (shown by •).

This can be seen as an indication that using conventional syngas feed ($CO/CO_2/H_2$=25 : 6.2 : 68.8), methanol and water are formed by reaction-2.11. The water thus formed reacts backward with CO in reaction-2.12 to give back CO_2 & H_2. Therefore, excess CO in the mixture acts to suppress the water formation and the methanol yield is not inhibited as seen in figure-2.2a (shown by ▲).

Skrzypek et al.[5] did a comprehensive study to determine the effects of initial feed composition, temperature and pressure on equilibrium conversion degrees and concentration of the reactants. They used CO instead of CO_2 to express equilibrium conversion degree because equation-2.12 runs backwards with the presence of CO, which makes CO_2, the product of the reaction instead of being the reactant. It was showed that both temperature and pressure exhibit a considerable effect on equilibrium conversion degrees. When the reactants contain no CO, then the degree of RWGS (ξ_2^{eq}) is always positive.

$$\xi_1^{eq} = \frac{N_{CH_3OH}^{eq} - N_{CH_3OH}^{\circ}}{N_{Total}^{\circ}} \quad ; \quad \xi_2^{eq} = \frac{N_{CO}^{eq} - N_{CO}^{\circ}}{N_{Total}^{\circ}} \tag{2.13}$$

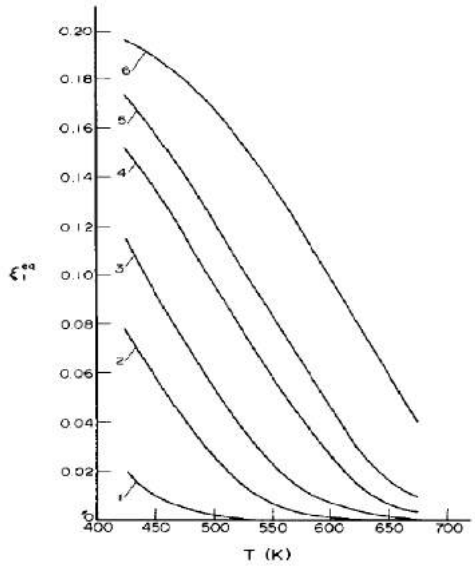

(a) *Equilibrium conversion degree of methanol synthesis reaction* (ξ_1^{eq}).

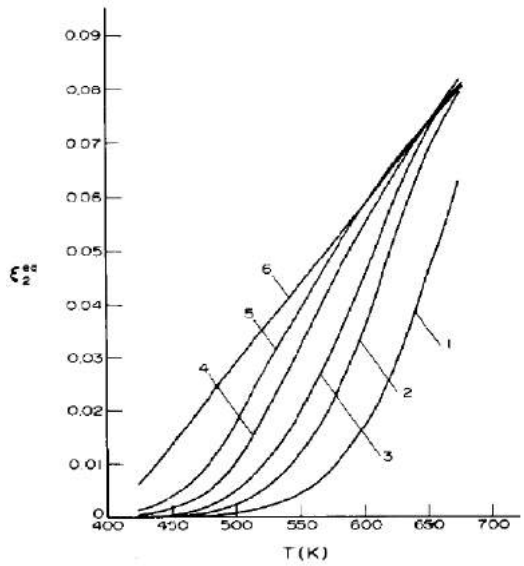

(b) *Equilibrium conversion degree of RWGS reaction* (ξ_2^{eq}).

Figure 2.3: Dependence of equilibrium conversion degrees on reaction variables of CO_2 hydrogenation without any initial presence of CO as observed by Skrzypek et. al[5] using numerically solving thermodynamic relations :
$x_{CO} = 0$, $x_{CO_2} = 0.20$, $x_{H_2} = 0.70$; **(1)** 0.5 MPa, **(2)** 2.5 MPa, **(3)** 5 MPa, **(4)** 10 MPa, **(5)** 15 MPa, **(6)** 30 MPa

Even though methanol synthesis is well studied by now, controversies exist among the research community over important questions such as the role of catalyst components, reactions steps leading upto the products and whether CO or CO_2 is the main source of carbon. These aspects will be looked into in the upcoming sections.

2.3. Methanol Reactors

"**The ZEF methanol reactor is a Packed bed reactor which is designed to function adiabatically as it is insulated and does not try to dissipate the reaction heat. But the reactor volume is less, so the chances of extreme thermal runaway is possible, but to a very low extent.**"

There are many types of reactors that can be employed for heterogeneous catalysis. But the two main main types, depending on the mobility of catalyst are: the Packed Bed Reactor (PBR) and the Fluidized Bed Reactor (FBR). In a FBR, small catalyst particles are suspended by enough upward

motion of the gas flow (fluidization) such that they are not carried out of the reactor or fall down [40]. The mobility of the bed is useful in getting uniform temperature distributions. Although, pressure and pumping required for fluidization at high reactor volume along with erosion due to catalyst particles remain the major shortcomings. On the other hand a PBR uses catalyst that is fixed in a column in random manner through which the gas flows. This allows the reactor to be compact. Therefore, they are the most conventionally used methanol reactors. [41].

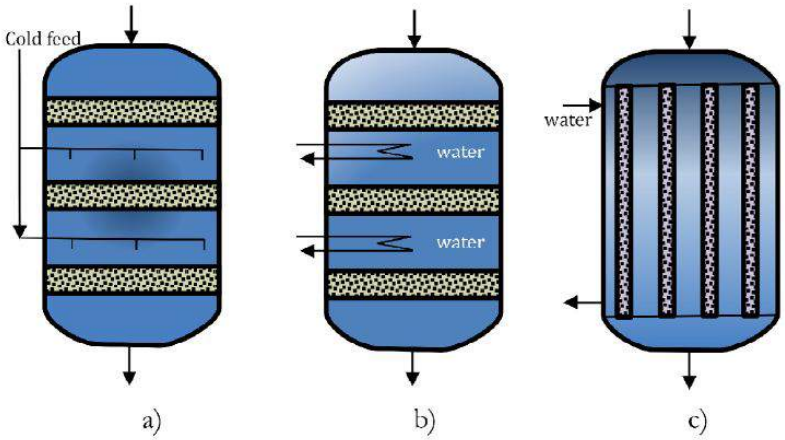

Figure 2.4: (a) Adiabatic reactor with direct cooling; (b) adiabatic reactor with indirect heat exchange; (c) water cooled reactor. [6]

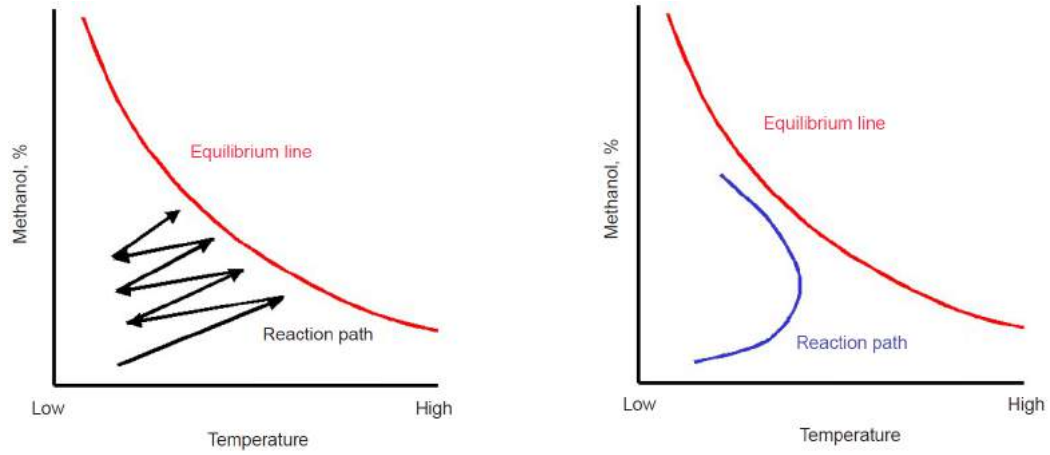

(a) *Reaction pathway for a quench reactor (Adiabatic)* (b) *Reaction pathway for a boiling water cooled reactor (Isothermal)*

Figure 2.5: Reaction path difference between adiabatic and isothermal reactor. [7]

Arguably the most distinguishing feature about any Packed Bed Reactor is the type of temperature control used for synthesis; either adiabatic or isothermal [42]. Adiabatic reactors are insulated from the outside, and the exothermicity of the synthesis reaction stays within the reactor which can cause non uniform runaway temperatures. Adiabatic reactors normally have multiple catalyst beds where cold unreacted gas is injected after each stage using nozzles to bring the gas temperature down (figure-2.4). Such a design is simple to construct and can have a production capacity upto 3000 t/d [7]. Although, addition of fresh quench gas leads to irregular flow distributions across the bed. Therefore, no two catalyst pellets receive the same gas flow that may create cold and hot zones. In some designs, even heat exchangers are used between subsequent catalyst beds (indirect cooling). The reaction pathway taken by such a process is illustrated in figure-2.5a. As showed, the

temperature rapidly rises due to reaction exothermicity and reaches thermodynamic limit. The successive addition of the quench gas takes the temperature away from the equilibrium line every time to increase conversion.

On the other hand, isothermal conditions at the bed are created by placing it in a shell surrounded by boiling water [6]. The temperature is controlled by the pressure of the water and thus, calls for an expensive design. As a result, uniform temperature distribution is achieved because excess heat is removed, which enables the catalyst bed to effectively track the point of maximum reaction rate without crossing the equilibrium limitation, as seen in figure-2.5b. It can be seen that the temperature rises due to exothermicity, but the heat is then taken out to improve the yield. It is understood that the power requirement is higher than an adiabatic reactor.

2.4. Methanol Synthesis Reaction Mechanism

"**The methanol synthesis reaction with CO_2 feed proceeds via Langmuir-Hinshelwood dual site mechanism via formate route, which is the longest living intermediate. The reaction mechanism that emerges from it is consistent with observations in literature. The kinetic models using this mechanisms have been accepted well by the research community.**"

The solid-gas interface is extremely important for heterogeneous catalysis as the reaction is known to happen exclusively at the surface. As such, two different approaches are very oftenly used in the literature; Langmuir-Hinshelwood dual site (s_1 & s_2) mechanism, and the Eley-Rideal single site mechanism [8]. In the first, both the reactant species are adsorbed on neighbouring sites and the product formation happens due to a bimolecular reaction between them, as shown in figure-2.6. In the second, only one reactant species adsorbs to the surface of the catalyst and the other reacts with it from the gaseous phase without adsorbing. Langmuir-Hinshelwood is the most widely accepted mechanism for methanol synthesis where CO and CO_2 compete to adsorb at s_1, while H_2 and H_2O compete to adsorb at s_2 [43].

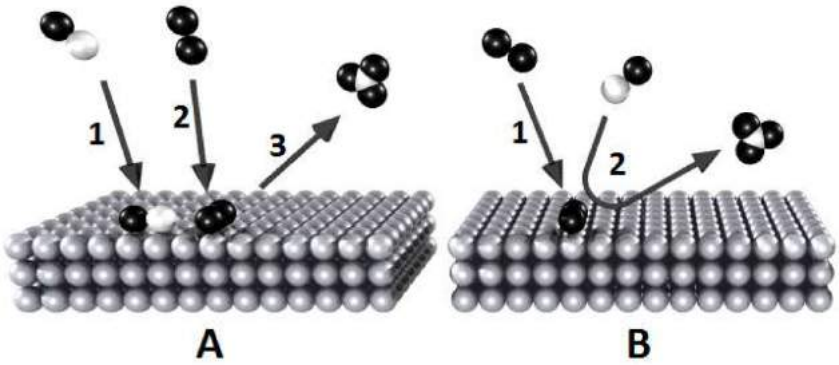

Figure 2.6: Mechanims for surface catalysed reactions; A) Langmuir-Hinshelwood mechanism, B) Eley-Rideal mechanism [8]

A comprehensive mechanism of methanol formation from only CO was first proposed by boomer and Morris [44] where they considered the role of CO_2 as merely to improve the oxidation state and the dispersion of Cu particles in the catalyst structure. Herman et al. [45] and Klier [46] also posited that only after getting converted back to CO by RWGS reaction, it produced methanol. However, Rozovskii [47] and Chinchen et al. [48] showed with complete agreement using isotope labelling experiments (C^{14}) that under industrial conditions and catalyst, almost all methanol was formed from CO_2 even at very low CO_2 /CO ratio. This was further confirmed by Lunkenbein et al.[49] who used 13-Labelled (C^{13}) CO_2. As such, broadly speaking, the reaction involved at the catalyst surface is 2.14, where O(s) is the surface oxygen atom. It has been established that the role of CO or H_2 is to

scavenge the surface oxygen using reactions- 2.15 & 2.16 [36]. The presence of this surface oxygen atom is therefore indicative of Cu^{2+} which promotes CO_2 chemisorption and later hydrogenation [50].

$$CO_2 + 2H_2 \longrightarrow CH_3OH + O(s) \tag{2.14}$$

$$CO + O(s) \longrightarrow CO_2 \tag{2.15}$$

$$H_2 + O(s) \longrightarrow H_2O \tag{2.16}$$

Bussche & Froment[9] came up with a much more detailed approach to methanol formation (Figure-2.7). They suggested that the reactions progress by dissociative adsorption of H_2 and CO_2 at first on the copper surface. The CO_2 adsorption is oxidative and leaves behind a surface oxygen atom, which attracts another CO_2 to form carbonates ($CO_3{}^{2-}$). These carbonates rapidly hydrogenate using the surface hydrogen atom at first to bicarbonates ($HCO_3{}^{-}$), then further to formate ($HCO_2{}^{-}$), formaldehyde (HCOOH), methoxy species (H_3CO^{-}), and then finally to methanol. The hydrogenation of the formate is thought to be the rate determining step, as it is the longest living intermediate. Apart from these, there is also hydrogenation of surface oxygen to form hydroxyl (OH^{-}) group and further, water. The right hand side of figure-2.7 shows the RWGS mechanism, where CO_2 dissociation is the rate determining step. It must be noted that this proposed mechanism is also in agreement with Chinchen et al. [50] and Tagawa et al. [51], where they also showed that RWGS reaction has no carbon containing intermediate, while formate species is the intermediate for methanol production from CO_2 using techniques such as Infrared spectroscopy and Temperature Programmed Desorption (TPD).

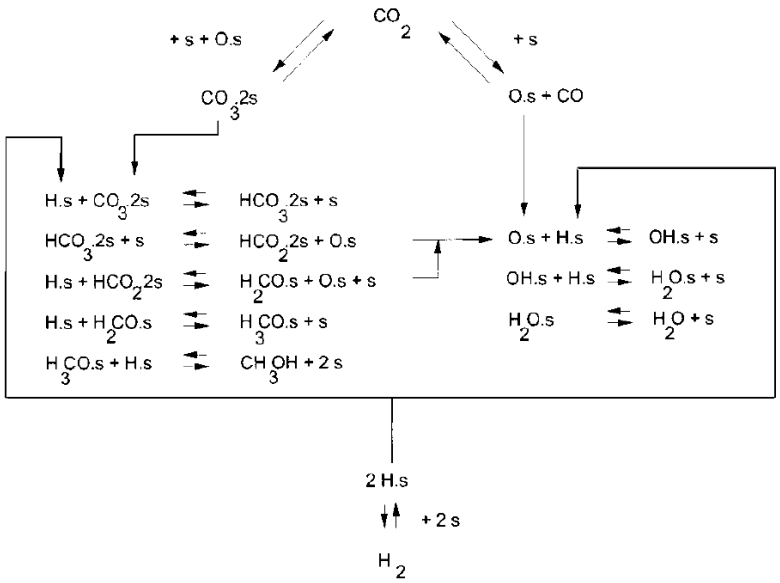

Figure 2.7: Proposed reaction mechanisms for methanol synthesis and water gas shift reactions.[9]

2.5. Methanol Synthesis Catalysts

"**The primary element of most of the methanol catalysts nowadays, is copper due to its high selectivity for methanol. However, the use of copper alone is not viable because it looses its activity soon sue to Thermal sintering. ZnO acts as a stabilizer that mitigates the effect of sintering. Addive oxides such as Al_2O_3 acts as a promoter for higher activity.**"

A practical methanol synthesis process requires a catalyst that is very active, selective and stable for long term operation. The early researches to find a suitable catalyst were quite extensive and in-

volved candidates that were all over the periodic table; zirconium, uranium, bismuth, antimony and even some rare earth elements. Iron was a major contender due to its effectiveness with the Haber-Bosch process for nitrogen hydrogenation. But it was observed that iron reacts with CO to form iron carbonyl, which decomposes to iron metal [7]. This phenomenon made the catalyst more suitable for the Fischer-Tropsch process for creation of higher saturated hydrocarbons and therefore, was discontinued. The first catalyst that was employed for large scale methanol production was developed by BASF in 1923. It was Cr_2O_3-ZnO or zinc chromite and the reaction took place at 300 bar and 573-673 K. The syngas used for the production was obtained from coal and hence contained impurities such as, sulfur, nitrogen, halogenated compounds and heavy metals [34]. The advent of modern desulphurization techniques in 1960, made it possible to clean the syngas stream better and use more selective catalyst $Cu/ZnO/Al_2O_3$ (Low pressure) or $Cu/ZnO/Cr_2O_3$ (High pressure)[52]. It was only after this catalyst was employed that the reaction conditions were lowered to 6-8 Mpa and 523-553 K [53]. However, these catalysts cannot be used for temperatures above 553 K and are prone to poisoning in the presence of sulphur. Either of these is not the case with the methanol reactor at ZEF BV that is under study for this thesis.

The literature on methanol synthesis catalysts suggests that various metal oxides can be introduced using co-precipitation method to boost the Cu/ZnO micro-structure to achieve different effects. Ramaroson et al.[54] noted that the nature of the added metal oxide also plays its hand in the selectivity, when using different reactant compositions. For instance, they showed that SiO_2 had a property to promote methane formation. Other metal oxides include Ga_2O_3, Al_2O_3, ZrO_2, Cr_2O_3 etc. Saito et al.[4] studied the optimum compositions of these metal oxides, the results of which are tabulated in Table-2.1. The Cu surface area was determined using a N_2O Reactive Frontal Chromatography (RFC), which is a well established technique. They observed that the specific activity was dependent only on the type of metal oxide species, but not its content. Ga_2O_3 and Cr_2O_3 improved the specific activity, but not Cu surface area. While, Al_2O_3 and ZrO_2 improved Cu surface area but not the specific activity.

Table 2.1: Activities of $Cu/ZnO/M_xO_y$ ternary catalysts at optimum compositions. Reaction conditions: catalyst weight = 1 g, H_2/CO_2 feed ratio = 3, feed gas rate 300 mL/min, Temperature = 523 K, Pressure = 50 bar.[4]

Catalyst	**Composition** [wt.%]	**Cu surface area** [m^2/g-cat]	**Methanol synthesis activity** [g-MeOH/kg-cat h]	**Specific activity** [mg-MeOH/m^2 h]
Cu/ZnO	50/50	36.5	516	14.1
$Cu/ZnO/Ga_2O_3$	50/25/25	37.6	738	19.6
$Cu/ZnO/Al_2O_3$	50/45/5	47.1	721	15.3
$Cu/ZnO/ZrO_2$	50/40/10	46.0	665	14.5
$Cu/ZnO/Cr_2O_3$	50/45/5	32.8	602	18.4

The addition of trace amounts of silica in the catalyst is shown to improve the longevity of Cu/ZnO based catalysts. Moreover, calcination at high temperatures such as 873 K also improves stability. Hirano et al. [55] did tests on different compositions and concluded that different catalyst cocktails may show similar activity, but they greatly differ in performance over longer durations which points towards their stability. Denise & Sneeden [56] reported that copper catalysts supported by MgO, La_2O_3, Sm_2O_3 had high activity for CO/H_2 feed, than CO_2/H_2. On the other hand, when they are supported by ZnO, Al_2O_3, the exact opposite behaviour is seen. ZrO_2, ThO_2-K supported catalysts take the middle ground and are active for both CO/H_2 & CO_2/H_2.

Thermal sintering of the Cu particles remain the major cause of catalyst deactivation in methanol synthesis using CO_2 feeds [34]. This is due to the low Huttig temperature (temperature at which the surface atoms become mobile) for copper that leads to particle coalescence and reduction in active

sites for reaction [33]. The Huttig temperature is dependent on the melting point of metal ($0.3T_m$), which is lower for copper (1063 °C) as compared to Iron (1535 °C) or Nickel (1455 °C). Therefore the sintering temperature for copper is close to 300 °C. Presence of ZnO minimizes this sintering effect [39].

2.6. Kinetic Models & Catalysis

Kinetic modelling remains the most fundamental challenge towards the design and optimization of any PBR. Understanding of the kinetic pathways is pivotal to creating any kinetic model. All early models to predict the methanol production rate were based on zinc chromite (ZnO/Cr_2O_3) catalyst that was in use then by BASF in the high pressure process and only considered CO hydrogenation [57]. As the understanding of the overall process evolved, CO_2 hydrogenation and water gas shift reactions were also introduced in the models. Most notable among these models are the ones proposed by Graaf et al.[43] and the model of Bussche & Froment [58]. Both these models make use of the Langmuir-Hinshelwood dual site mechanism and are the two main kinetic models used by the industry. The success of these models is attributed to their much more detailed mechanistic approach.

Global kinetic model of Graaf et al.

Graaf et al. [43] pointed out that regardless of the carbon source for methanol, both CO and CO_2 hydrogenation must be considered to create a sound kinetic model even though the role of CO_2 is disputed. Since Cu-Zn-Al is known to catalyse water gas shift reaction, it was also included in their model. They made use of the Langmuir-Hinshelwood dual site mechanism and assumed that CO and CO_2 compete to adsorb at site s_1, while H_2 and H_2O compete to adsorb at site s_2. The adsorption of methanol was assumed to be negligible. A detailed list of elementary reactions used by Graaf at al. that lead to the overall reaction is given below for reference. Although 48 different combinations of kinetic models can be made from these reactions, A3-B2-C3 was shown to be most accurate with experimental data. The rate equations that culminated from considering A3-B2-C3 as rate determining steps is shown in equations-2.17, 2.18, 2.19.

$$
\begin{aligned}
CO\cdot s_1 + H\cdot s_2 &\rightleftharpoons HCO\cdot s_1 + s_2 && \dots(A1)\\
HCO\cdot s_1 + H\cdot s_2 &\rightleftharpoons H_2CO\cdot s_1 + s_2 && \dots(A2)\\
H_2CO\cdot s_1 + H\cdot s_2 &\rightleftharpoons H_3CO\cdot s_1 + s_2 && \dots(A3)\\
H_3CO\cdot s_1 + H\cdot s_2 &\rightleftharpoons CH_3OH + s_1 + s_2 && \dots(A4)\\
CO_2\cdot s_1 + H\cdot s_2 &\rightleftharpoons HCO_3\cdot s_1 + s_2 && \dots(B1)\\
HCO_2\cdot s_1 + H\cdot s_2 &\rightleftharpoons CO\cdot s_1 + H_2O\cdot s_2 && \dots(B2)\\
CO_2\cdot s_1 + H\cdot s_2 &\rightleftharpoons HCO_2\cdot s_1 + s_2 && \dots(C1)\\
HCO_2\cdot s_1 + H\cdot s_2 &\rightleftharpoons H_2CO_2\cdot s_1 + s_2 && \dots(C2)\\
H_2CO_2\cdot s_1 + H\cdot s_2 &\rightleftharpoons H_3CO_2\cdot s_1 + s_2 && \dots(C3)\\
H_3CO_2\cdot s_1 + H\cdot s_2 &\rightleftharpoons H_2CO\cdot s_1 + H_2O\cdot s_2 && \dots(C4)\\
H_2CO\cdot s_1 + H\cdot s_2 &\rightleftharpoons H_3CO\cdot s_1 + s_2 && \dots(C5)\\
H_2CO\cdot s_1 + H\cdot s_2 &\rightleftharpoons CH_3OH + s_1 + s_2 && \dots(C6)
\end{aligned}
$$

$$
r_{MeOH,CO} = \frac{k'_{ps,A3}K_{CO}\left[f_{CO}f_{H_2}^{3/2} - \dfrac{f_{CH_3OH}}{f_{H_2}^{1/2}K_1^{eq}}\right]}{\left(1 + K_{CO}f_{CO} + K_{CO_2}f_{CO_2}\right)\left[f_{H_2}^{1/2} + \dfrac{K_{H_2O}}{K_{H_2}^{1/2}}f_{H_2O}\right]} \tag{2.17}
$$

$$r_{RWGS} = \frac{k'_{ps,B2} K_{CO_2} \left[f_{CO_2} f_{H_2} - \frac{f_{H_2O} f_{CO}}{K_2^{eq}} \right]}{\left(1 + K_{CO} f_{CO} + K_{CO_2} f_{CO_2}\right) \left[f_{H_2}^{1/2} + \frac{K_{H_2O}}{K_{H_2}^{1/2}} f_{H_2O} \right]} \tag{2.18}$$

$$r_{MeOH,CO_2} = \frac{k'_{ps,C3} K_{CO_2} \left[f_{CO_2} f_{H_2}^{3/2} - \frac{f_{CH_3OH} f_{H_2O}}{f_{H_2}^{3/2} K_3^{eq}} \right]}{\left(1 + K_{CO} f_{CO} + K_{CO_2} f_{CO_2}\right) \left[f_{H_2}^{1/2} + \frac{K_{H_2O}}{K_{H_2}^{1/2}} f_{H_2O} \right]} \tag{2.19}$$

It was observed that adsorption of hydrogen is better explained when considered rather dissociative than molecular. Even though they considered both CO and CO_2 hydrogenation, it was seen that CO_2 was much more dominant. A problem that they spotted was that equations-A3, C5 have the same stochiometry, and hence they give different concentrations of the same species (Formyl & Methoxy).

Global kinetic model of Bussche & Froment

Most notable and relevant to this thesis among these models is the Bussche & Froment model [9] for $Cu/ZnO/Al_2O_3$ catalyst (equation-2.20, 2.20). Adapting to the findings of the previously stated model of Graaf et al., it considers CO_2 as the carbon carrier and also takes into account water gas shift reaction. Both methanol formation, and RWGS proceed on the copper phase of the catalyst. While, ZnO acts as a promoter. Intermediate reactions and their equilibrium and rate constant connotations that are used in the model are presented below for reference.

$$\begin{aligned}
H_{2(g)} + 2s &\rightleftharpoons 2H\cdot s && \dots (K_{H_2}) \\
CO_{2(g)} + s &\rightleftharpoons O\cdot s + CO_{(g)} && \dots (K_1, k_1) \\
CO_{2(g)} + O\cdot s + s &\rightleftharpoons CO_3\cdot 2s && \dots (K_2) \\
CO_3\cdot 2s + H\cdot s &\rightleftharpoons HCO_3\cdot 2s + s && \dots (K_3) \\
HCO_3\cdot 2s + s &\rightleftharpoons HCO_2\cdot 2s + O\cdot s && \dots (K_4) \\
HCO_2\cdot 2s + H\cdot s &\rightleftharpoons H_2CO_2\cdot 2s + s && \dots (K_{5a}) \\
H_2CO_2\cdot 2s &\rightleftharpoons H_2CO\cdot s + O\cdot s && \dots (K_{5b}) \\
H_2CO\cdot s + H\cdot s &\rightleftharpoons H_3CO\cdot s + s && \dots (K_6) \\
H_3CO\cdot s + H\cdot s &\rightleftharpoons CH_3OH_{(g)} + 2s && \dots (K_7) \\
O\cdot s + H\cdot s &\rightleftharpoons OH\cdot s + s && \dots (K_8) \\
OH\cdot s + H\cdot s &\rightleftharpoons H_2O\cdot s + s && \dots (K_9) \\
H_2O\cdot s &\rightleftharpoons H_2O_{(g)} + s && \dots (K_{H_2O})
\end{aligned}$$

$$r_{MeOH} = \frac{k'_{5a} K'_2 K_3 K_4 K_{H_2} p_{CO_2} p_{H_2} \left[1 - \left(\frac{1}{K^*} \right) \left(\frac{p_{H_2O} p_{CH_3OH}}{p_{H_2}^3 p_{CO_2}} \right) \right]}{\left(1 + \left(\frac{K_{H_2O}}{K_8 K_9 K_{H_2}} \right) \left(\frac{p_{H_2O}}{p_{H_2}} \right) + \sqrt{K_{H_2} p_{H_2}} + K_{H_2O} p_{H_2O} \right)^3} \tag{2.20}$$

$$r_{RWGS} = \frac{k'_1 p_{CO_2} \left[1 - K_3^* \left(\frac{p_{H_2O} p_{CO}}{p_{CO_2} p_{H_2}} \right) \right]}{\left(1 + \left(\frac{K_{H_2O}}{K_8 K_9 K_{H_2}} \right) \left(\frac{p_{H_2O}}{p_{H_2}} \right) + \sqrt{K_{H_2} p_{H_2}} + K_{H_2O} p_{H_2O} \right)} \tag{2.21}$$

In the above equation, K_i denotes equilibrium constants while k_i denotes rate constants. The values of equilibrium constants K_1^* and K_3^* are calculated thermodynamically using the findings of an earler work from Graaf et al. [59].

$$\log k_1^* = \frac{3066}{T} - 10.592 \tag{2.22}$$

$$\log \frac{1}{K_3^*} = \frac{-2073}{T} + 2.029 \tag{2.23}$$

The model very effectively captures the experimental observations of previous works in literature. Effects of pressure and inlet temperatures are also accounted. Concentration of both reactant and product species are predicted along the bed (see figure-2.8).

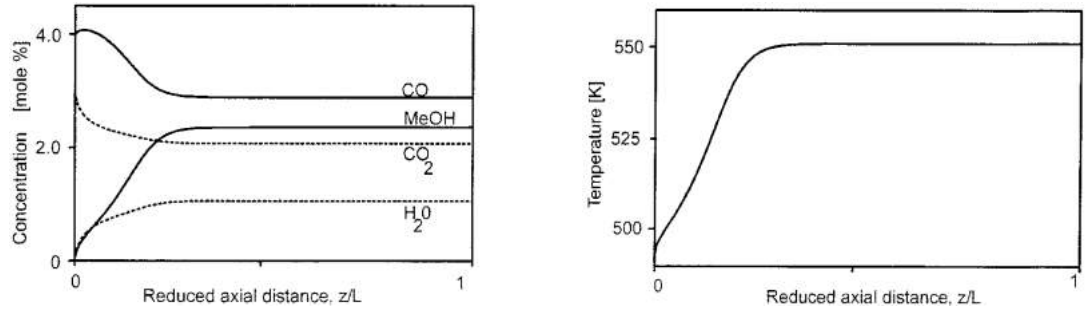

(a) *Concentration profile along the bed* (b) *Temperature profile along the bed*

Figure 2.8: Simulated concentration and temperature profiles in an adiabatic reactor modelled by Bussche & Froment [9]. Operating conditions:Inlet temperature = 493 K, P= 50 bar

2.7. Methanol synthesis from captured CO_2

" **Synthesis of methanol from CO_2 proceeds 20 times faster than that of CO. The selectivity is also very high and by product formation is less. The low exothermicity of CO_2 as compared to CO also helps in better temperature control. However, the equilibrium yield is lower than syngas based system. Condensation of products and their removal reveal prospect for future of CO_2 valorization to methanol. A purge outlet has no impact on methanol yield by direct CO_2 hydrogenation.**"

Lee et al. [60] as well as Sahibzada et al.[61] reported that the methanol production from CO_2 happens at much faster (20 times) rates than CO, especially at low temperatures. This may be the reason why Rozovskii et al.[47] found higher methanol production from CO_2 when operating at 495 K, which is in the lower range of typical methanol synthesis conditions 500-575 K. As discussed earlier, it is now widely accepted that methanol is almost exclusively formed at the surface of the catalyst by CO_2 content of the syngas by hydrogenation. The water gas shift reaction only acts to suppress the CO and also provide more H_2. Some quantity of CO_2 is always necessary for the process to kick start and proceed. Experiments in the literature from only CO/H_2 containing yielded in negligible amounts of methanol (Ipatieff & Monroe [62]) where they found higher concentrations of di-methyl ether instead of methanol by using CO. This is because CO hydrogenation is more exothermic and caused an average 30 °C rise in the bed temperature in their experiments. This in turn causes the dehydration of methanol into ether.

The capital investment for a CO_2 based plant is estimated to be about the same as that of a conventional syngas plant[10]. CO_2 as a raw material can be captured from various sources; like exhaust of power plants or other industrial plants, geothermal wells, natural gas wells, even from the small concentration of CO_2 from the air. Additional purification steps are required when pollutants such

as H_2S, SO_x are present. A wide range of processes, both physical and chemical are available to separate CO_2 from a gas; such as absorption into a liquid, adsorption onto a solid surface, membrane separation, cryogenic separation etc. Out of the above mentioned techniques, the absorption into a solution is most prominently used and some common sorbents are: monoethanolamine (MEA), diethanolamine (DEA), polyethyleneimine (PEI), tetraethylenepentamine (TEPA). CO_2 [63]. Absorption is an exothermic process and can even be simply achieved by contacting it with an adequate base like $Ca(OH)_2$ or KOH to form carbonates. The energy taxing step is the regeneration of the base that releases CO_2.

The methanol yield of syngas feed plants is considerably higher than that of the CO_2 feed plants, as seen in Figure-2.9 [10]. This is because single pass conversion with CO_2 is very low, which calls for very high recycle ratio. In order to reduce the operational and capital costs associated with having high recycle ratios, several methods have been suggested in the literature to shift the equilibrium towards methanol when using only H_2/CO_2 feed. Most of them involve the *in-situ* removal of methanol and water. As the products of an equilibrium reactions are removed, the reaction shifts towards the right according to Le Chatelier's principle. For instance, methanol adsorption on silica-alumina powder[64] or solvents such as tetraethylene glycol dimethyl ether (TEGDME)[65], supercritical 2-butanol[66], or n-dodecane. Equilibrium can also be shifted by using membranes. A different approach was suggested by Haut et.al[67] by condensing the reaction products on a condenser surface. Another technique is by condensing the products using very high pressures(>360 bar). However, these methods result in very high costs due to high pressure equipments, extra process steps and introduction of foreign chemicals. Due to these limitations ZEF has embarked on a path which uses an internal recycle stream, by having temperature gradients inside the reactor itself. This design is inspired from the work of Brilman & Bos[10]. As such the flow inside the reactor is not pressure driven but rather temperature driven, thus based on natural convection.

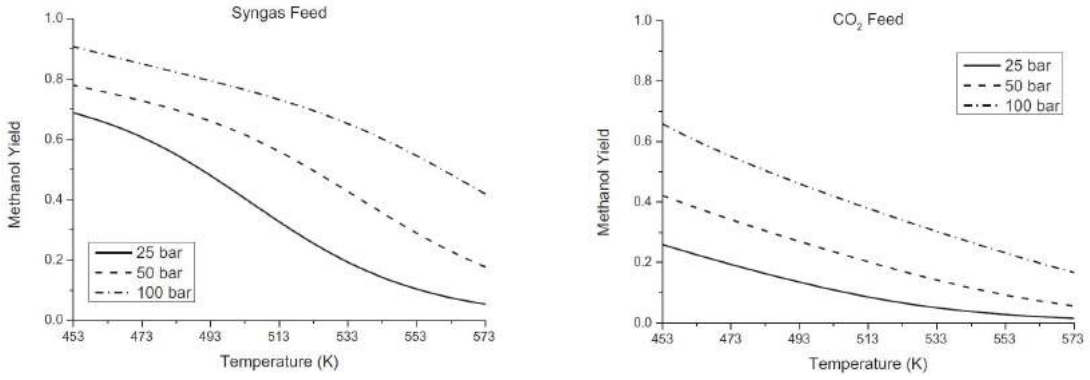

(a) *Methanol synthesis from Syngas feed.* $H_2/CO/CO_2$ *: 75.9/16.9/7.2* (b) *Methanol synthesis from* CO_2 *feed.* $H_2/CO/CO_2$ *: 75/0/25*

Figure 2.9: Comparison of equilibrium methanol yield for two feed options. [10]

Studies done by Ushikoshi et al.[68] revealed that methanol synthesis from CO_2 hydrogenation has the following advantages over syngas hydrogenation.

- The selectivity for methanol formation is extremely high(99.7%) with CO_2 hydrogenation instead of CO hydrogenation.
- Byproducts such as higher alcohols and ketones which are difficult to separate are in low concentration (<0.1%).
- Methane and other alkane formation is so less that a purge operation is not necessary. These by products get reformed inside the reactor and reused for methanol production.
- $Cu/ZnO/Al_2O_3$ based catalysts show long term stability.
- Presence of a purge valve at the reactor outlet has no effect on methanol synthesis from CO_2

hydrogenation, unlike the case with syngas.

2.8. Transient observations in literature on methanol synthesis

Synthesis of methanol is one of the ways of converting the anthropogenic CO_2 into a useful chemical [3]. The intricate nature of the processes concerning methanol synthesis totally justify an experimental study for transient behaviour to assess the system and gain a better understanding of the reactor behaviour. Such experiments are really important for a myriad of reasons: Safety, control, optimization, start-up and shut-down protocols, process intensification, and in general the entire operability study [14]. The need for such an understanding becomes even more heightened in presence of factors that affect catalyst activity (Gas composition, Temperature etc). Methanol reactors that employ fixed bed catalysis are often very difficult to control because the reaction is highly exothermic. Therefore, it is important to predict the possibility of hot spot formation and thermal runaway occurrences. More often than not, wide fluctuations in temperatures occur from relatively minor fluctuations in control variables [69]. These erratic temperature zones may lead to poor yield and wastage of valuable feed-stock and power.

The transitory behaviors can be tested experimentally or by modelling the reactor itself. Modelling the reactor with recycle streams poses a lot of complex problems because the boundaries of the system and their interactions are complicated, to put it lightly. It involves solving system of non linear differential equations while evaluating various transport and chemical parameters like: the diffusion of gas through a solid matrix coupled with catalyst deactivation, intra-particle mass diffusion etc. Even if all such problems are somehow resolved, and the transient behavior appears to be reasonable, it does not mean anything unless it is corroborated with experimental data. If the reactor parameters are controlled properly, the experimental data tells more about the real transient behavior, no matter how unreasonable it looks.

Unfortunately, typical methanol reactors are huge and companies are reluctant to spend so much on experimenting with the reactor as it involves significant capital and time, which is why they rather go for modelling. Some investigations that may even have been done by firms are confidential and are not readily available. This makes it hard to find similar works in the literature. But ZEF has a much more small scale plant and it is possible to see its transient behaviour with experiments and observations.

Therefore the following sections try to gain insights from the modelling and lab scale works done by various researchers, and uses them to explain the behaviors observed in the methanol reactor that is under study for this thesis.

2.8.1. Transient response to morphology of the catalyst

"The morphology of the catalyst during production is not in the scope of this thesis, but it does change due to the gas environment. So it is better to keeps these effects in mind before moving further. When the feed becomes CO_2 rich it creates a more oxidizing environment. An oxidizing environment causes the copper nano particles to acquire less surface area, thereby reducing the active site for methanol production. Some oxygen atom coverage on the catalyst surface is inevitable during synthesis. But it may leave the catalyst oxidized, if not scavenged by H_2 to make water and re-reduce the catalyst."

Chinchen et al.[48] demonstrated that the oxidation state of the copper surface during methanol synthesis is highly correlated with methanol synthesis activity because it promotes CO chemisorption. They tested for available copper area for different metal oxide support and compositions using N_2O chemisorption based Reactive Frontal Chromatography[1] and found strong correlation with

[1] RFC: It is a well know technique in which known amount of N_2O is passed through the catalyst. After adsorption on the copper site N_2 is released and Oxygen atoms remain chemisorbed on the catalyst surface. The N_2 received at the outlet, compared to the N_2O supplied to the inlet is calibrated to find the active surface area of the catalyst.

synthesis activity; higher the surface area, higher the activity. In a followup of this experiment they also determined the apparent copper surface area before and after methanol synthesis, which was indicative of the oxygen coverage of the copper surface. They observed that the oxygen coverage is dependent on the feed gas composition, especially CO which is the dominant reducing agent for the copper surface. Therefore, higher the CO_2 content of the feed gas, higher the oxygen coverage of the catalyst surface.

As shown before, several isotope labelling experiments with Cu/ZnO based catalysts have been conducted to show that the hydrogenation of CO_2 is the dominant route to methanol [50, 70], which produces water. Although industrial methanol is produced using syngas which contains CO, experiments with and without CO_2 in CO/H_2 feed suggests that direct hydrogenation of CO is insignificant [71]. Steam is a natural byproduct of CO_2 hydrogenation and the CO component of the syngas only acts to suppress the steam using the reverse water gas shift reaction. In absence of CO, the catalyst is always at risk of deactivation due to water, which enhances recrystallization and sintering [39].

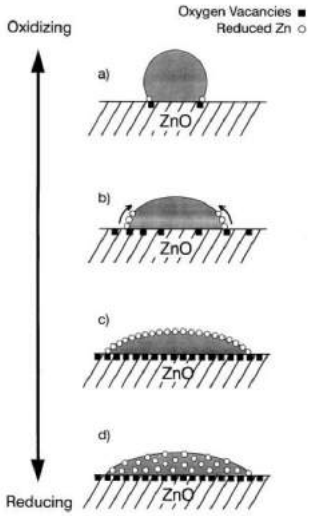

Figure 2.10: Illustration for the wetting/nonwetting of the Cu particles on the Zn support, surface alloying, and bulk alloy formation due to change in reduction potential of the feed gas: (a) round-shaped particle under oxidizing syngas conditions; (b) disk-like particle under more reducing conditions; (c) surface Zn–Cu alloying due to stronger reducing conditions; (d) brass alloy formation due to severe reducing conditions. [11]

Cu and ZnO may be used alone as methanol synthesis catalyst, but the activity increases significantly when Cu particles are supported by ZnO. The true nature of this metal-support synergy is not understood fully and several explanations have been levied. Some propose that it is due to the support induced strain in Cu particles [72] while some propose that it is due to the dispersion of Cu species on ZnO [6]. There is also literature that says it is due to the formation of Cu–Zn alloy [73]. But the most promising one is the gas dependent morphology of Cu on ZnO, which says that the shape of Cu particles is dependent on the composition of the methanol synthesis gas environment.

Vesborg et al [12] studied these dynamic changes of the catalyst using *in-situ* Extended X-Ray Absorption Fine Structure (EXAFS) and observed this dynamic morphology. They showed that these changes can be attributed to the reduction potential of gas environment. Essentially, their findings suggest a shape-activity relationship where flatter Cu nano-particles have a higher activity than the more spherical particles because they have lower coordination number. Qualitatively, in figure-2.11 the Cu nano-particles appear to be more flat under more reducing conditions and more spherical during exposure to more oxidizing gases. Their experiments showed that the methanol production spikes after being treated with a reducing environment. If such a relationship does exist, then it may cause transient behaviours in the reactor. As the composition of the feed changes, so does the

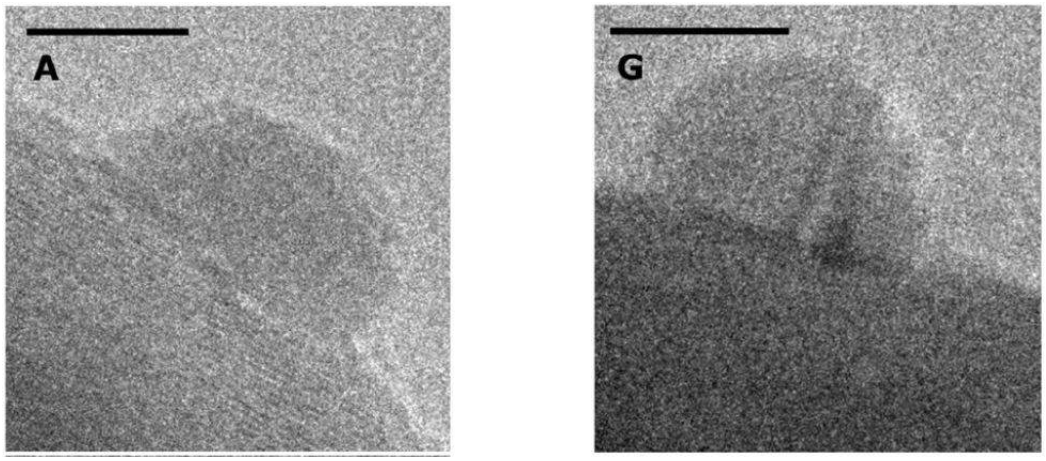

(a) *50:50 CO:H_2*

(b) *50:50 CO_2:H_2*

Figure 2.11: Representative ETEM images of Cu nanoparticles on ZnO obtained in situ during exposure to 2 mbar gas at 500 K [12].

reduction potential of the gas environment. As such it can cause the morphology of the Cu/ZnO interface to change and affect production.

2.8.2. Transient response to composition of the feed

"The activity of the catalyst is dependent on the feed gas composition as it affects its oxidation state and morphology. If the ZEF reactor while in operation, faces shortage in any reactant, it may need to operate at a composition that is not stochiometric. In such a case the temperature of the bed needs to be changed to the T_{opt}, which is commensurate with the varying composition. For a given temperature, the reactor yield drops on either side of the ideal composition of $H_2 : CO_2$ = 3:1."

A process that relies on the feed stock obtained from intermittent energy source such as sun, necessitates a proper understanding of the dynamics which can define a robust control design. The compositions and conversions which are attained at equilibrium are highly dependent on the initial composition of the feed. Total Gibbs free energy minimization is used generally to obtain the equilibrium compositions [74].

The temperature of the reacting gases while passing the reactor bed strongly influences the methanol yield and thermal stability. It can be seen in the work done by Sharokhi et. al. [13] (figure-2.12a) that there is an optimum temperature which maximizes the methanol conversion for a given feed composition. However, when the feed composition is changed the reaction temperature must also be changed accordingly in order to have maximum conversion. Therefore, a changing feed composition can be introduced to get a surface plot that can tell us the optimum operating line, as shown in figure-2.12b. Experiments done by Lee et al. [75] suggests that higher concentration of CO_2 in the feed leads to higher oxygen coverage of the catalyst which leads to better yield. It has already been discussed that the surface oxygen is seen as a reactant and promoter of CO_2 adsorption on the catalyst [48] [58]. Liu et al. [76] also reported that the activity is dependent on the oxidation state of the catalyst, which in turn depends on the composition of the gas environment. These findings must be coupled with those of Tagawa et al.[51], who found that there exists a T_{Max} for any catalyst for maximum methanol production and different catalysts with same activity have similar T_{Max}. Therefore, if the activity of the catalyst is somehow changed due to the feed gas composition, the reactor must be adjusted to the new T_{Max} to give optimum yield.

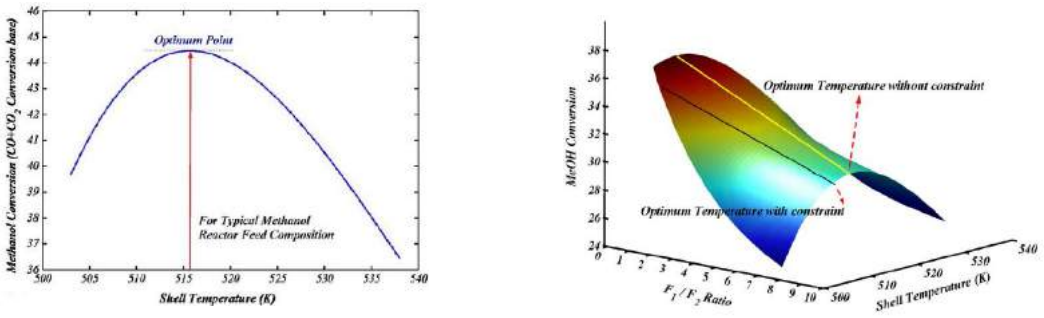

(a) *Effect of reaction temperature on the methanol conversion for a given feed composition*

(b) *Optimal shell temperature for different feed compositions*

Figure 2.12: Effect of various parameters on the methanol activity [13].

2.8.3. TRANSIENT RESPONSE TO TEMPERATURE

"The equilibrium methanol yield increases with temperature to a maximum point, and then starts decreasing. However, temperature greatly enhances reaction rate by affecting kinetics. Therefore, an increase in temperature may decrease the equilibrium methanol yield, but still increase the methanol production, if the reactor is away from equilibrium. In such a case the reactor is said to be kinetically limited and not equilibrium limited. In the current work the temperature of reactor bed has not been varied as a parameter. Although, the gas inlet temperature can show variations depending on the internal mass flow due to natural circulation. The temperature can exert its effect on the kinetics of methanol production and increase yield."

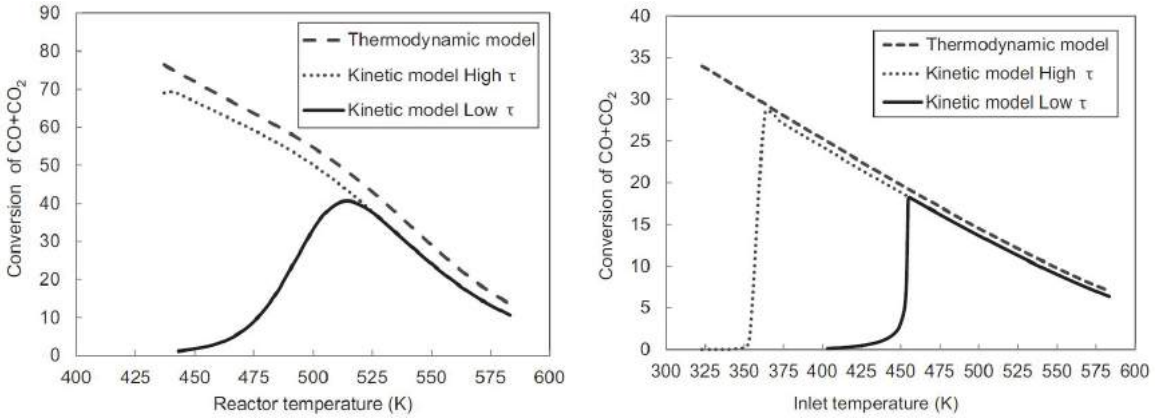

(a) *Comparison of CO+CO_2 conversion predicted by kinetic model and thermodynamic model under isothermal conditions*

(b) *Comparison of CO+CO_2 conversion predicted by kinetic model and thermodynamic model under adiabatic conditions*

Figure 2.13: Results of simulations by Iyer et al.[14]. High τ = 2000-3000 s, Low τ = 5-7 s

$$X_{\mathrm{CO+CO_2}} = \frac{CO_{in} + CO_{2in} - CO_{out} - CO_{2out}}{CO_{in} + CO_{2in}} \times 100 \tag{2.24}$$

Temperature very intricately affects the kinetics and thermodynamics in any reactor. It is important to realize whether the yield is being limited by the equilibrium or by kinetics. Iyer et.al.[14] did a comparison of kinetic model with thermodynamic model to study the CO+CO_2 conversion as a function of temperature in an isothermal and an adiabatic reactor at 50 Bar. The kinetic model used the Vanden Bussche and Froment[58] proposed Langmuir-Hinshelwood-Hougen-Watson(LHHW) based approach to predict the performance. While the thermodynamic model used the minimum of the total Gibbs energy to predict the equilibrium compositions[74]. It can be seen in figure-2.13a

that for low residence time and isothermal case, the kinetic model predicts an increase in conversion with temperature and reaches a maximum at around 510 K. This is the point where the reactions exhibit a transition from kinetic to an equilibrium regime. In other words it has reached the thermodynamic limit. While in the case of high residence time, equilibrium is reached in the reactor due to more time. Figure-2.13b shows the same analysis for adiabatic conditions. They concluded that the reaction reaches equilibrium very quickly due to its exothermic nature. When the heat loss is locked, the outlet temperature of reactor rises drastically and high reaction rates approach equilibrium condition. At this point it must also be brought to light that experiments conducted by Ipatieff & Monroe [62] showed that with increase in temperature, the methanol production goes down drastically, while the production of methane is favored over $Cu/ZnO/Al_2O_3$ based catalysts. This is also supported by the work of Bukhtiyar et al. [15] and Urakawa et al.[77]. In figure-2.14b, the selectivity goes down with temperature.

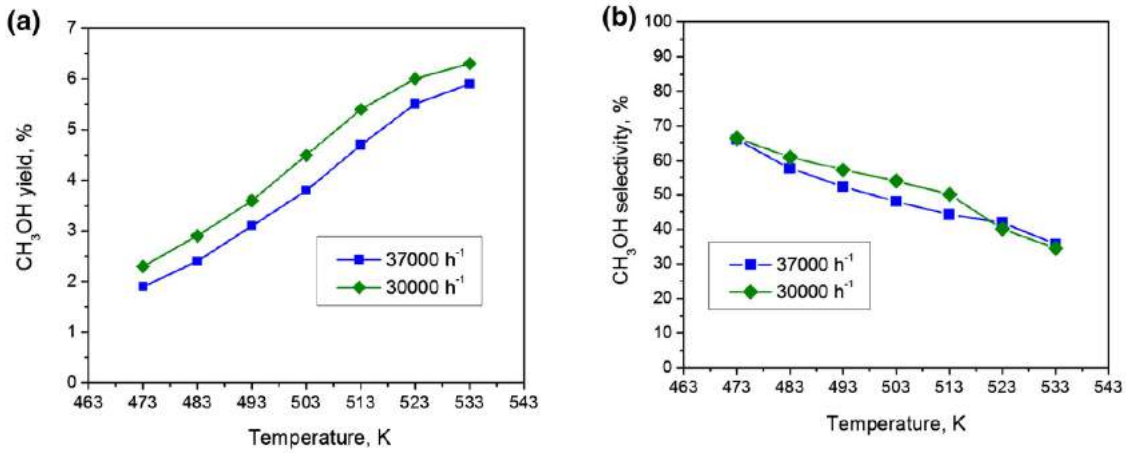

(a) *Effect on methanol yield.*

(b) *Effect on selectivity.*

Figure 2.14: MeOH yield and selectivity at 30 bar and varying temperatures over the $Cu/ZnO/Al_2O_3$ catalyst. Bukhtiyar et al. [15]

2.8.4. Transient response to pressure

" Pressure has a positive impact on the methanol synthesis process due to Le Chatelier's Principle. The equilibrium methanol yield is raised by increasing pressure. However, in the current work, the pressure also affects density of gas inside the reactor and hence, the natural circulation. Therefore, the observed effects may digress from the trends of pressure at equilibrium."

The methanol synthesis process is favored by higher pressures (Le Chatelier's Principle) because the synthesis reaction proceeds by reduction in the number of moles of the reactant species as compared to products. On the other hand it has only mild effect on the RWGS reaction. Ushikoshi et al.[68] did an experimental analysis on a small scale test plant with methanol production capacity of 50 kg/day over $Cu/ZnO/Al_2O_3/SiO_2$ catalyst and only CO_2/H_2 feed. It can be seen in Figure-2.15a that the production rate was 580 g/hr per liter of catalyst under the conditions 523 K and 50 bar, which is 20% lesser than the reaction equilibrium production rate at same pressure (dashed lines). At 50 bar the yield reaches a maximum around 533 K and it also increases by increasing the reaction pressure. Similar results have been corroborated by other works in the literature too (Ipatieff and Monroe [62]).

Moreover, they analysed the reaction products for presence of byproducts (Thermal Conductivity Detector (TCD), Flame Ionization Detector (FID)). It was reported that the selectivity was 99.7% for methanol and the concentration of CO remained the same throughout the test, which was the

equilibrium concentration of CO for the reverse water gas shift reaction at that reaction temperature. The main composition of the liquid product was methanol and water, with trace amounts of methyl formate and ethanol. The purity of the product at 523 K and 50 bar was the highest at 99.9 wt%. They showed that it is because, at 473 K production of methyl formate is more and at higher temperatures like 543 K it had more higher alcohol production. In figure-2.15b it has been shown

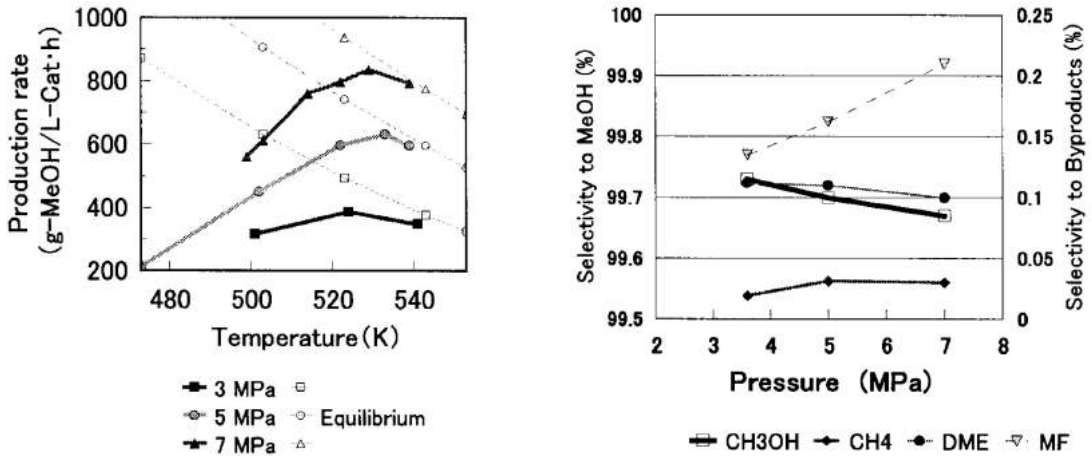

(a) *Effect of pressure on methanol production. Conditions: GHSV = 10000 h^{-1}, T = 523 K, P = 50 Bar, Cu/ZnO/Al_2O_3/SiO_2, H_2 : CO_2 = 3:1. [68]*

(b) *Effect of pressure on methanol selectivity. Conditions:GHSV = 10000 h^{-1}, T = 523 K, P = 50 Bar, Cu/ZnO/Al_2O_3/SiO_2, H_2 : CO_2 = 3:1. [68]*

Figure 2.15: Effect of pressure on methanol production and selectivity.

that, from the stand point of selectivity to methanol, pressure has a negative effect. Higher pressures declined methanol selectivity and favored Methyl formate selectivity.

2.8.5. Transient response to Gas Hourly Space Velocity (GHSV)

"GHSV experiments in the literature are done on single pass reactors with mass flow controllers. Although, in the ZEF reactor it is not the flow of feed gases from cylinders, but rather the internal circulation because it works on feed recycle. Even though a comparison will be impractical, it is better to note the underlying phenomenons. A high space velocity gives more mass diffusion to the catalyst bed, but reduces the contact time needed for the reaction, giving rise to a trade-off situation that requires maximization. It does not affect the selectivity."

GHSV is defined as the hourly volumetric flow rate of feed gas per unit of catalyst volume and has a unit of $L_{feedgas}.L_{Cat}^{-1}.h^{-1}$, also abbreviated as h^{-1}. Doss et al.[78] built a pilot scale, single pass, isothermal methanol synthesis reactor working on only CO_2 & H_2 feed. A monotonic decrease in CO_2 conversion is observed when GHSV is increased (figure-2.16a). A high GHSV is indicative of low residence time of feed gases on the catalyst bed thereby decreasing the methanol synthesis. As such a high percent of the feed gas can be expected to go un-reacted and the conversion decreases. However, it is also seen that the STY increases with the GHSV (Figure-2.16b). This is because even though the percentage of CO_2 converted to methanol is lowered, the total CO_2 flow into the reactor is much higher. Lo and Wu [79] also did similar tests and found that the methanol production rate is directly proportional to the GHSV. In addition they also noted two different factors that oppose each other. In any catalytic reduction process there are several intermediate steps at the catalyst surface that need to be completed to reach the final product. Reactant gases must therefore, diffuse into the catalyst where they can join the surface reaction. The diffusion is affected by the GHSV but the surface reaction is affected by the residence time. They showed that after increasing the GHSV beyond a certain point, even the methanol production rate goes down.

Lee et al. [75] confirmed this behaviour of production rate going up and the further down after

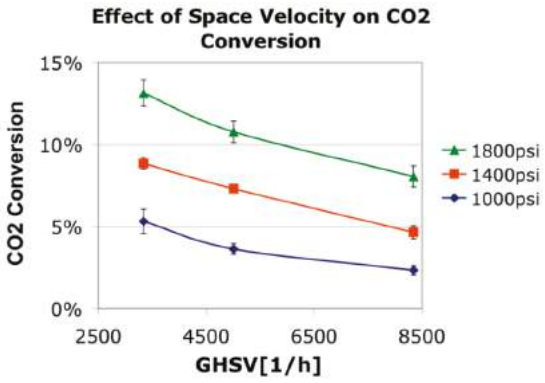

(a) *CO_2 conversion as a function of GHSV at different pressures; T = 240 °C. H_2 : CO_2 = 3.5:1[78]*

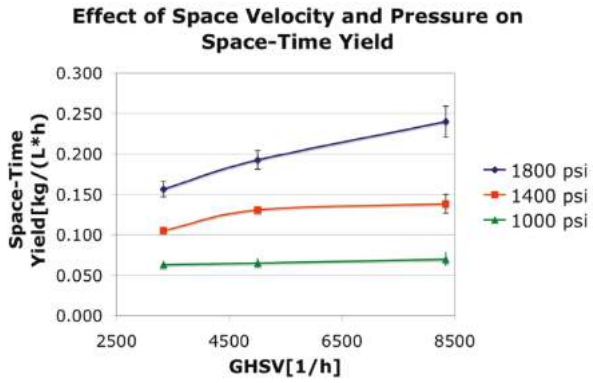

(b) *Space Time Yield (STY) as a function of GHSV at different pressures; T = 240 °C. H_2 : CO_2 = 3.5:1[78]*

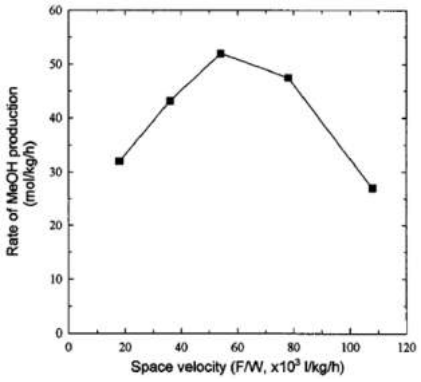

(c) *Occurrence of an optimal space velocity for maximum yield. Experimental: $Cu/ZnO/Al_2O_3$ with synthesis gas containing 10 vol% CO_2. Reaction conditions: T =523 K, P=30 Bar [75].*

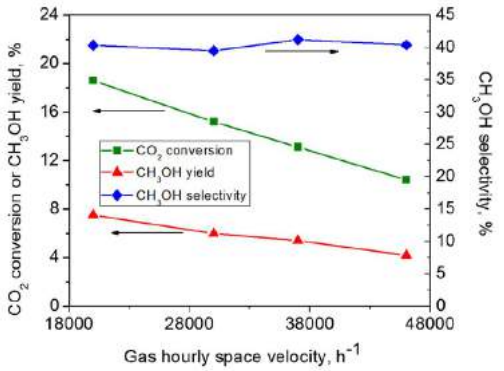

(d) *Catalytic performance of the $Cu/ZnO/Al_2O_3$ catalyst at 30 bar, 523 K, and different space velocities. [15]*

Figure 2.16: Results from literature about the effects of space velocity on methanol yield.

increasing the space velocity (figure-2.16c). Bukhtiyar et al. [15] demonstrated similar results with their experiments. Their CO_2 conversion trends with GHSV match with that of Doss et al.[78] as seen in figure-2.16d. However, their methanol production trends do not match. This can be understood by the concept proposed by Lo and Wu[79], as the GHSV value used by the former is higher.

2.8.6. Transient response to long term operation.

"Even though long term methanol production experiments were not conducted during this thesis, its effects cannot be excluded and should be kept in mind. The water formed during production can slowly deactivate the catalyst by promoting Cu sintering for the first 500 hrs of operation."

Most catalysts show an initial decrease in the productivity before reaching a stable state Economic feasibility of methanol synthesis dictates that the catalyst should reveal long term stability during production. Ushikoshi et al.[68] conducted a long term methanol synthesis test for 3500 h. Figure-2.17a shows their experimental findings. It can be seen that methanol production rate was 700 g h^{-1} initially, but reduced to 580 g h^{-1} after 1000 h. The extrapolation of regression line also estimates that it will be around 500 g h^{-1} in 3 years. Hirano et al. [55] also did similar long term tests and observed that methanol yield drops to 90% of the initial value during first 500 h and then stays stable after it. Bukhtiyar et al. [15] found a reduction by 9.8% in first 48 hrs (figure-2.17b). This behavior was attributed to the stability of the catalyst but points towards the transitory behaviour in production over long duration. The sintering of the catalyst is the prime suspect for this behaviour [34]. As works done by Wu et al. [80] showed that the crystallization of Cu and ZnO particles can be

accelerated by water formation due to methanol production. Due to this loss of productivity, some researchers also suggest a gradual increase in pressure to compensate for the loss of production [36], as temperature increase is not a viable option due to its promoting behavior on catalyst sintering.

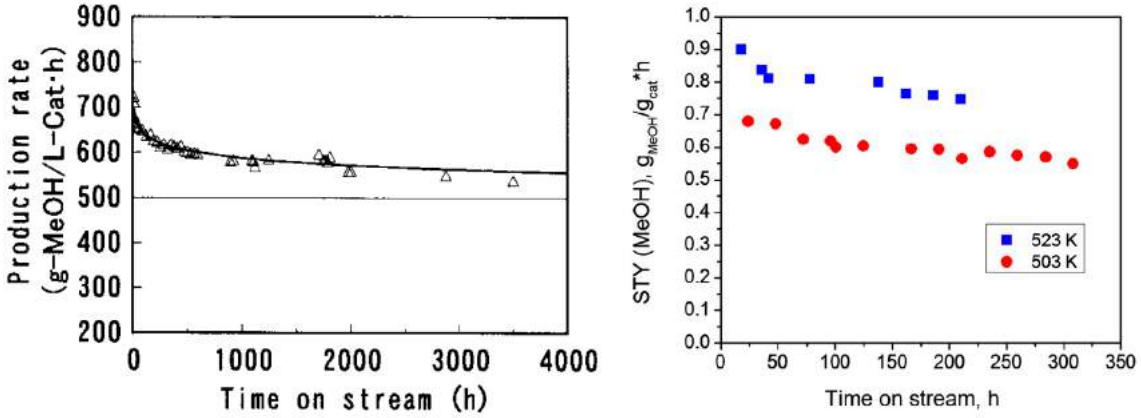

(a) *Production rate of methanol as a function of time. Reaction conditions: 50 Bar, T = 523 K, SV = 10000 h^{-1}, H_2 : CO_2 = 3:1, Cu/ZnO based catalyst [68].*

(b) *Time-on-stream measurements at the following reaction conditions: 30 bar, SV = 37000 h^{-1} and H_2 : CO_2 = 7:2 over the Cu/ZnO/Al_2O_3 catalyst[15]*

Figure 2.17: Effects of long term production on methanol productivity in literature.

2.9. Background of methanol reactor at Zero Emission Fuels BV

This section focuses on outlining the previous works that have been carried out at Zero Emission Fuels (ZEF) in light of the methanol reactor development. Brilman & Bos [10] from University of Twente, were the first to lay down the foundation for a reactor that bypasses the reaction equilibrium via *in-situ* condensation of products while operating under natural convection. The idea was furthered by Roy Lammerink [81] who theorised a possibility for heat integration and autothermal operation. The methanol reactor at ZEF has undergone two developmental stages. Basarkar [16] was the first to adapt this idea to suit the production needs for ZEF. His work was complemented by the modeling and analysis of Gutierrez [82]. Following up on their findings van laake [17] built a new reactor at base case.

2.9.1. Brilman reactor

Brilman and Bos[10], from University of Twente designed a novel reactor in 2015 for converting CO_2 and H_2 to methanol. This reactor uses *in-situ* condensation of methanol/water mixture by having two separate temperature zones for reaction and condensation. Such a design uses natural convection for circulation and obviates the use of external recycle streams. Figure-2.18 shows a design of the reactor used by them. The catalyst is packed in the green region inside an annulus. It is the commercially available Cu/ZnO/Al_2O_3 (CP-488). The feed gas enters from the top inlet and moves to the bottom where it is redirected towards the catalyst bed. The bed is maintained at a constant temperature of 473-533 K using heating jackets. The reaction takes place at the bed and the product vapours move upwards to the condensation zone. They exchange heat with the cooling coils and collect in liquid phase at the vessel, where they are siphoned out at regular intervals. Due to this kind of operation, it is termed Liquid Out Gas In Concept (LOGIC). Consequently, any losses due to the selectivity of the reaction to form CO is rendered irrelevant due to this concept because CO does not leave the reactor in gaseous phase.

They identified CO_2 as a better carbon carrier than CO for direct hydrogenation into methanol. The reason behind this decision comes from a thermodynamic consideration. It can bee seen from equations-2.26,2.25 that the energy required to remove oxygen from water or carbon dioxide is al-

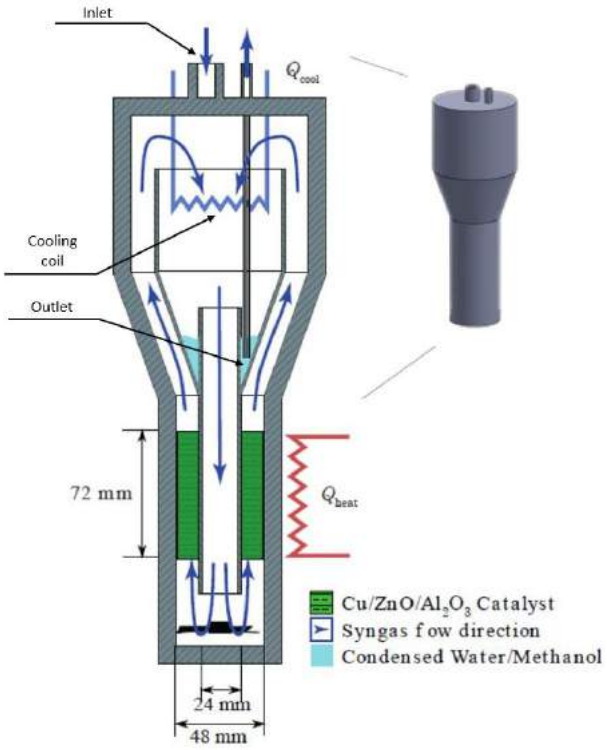

Figure 2.18: Design of reactor proposed by Brilman et al.[10]. The feed enters the reactor through the inlet and passes through the catalyst which is on the tube annulus. The methanol and water mixture is condensed at the top using cooling coils. The products need to be taken out at regular intervals.

most the same. However, technologically speaking, the former can be done much more efficiently by electrolysis. The power consumption at 100% theoretical efficiency is 39.4 kWh/kg of hydrogen. Although, in practice it is somewhat closer to 50-65 kWh/kg [83]. Therefore, given CO_2 as the starting point and a totally thermodynamic point of view, it is better to make more H_2 and go for direct hydrogenation to methanol, rather than converting CO_2 into CO.

$$H_2O \rightleftharpoons H_2 + \frac{1}{2}O_2 \quad \Delta H_{298K} = 286\,kJ/mol \tag{2.25}$$

$$CO_2 \rightleftharpoons CO + \frac{1}{2}O_2 \quad \Delta H_{298K} = 283\,kJ/mol \tag{2.26}$$

The condensation of the products start when the temperature of the condensation zone reaches the dew point temperature. The dew point temperature is the highest temperature at which for a given gas composition and pressure, the fugacity of a component in the vapor phase equals the fugacity of the liquid phase. This means that the gas enters the two phase region from vapor region. Figure-2.19 shows that at high pressure(>100 bar) the dew point temperature is close to the reaction temperature. This may not be suitable as products will start condensing in the reaction zone and pose problems with product extraction. At a pressure of 50 bar, condensation occurs at 403-413 K. This can be achieved by introducing a temperature gradient inside the reactor that will lead to a separate condensation zone.

The formation of such temperature gradients also posits the formation of density gradients. As such, the flow inside the reactor can be buoyancy driven, or simply natural convection. To enhance this even further, the cold section is kept at the top and the hot section is kept at the bottom. The methanol production was observed to be a strong function of condenser temperature. When the temperature of condenser approached 418 K, the production dropped to zero and also the reaction

started reaching its equilibrium concentration as reaction products do not condense. Key takeaways are:

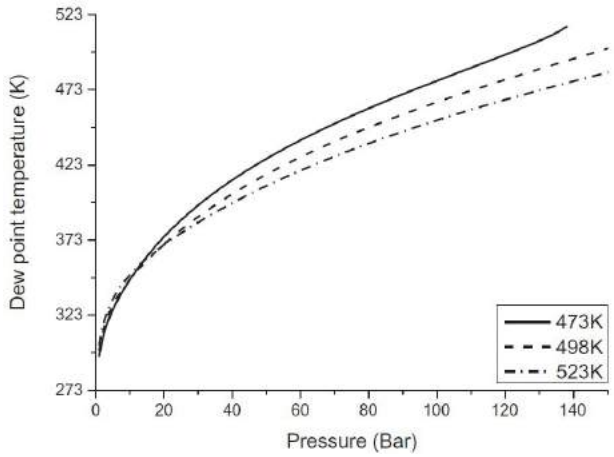

Figure 2.19: Dew point of the product mixture as a function of pressure at different temperatures (473/498/523 K). These are results of solving thermodynamic relations for vapor liquid equilibrium of methanol and water mixture for a $H_2 : CO_2$ feed of 3:1.[10]

- Lower condenser temperatures led to higher methanol yield. Productivity reached 0 for a condenser temperature of 418 K, which is the calculated dew point temperature. The system reached equilibrium composition and reaction stopped.
- 99.5 mol% pure methanol was formed with only trace amounts of ethanol, 1-propanol and formic acid.
- The energy input was reported to be around 66 MJ/Kg of methanol produced, which is 3 times higher than the Higher Heating Value (HHV) value of methanol (22.4 MJ/Kg). These losses can be attributed to the condenser, fan duty and heat loss from the insulation. Such an observation paves way for better design and heat integration.
- The reactor performed equally well with or without the provision of external forced convection suggesting a reactor without the need of moving parts.

2.9.2. TEAM-I, 2017-2018 (MODIFIED BRILMAN REACTOR)

The findings and suggestions laid out by Brilman et.al[10] & Lammerink[81] were followed up by master thesis of Basarkar [16] in 2018 with ZEF BV. The schematic of the reactor is shown in the Figure-2.20. The design changes were attributed to the methanol production target set by ZEF BV of 135 g/day, which was higher than Brilman reactor. The MBR was entirely built from aluminium due to the fact that it has very high thermal diffusivity(97 mm^2/s) and heat conduction is very rapid. A new heat integration system was also used to increase efficiency. Six aluminium blocks can be seen which transfer the heat from hot effluent gases to pre-heat the gases entering the reaction zone. This reduced the energy spent in the reaction zone for heating and also in the condensation zone for cooling as it lowered the temperature of the effluent gases. This was also advantageous for maintaining the temperature gradient between the hot & cold section. Some key findings of Basarkar's work are summarised below:

- Methanol space time yield of 6.76 mmol/g_{cat}/hr was reported at a reaction temperature of 228 $^{\circ}C$, which was identified as the optimum wall temperature. However, this STY was lower than the designed criteria of 18.8 mmol/g_{cat}/hr.

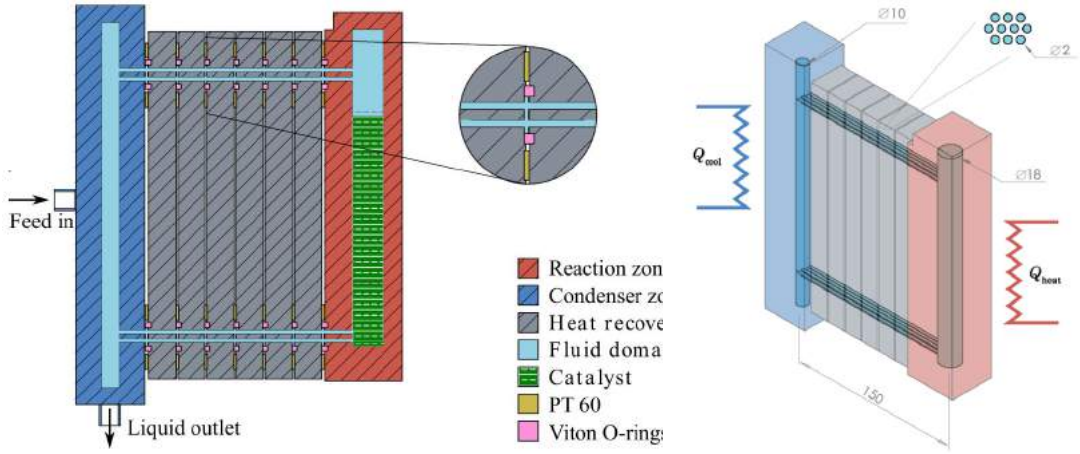

(a) *Cross section of the MBR* (b) *Schematic model of the MBR*

Figure 2.20: Design of Basarkar's methanol reactor(Modified Brilman Reactor)[16]

- Lower condensation temperature were accompanied by higher methanol yield due to better condensation of the products. It also ensured better driving force for the gasses inside the reactor.
- Aluminium was found to be vulnerable to corrosion in an environment that contains water and methanol. Therefore other alternatives such as stainless steel must be looked into.
- The reactor mass should be as low as possible because it is linked with the reactor startup time. A Heavier reactor has higher amount of heat needed to raise its temperature to the reaction conditions. The weight of Basarkar's reactor was close to 5 Kg.
- The inclusion of a heat integration system improved the overall efficiency of the process. The heat duty of the system was 64.8 W after 11.2 W was saved by the heat integration network, leading to an overall efficiency of 44.3% (η_{energy} defined later in section-3.9.6). If there were no heat integration the overall efficiency would have been 41.0%.
- Major part of the heat losses in the reactor were linked to insulation which hampers the autothermal operation. If the heat losses were all mitigated, then autothermal operation could have been achieved by additional 14.6 W of heat. It was suggested that this can be achieved by both improving the heat integration (Heat pipes) or by increasing the mass of catalyst (Exothermic nature of the methanol synthesis reaction).
- Better heat integration corresponds to higher mass flow inside the reactor which is conducive to higher methanol yield.
- Removal of products with manual operation led to excess gas leaks. This should be mitigated by using automated valves and appropriate level sensing mechanisms. It was also seen that the yield strongly depended on the sampling time.
- Crushing the catalyst pellets reduced the porosity of the bed to such an extent that buoyancy forces were insignificant to cause a convective flow. As such the pressure drop across the bed became too high and mass flow approached zero along with the methanol yield.
- All the thermocouples used in the reactor measured the surface temperature of aluminium block and not the actual gas temperature inside the reactor. Therefore, some mechanism needs to be designed which can withstand 50 bar while at the same time be isolated from the body of the reactor, so as to facilitate the placement of a thermocouple.

2.9.3. TEAM-III, 2018-2019

During Basarkar's work with the MBR, another idea of using heat pipes for better heat integration was developed at ZEF BV which culminated into the work of van Laake [17]. The reactor was built using Tri-Clamp standard parts which are made up of stainless steel and designed to withstand high pressures(failure pressure of 100 bar). It also made the design completely modular as seen in figure-2.21. The pipe diameter was chosen as 35 mm and the catalyst pellets had a diameter of 5 mm(Instead of 6 mm for MBR). Consequently, the bed to catalyst diameter ratio, d_t/d_p was 5.8(instead of 3.6 in case of MBR). The length of the bed was 100 mm leading to a L/d_p ratio of 20, which ensured near plug flow as it is greater than 10. Effects of tilting the reactor were also studied experimentally in van Laake's work after modelling and simulations done by Gutierrez [82] suggested that it can have a negative impact on the flow rate inside the reactor due to decreased natural circulation. Key takeaways are:

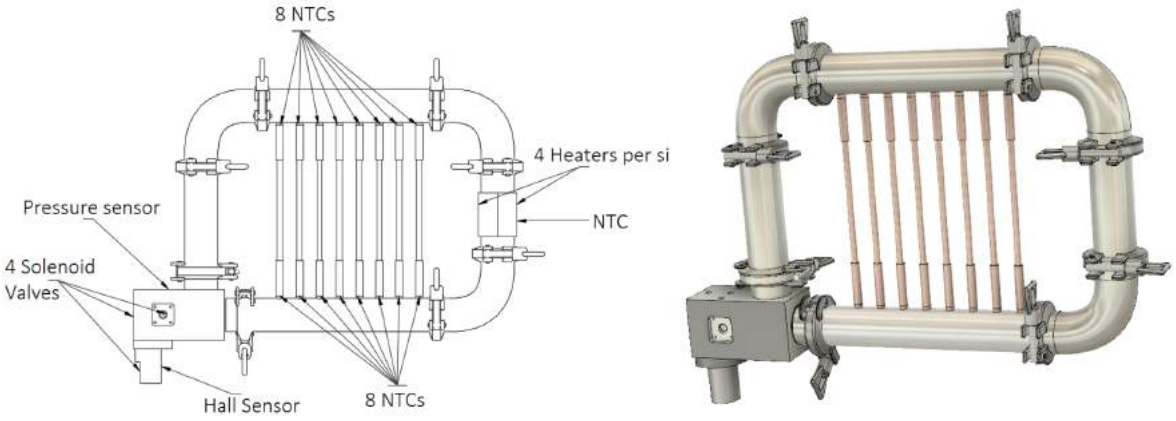

(a) *Schematic of van Laake's methanol reactor.* (b) *3D Fusion model of van Laake's reactor.*

Figure 2.21: van laake's Methanol reactor[17]

- Space Time Yield (STY) was seen to improve with the tilting angle. It was 2.61 mmol/g_{cat}/hr at 0° tilt, 3.21 mmol/g_{cat}/hr at 10° tilt and 4.10 mmol/g_{cat}/hr at 20° tilt. However, this was lower than the STY of Basarkar (6.4 mmol/g_{cat}/hr) due to non homogeneous heating of the reacting gases at the walls and at the center of reactor tube.

- Tilting the reactor had a negative impact on the mass flow rate inside the reactor which is strongly correlated to other performance indexes such as STY, overall energy efficiency, heater duty & reactor outlet temperature. Respectively, the STY increased; Energy efficiency increased; heater duty decreased and reactor bed outlet temperature increased due to tilting. Therefore, it showed that high mass flow rate was limiting the reactor performance and tilting had a positive impact overall.

- The heat exchanger performance was higher than Basarkar's reactor. The heat integration duty was seen to increase from 11.2 W to 62 W.

- The mass flow rate increased significantly as compared to the Modified Brilman Reactor (MBR). This was attributed to the increased reactor dimensions. Basarkar [16] had high pressure drop across the bed due to smaller channels. This was not the case with van Laake's reactor and high natural circulation was seen even though the temperature gradient from reactor bed to condenser was almost the same.

2.9.4. Overview of modifications in the current reactor

Based on the research questions posed for this thesis as well as the suggestions given by earlier works at ZEF, the following improvements were made in the reactor:

- **Automated Liquid sluicing:** A level sensor was implemented that facilitated automatic liquid removal, thereby significantly lowering feed gas loss due to sluicing. Such a system also helps in accurately tracking the production by making the sampling time and volume uniform. Every sluicing operation is very accurately logged and can be used to correlate changes in the temperature data.
- **New heat integration network:** In the previous reactor version 8×200 mm heat pipes were used. In the current setup 16×(2×150 mm) heat pipes have been used.
- **Gas flow temperature sensors:** Two sensors were implemented to measure the actual gas flow temperature before and after the catalyst bed. Earlier, the same was done by measuring wall temperature instead, which does not reveal the true gas temperature [84]. The reaction temperature is always lower than the bed temperature. True gas temperatures also help in calculating mass flow rate effectively.

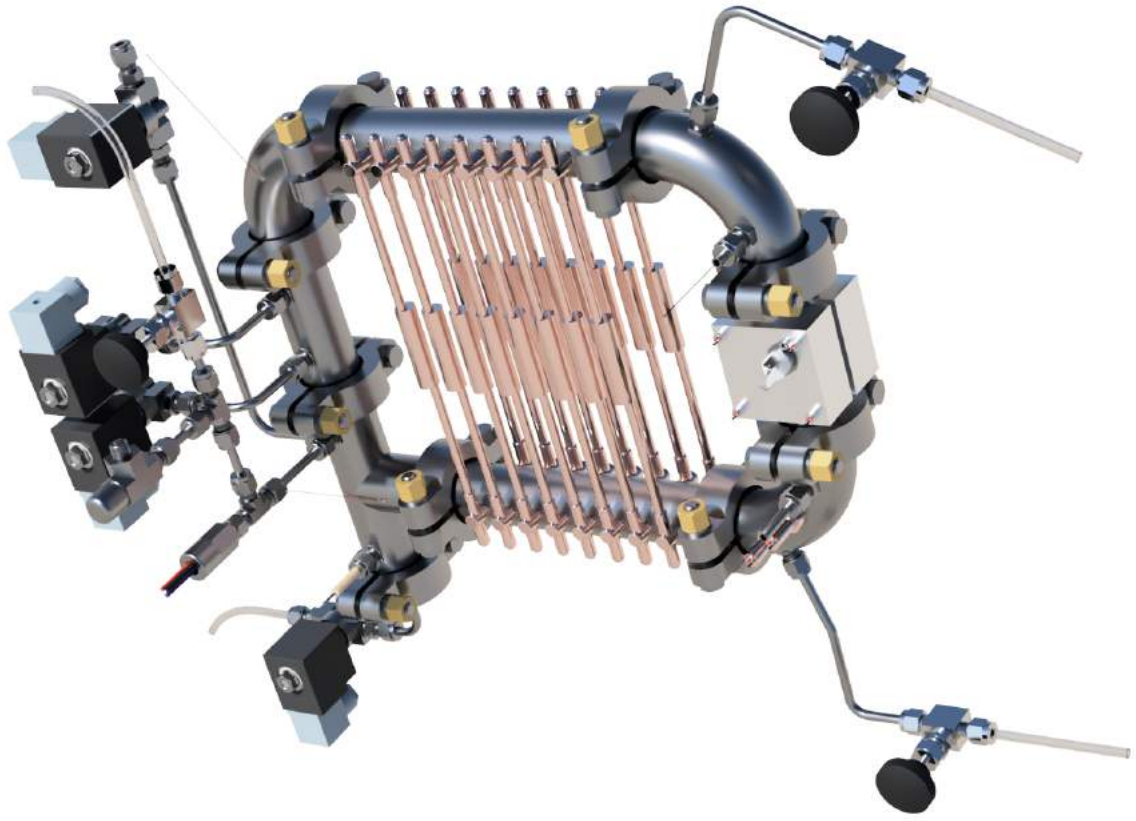

Figure 2.22: A 3D model of the current reactor design made in Fusion 360

- **Gas flow valves:** Four valves were implemented to regulate the mass flow in and out of the reactor. Earlier, this was done by connecting the cylinder to the reactor and leave it opened continuously. As a result the pressure response was a straight line. The use of valves allows the current reactor to exploit the pressure sensor feedback loop and obtain pressure decline response of the reactor, while in operation. The pressure decline data can be used therefore, to get information about the production rate and kinetics.

- **Customized feed gas compositions:** Separate inlet valves allow the use of separate gas cylinders to change the composition inside the reactor. Pure H_2 and CO_2 cylinders were used to get the reactor performance data at different compositions.
- **Reactant heater section:** In order to heat the gases up to the reaction temperature before entering the catalyst bed, four heaters were implemented in the Tri-Clamp pipe before it. In earlier works, only the catalyst bed was heated. Due to this the reactant gases could not attain the reaction temperature and therefore, rendered the catalyst bed partially inactive.
- **Improved Data acquisition:** Various changes were made in the electrical circuit to improve the quality of data obtained from the reactor. This includes two dedicated Printed Circuit Boards that segregate the sensitive electric circuit from heavy current circuits. Voltage regulation circuits were also added to reduce the temperature sensor noise. Valves and heaters were automated with the PCB controller.

A 3D model of the current reactor design is shown in figure-2.22. All the above mentioned modifications are discussed and explained in detail in the following chapter.

3

EXPERIMENTAL SETUP DEVELOPMENT & TESTING METHODOLOGY

"You must realize that knowing how to think, empowers you far beyond those who only know what to think. The thought process is far more important than the answer."
-Neil deGrasse Tyson-

This chapter focuses on describing the test setup that is under study for this thesis. Several changes have been made to the reactor as compared to its predecessor, van Laake, 2019 [17]. These changes are mostly attributed to the research questions posed for this thesis, which warranted a better control over the feed composition, temperature & pressure and overall reliability of the sensor data. All these modifications are addressed in the upcoming sections.

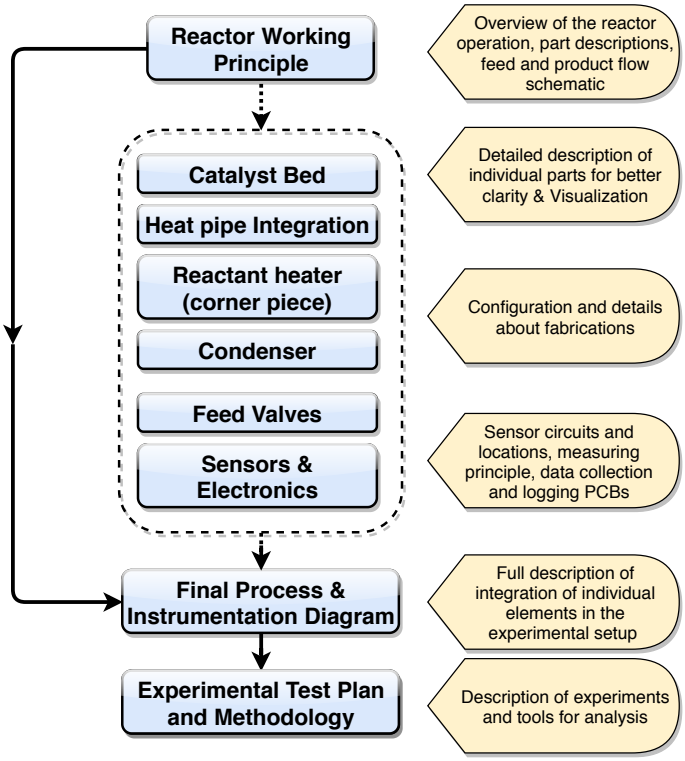

Figure 3.1: Chapter Structure

3.1. Reactor Working Principle

A 3D model of the current Methanol Synthesis reactor (MSR) was introduced in the previous chapter and a brief schematic of the same is shown in Figure-3.2. The dashed lines denote different blocks of the reactor which are addressed separately in sections that follow.

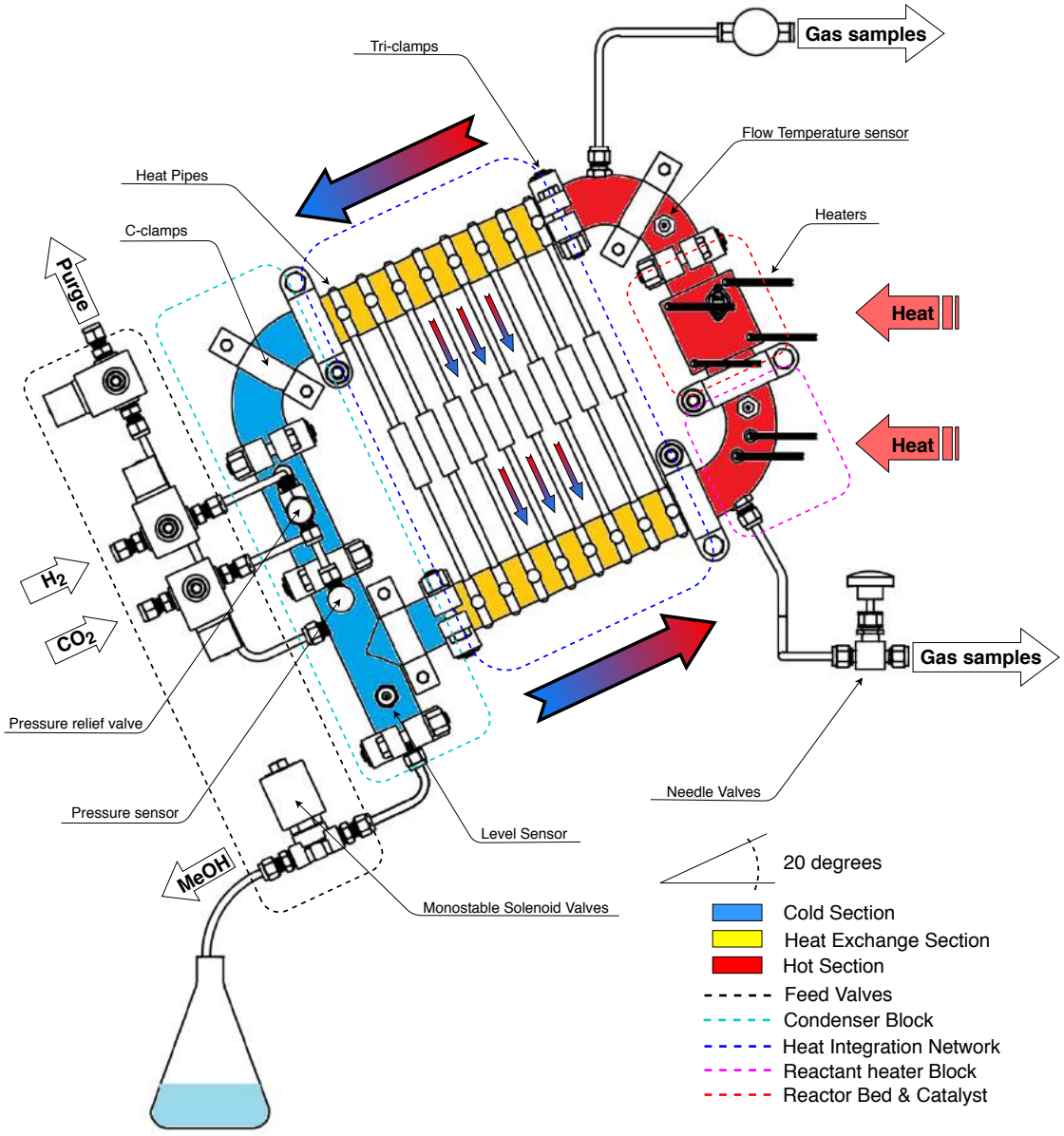

Figure 3.2: Schematic of the current reactor design

It can be seen that there are three zones in the reactor piping. Condensation zone or cold section(marked blue), reaction zone or hot section(marked red) & the heat exchange zone(marked yellow). The feed gases, H_2 & CO_2 enter the reactor at the cold section. As the reactor heats up, the gas in the hot section becomes hotter than the rest of the gas in the reactor and starts to rise upwards. The negative pressure gradient induced, causes the cold gas to flow from the cold section and fill up the hot section. This gives rise to a natural circulation inside the reactor. The rising hot gases pass through a packed bed of catalyst which is kept at the reaction temperature (210 °C). When the gas temperature also approaches the reaction temperature, then methanol and water are formed as reaction products. The reactor outlet gas stream containing mainly reactants but also products

of methanol synthesis reaction goes through the heat exchange section. Here it exchanges heat with the copper mesh attached to the heat pipes and becomes cooler after passing through subsequent heat pipes. The temperature of methanol and H_2O mixture becomes lower than the dew point temperature as it reaches the cold section, causing it to condense and form droplets. These droplets move downwards in the condenser due to gravity and collect at the bottom cap. When a fixed amount of condensate is collected, it is sensed by the level sensor and sluiced out through the extraction valve. There is a purge valve too in the system which is used to remove gases during startup, shutdown & catalyst activation. During reactor operation the purge valve is not used. It can also be seen that needle valves are provided before & after the reactor bed, to extract gas samples and analyse using gas chromatography.

3.2. Reactor Bed & Catalyst

The reactor bed used in the current study is what is called a fixed bed reactor because the pellets do not move during the reactor operation. The design of such packed beds is governed by structure of the packing matrix which includes the shape, dimensions & surface properties of both catalyst as well as container, and also the loading. Generally in industrial applications, such a decision is made by a trade off between conflicting and competing attributes. Such as active surface area per unit volume, void fraction, transport coefficients and structural strength (which are expected to be high). When these attributes are improved by making the pellet size smaller, other attributes such as pressure drop, cost and ease of manufacturing, suffer from it (which are expected to be low).

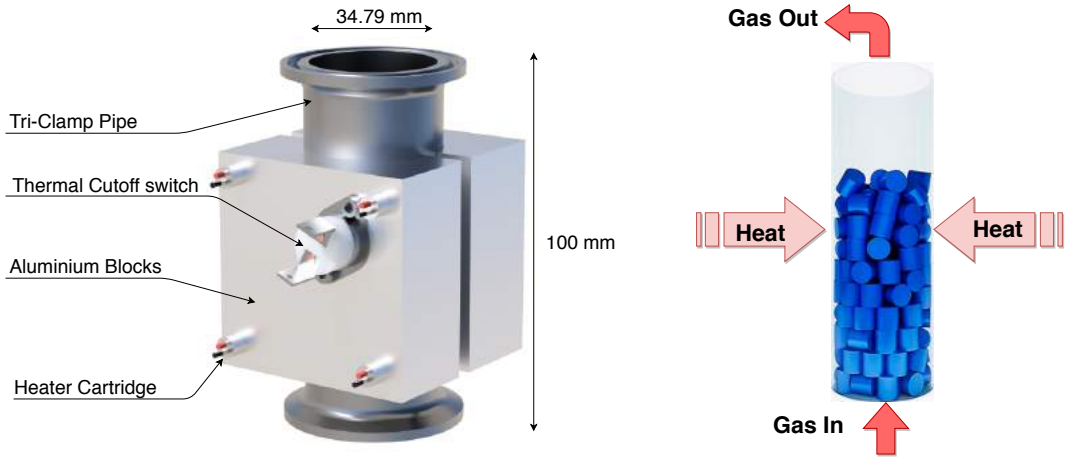

(a) 3D design of catalyst bed

(b) Random Catalyst Packing. [85]

Figure 3.3: Description of Reactor bed

The catalyst used in this reactor was HUC-98 ($Cu/ZnO/Al_2O_3$ in an undisclosed composition[1]) which was sourced from Hutong Global Co. in China. It is in the shape of a cylinder that has 5 mm diameter and 4 mm height, because for a given volume, cylindrical particles provide more surface area than their spherical counterparts. Aspect ratio of catalyst pellets (h_p/d_p) is 0.8, which is in the recommended range between 0.7 to 1.3 [86]. For tubular fixed bed reactors it is advised that the tube to catalyst pellet diameter (d_t/d_p) be kept between 5 to 10 (7 for this case). For plants that have higher production rates it is also not uncommon to use values up to 25. However, it must be noted that, values lower than 5 indicate that the catalyst pellet size is disproportionate to the tube diameter that leads to high mean bed voidage(ϵ). The pressure drop across the bed is a strong function of voidage, roughly proportional to ϵ^{-3} (Ergun's Equation). As such, there can be non homogeneous voids in the bed, that may lead to non uniform flow distribution across the bed. Pressure drop and

[1] CuO(>56%), ZnO(>21%), Al_2O_3(>8%)

production rate seems to be the two opposing and yet deciding factors for the loading consideration. Figure-3.3b, is taken from Moghaddam et.al.[85] on the effect of heterogeneities in randomly packed catalyst beds. It is not up to scale with the current reactor under study, but does depict very well the kind of random packing that is employed in it.

The catalyst needs to be reduced before methanol synthesis which is essentially the conversion of cupric oxide (CuO) into metallic copper. It is a strongly exothermic reaction which is is needed for catalyst activation (equation-3.1).

$$CuO + H_2 \longrightarrow Cu + H_2O \qquad \Delta H_{298K} = -86.7\,KJ/mol \tag{3.1}$$

Since the reactor bed and catalyst pellets are small in dimensions, aspects such as pellet charging and bed shrinkage due to settling, need not be considered.

3.3. Heat Integration network

The reaction and condensation sections of the reactor are separated by the heat integration section which provides the necessary temperature gradient between them. Heat pipes as a transfer medium is pivotal to this operation. The conductivity k of a heat pipe ranges from 10^2 to 10^3 orders of magnitude higher than ordinary conductive metals such as aluminium or copper[87]. Contrary to intuition, conduction through outside copper wall is not the dominant heat transfer mode for a heat pipe. Infact, it is the latent heat of vaporization of the working fluid.

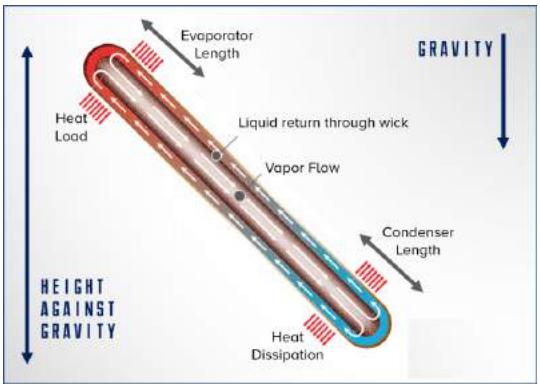

(a) *Working principle of a heat pipe[88].*

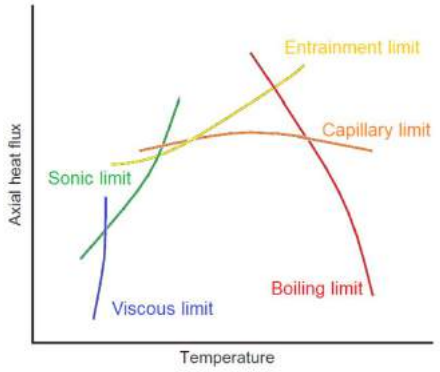

(b) *Variuos limitations with heat pipe design [17].*

Figure 3.4: Heat pipe working and design limitations.

It consists of a hollow copper tube with a working fluid at very low pressure, almost near vacuum. The working fluid is decided by operation temperatures, which can range from a staggering 30 K to 2000 K. The inner walls of the tube is lined with a Wick material [88]. Figure-3.4a depicts the working principle of a heat pipe. The hot end absorbs the heat and the transfers it to the working fluid. This heat is used to evaporate the working fluid and form vapor. Due to the low pressure inside the heat pipe, the boiling point of the working fluid is lowered. The mobile vapor phase travels through the heat pipe due to natural convection, towards the cold end. It releases the heat there and condenses back to liquid phase. This liquid is then returned to the hot end by Wick action. There are a lot of factors that determine the choice of working fluid. But as a rule, the operating temperature must be between the freezing point and the critical point of the working fluid. Apart from these, there are other limitations (figure-3.4b. For example, if the temperature gradient is too low, then the gradient in vapor pressure across the heat pipe may not be able to overcome the viscous forces, thereby preventing any flow (viscous limit). At a slightly higher temperature and heat flux, the vapor density may become too low and the speed of vapor may exceed the speed of sound creating a shock wave that blocks the flow (sonic limit). At even higher heat fluxes, this vapor speed may not cause shock

waves, but cause enough shear stress at the vapor-liquid interface, so as to draw the liquid back to the condenser (entrainment limit). Towards the top boundary of operating temperatures gradients, it may cause nucleate boiling of the liquid which gets trapped in the wick structure, preventing any liquid from replenishing. The result is an evaporator dryout (boiling limit). These limitations have been thoroughly evaluated in the master's thesis of van Laake [17]. It was observed that for the current choice of heat pipe and working fluid, capillary limitation is the most dominant among others. This is due to low surface tension at high temperatures and gravity (vertically aligned heat pipes).

Figure-3.5 shows a 3D rendered model of the heat integration section used in the reactor that is under study for this thesis. A total of 32 heat pipes (150 mm) were used that were compounded into 16 units (Right side figure-3.5) using a copper cylinder block at the center. The heat pipes are hollow copper vessels with sintered wick and water as the working fluid. As discussed earlier, the working fluid in a heat pipe is replenished at the hot end via Wick action. But gravity poses hindrance for the capillary forces which are required for it. The copper cylindrical blocks serve to mitigate this by providing an intermediate heat sink for the top side heat pipe and a heat source for the bottom side heat pipes. This is analogous to using stairs between two pedestals at different height in order to bridge the gradient between them over a single step. The method to estimate the heat flow through the heat pipes is discussed in detail in the methodology section (section-3.9.5).

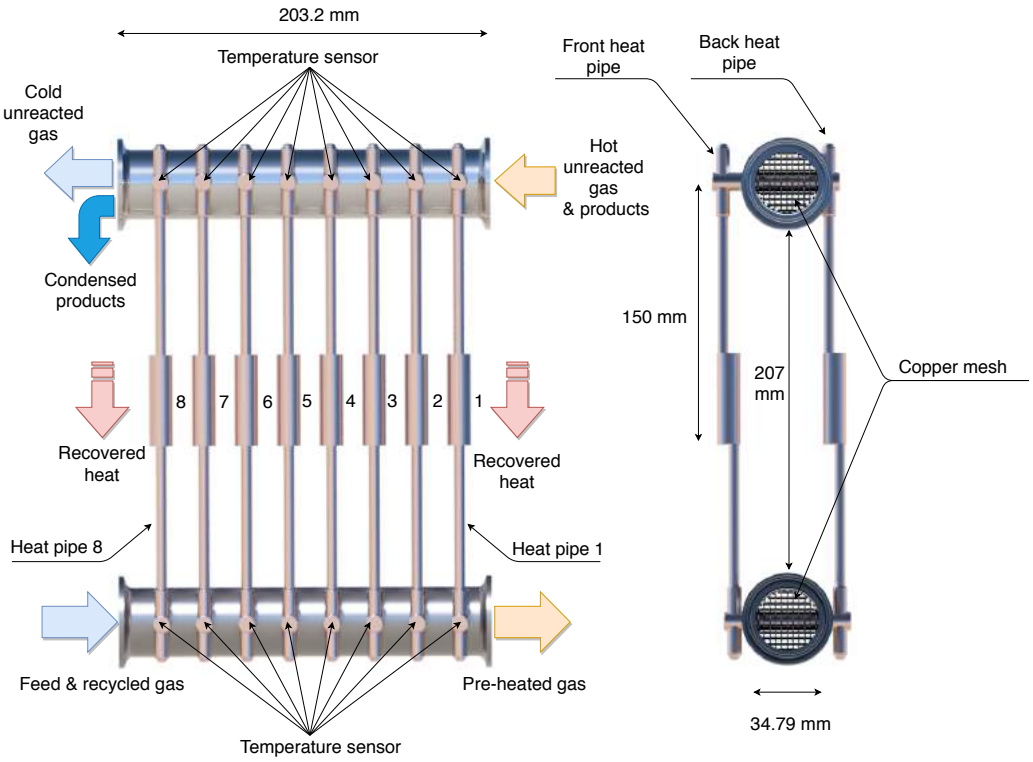

Figure 3.5: 3D render of the heat integration section of the reactor

3.4. Reactant heater block (Corner-piece)

Even though the catalyst bed is maintained above the reaction temperature (473 K), the temperature of the gas entering the bed is not high enough. As a result, a portion of the catalyst bed is always inactive, till the gas temperature is raised to reaction temperature. To circumvent this problem, a reactant heater block (or corner-piece) was placed before the catalyst bed.

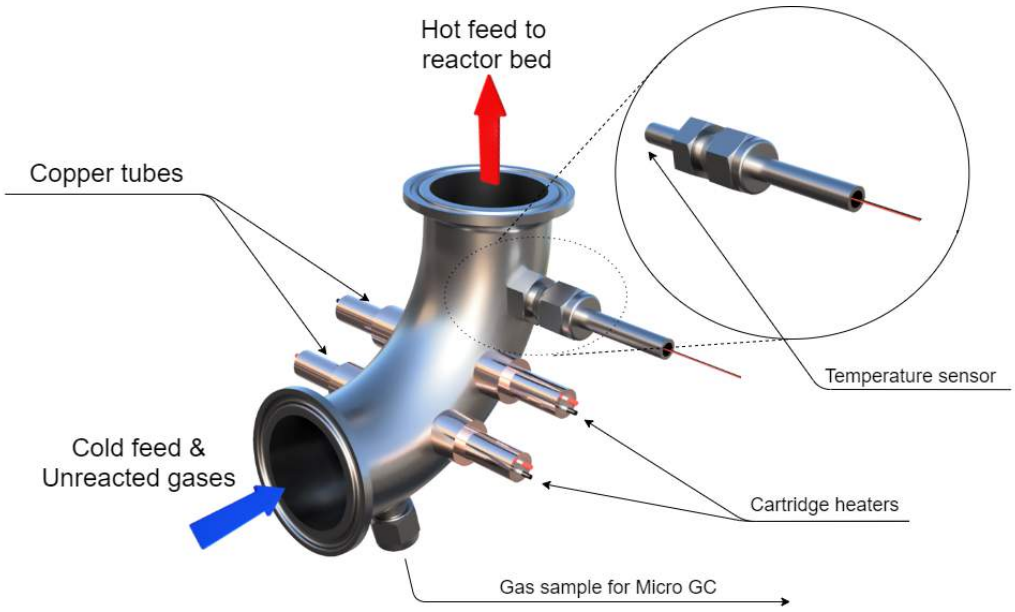

Figure 3.6: CAD model of the reactant heater block (Corner-piece).

Figure- 3.6 shows a model of the same. The pre-heated gas from the bottom heat exchanger section enters the corner-piece where it passes through a copper mesh that is heated using 4 Cartridge heaters (40 W each), raising its temperature. The heater cartridges are inserted in a copper tube that is welded to the Tri-clamp pipe. The temperature set-point for the heaters is monitored using two temperature sensors on the copper tubes on the outside. The exact temperature of the gas stream is measured using a temperature sensor placed at the center of the Tri-clamp pipe using an in-house built thermal well. The temperature sensor circuit must not come in contact with the body of the reactor. This is very important as the temperature sensor has Negative Temperature Coefficient (NTC), and measures the temperature by calibrating change in resistance. Therefore, it should be isolated enough such that the resistance of the body of reactor must not be in the circuit. A provision was also made at the bottom to extract gas sample for the Gas Chromatograph (GC), and ascertain the inlet gas compositions.

3.5. Condenser block

The condenser block of methanol synthesis reactor is pivotal to this thesis and answering its research questions. It contains the two Inlet valves (Feed) and two outlet valves (Products & Purge) that automate the reactor as seen in figure- 3.7. The unreacted gases and the products of methanol synthesis reaction enter the condenser block through the top elbow. Due to the heat exchange with heat pipes, the temperature is already lowered. Methanol and water begin to condense on the inside walls of the condenser section and travel downwards due to gravity to collect at the bottom cap. Unreacted gases, fresh feed and uncondensed methanol with water which are still in gaseous phase move out of the condenser block towards reactor bed for another pass. The amount of collected methanol and water is sensed by a level sensor and extracted out periodically from the reactor in an erlenmeyer. Therefore, only liquid products leaves the reactor as mentioned earlier (LOGIC).

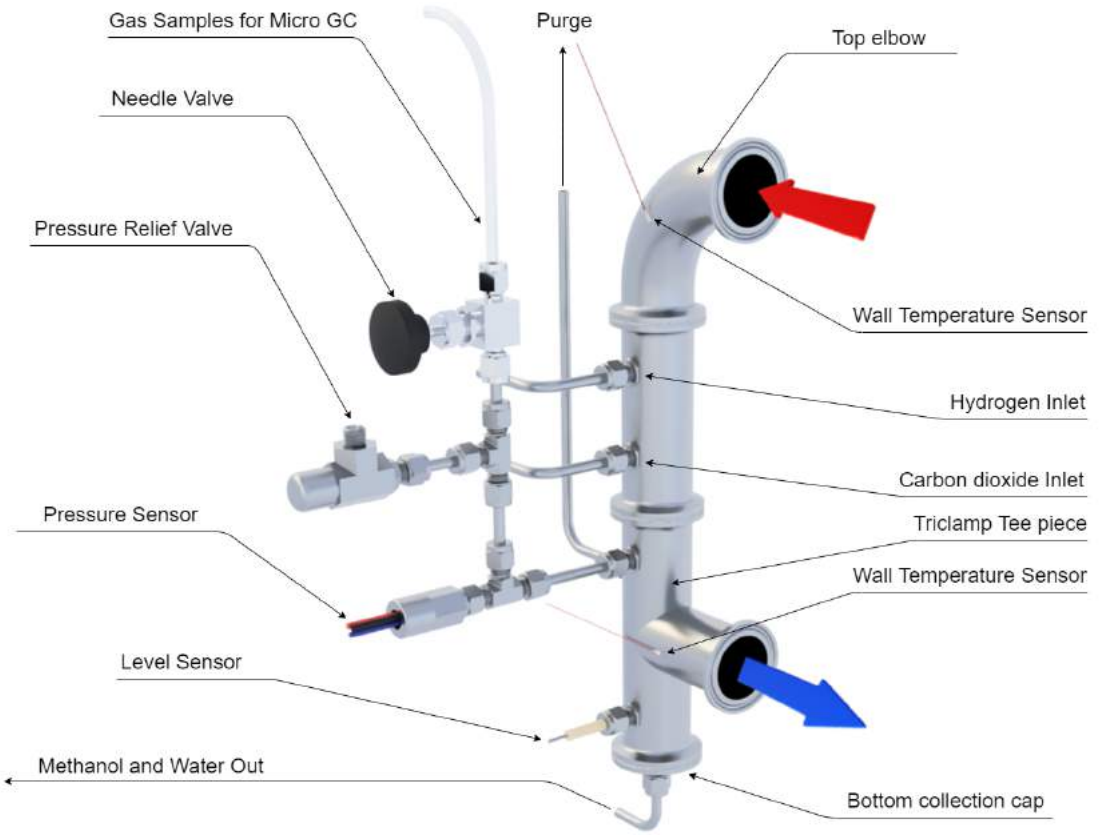

Figure 3.7: The Condenser block used in the methanol synthesis reactor

It is very important for the reactor operation, to circulate the gases inside by natural convection without the need of external power to drive the flow. Therefore, the wall temperature of the condenser needs to be monitored rigorously. To that end, two temperature sensors were placed; 1 at the top elbow bend and another at the Tee-piece. These sensors provide the data for top and bottom condenser temperature. For some experiments, an external fan was also used to lower the top condenser temperature and observe its effects. The dew point temperature calculations also mandate that the condenser temperature be maintained below 413 K (140 °C) for condensation to occur at 50 bar.

3.6. Feed valve block

Four Normally closed solenoid valves sourced from JP Fluid Control were used to regulate the reactor. Anything that goes in or comes out of the reactor was controlled by these valves. If the high pressure side and the low pressure side of the valve are appropriately connected it can withstand pressures upto 75 bar. Each valve has a flow area[2] of 0.79 mm^2. Inside the stainless steel housing seen in figure-3.8, there is a plunger that always keeps the passage closed using a spring. When a 12 V DC supply is given, it energises the solenoid coil which pulls the plunger and opens the passage. Two H-bridges connected to Arduino Nano, controlled the supply of these four valves. Due to this the valves can open can close with an accuracy of 30 milliseconds. Using different opening times for these valves that are connected to separate CO_2 and H_2 cylinders, it is possible to create different gas compositions inside the reactor.

[2]Passage width of 1 mm.

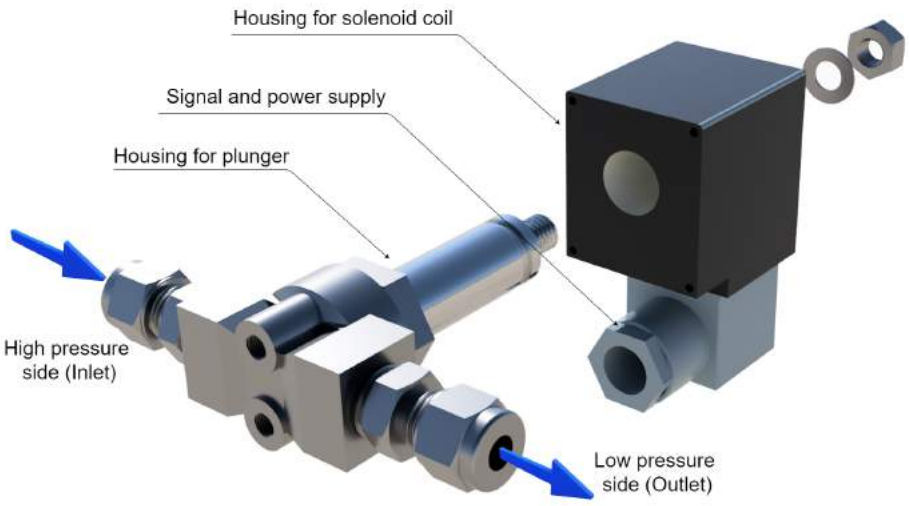

Figure 3.8: The mono-stable valves used in the methanol synthesis reactor

3.7. Sensors and Electronics

A vast multitude of sensors have been used in the reactor to accumulate data for further analysis. These include temperature sensors, pressure sensors and level sensor. Apart from these, several other electronic devices have also been used for varied purposes such as heaters, relays and H-bridges that play a pivotal role in controlling the reactor. These elements have been discussed further now.

3.7.1. Level sensor

"A conducting material that is fabricated near the liquid collection cap in such a way that it is isolated from the reactor body, can be given a known voltage supply and be used to detect liquid level as it conducts after a certain liquid buildup. When used against a resistor that is comparable to the resistance of the reactor body, it can even be used to get continuous liquid level data."

As pointed out by the previous works of both Basarkar [16] & Van Laake [17], automated product extraction is very important for accurate data regarding the reactor yield. They both faced problems with determining the optimum sampling time. Therefore, the aforementioned accuracy is improved due to a better accounting of the sluicing time during methanol production. Manual liquid sluicing valve operation always purges a lot of feed gas along with the liquid. Repetitive extraction from 50 Bar to ambient pressure also damages the valve after some time and leads to permanent leaks. Since the reactor is designed in keeping with the LOGIC concept, any reactor effluent in the gaseous phase must be avoided. If not, then it affects the carbon conversion calculations. This is because, any methanol output is assumed to be formed by consuming equal moles of CO_2 from the gas cylinders. However, if there are significant leaks or loses, then the conversion expressed by it becomes misleading. Based on the aforementioned suggestions, a level sensor was built and tested for the current methanol synthesis reactor.

As seen in figure-3.9, it comprises of a stainless steel nail that is jammed tightly by an interference fit into a hollow PEEK (Polyether ether ketone) cylinder. The outer diameter of the PEEK cylinder was kept 6 mm which is the standard for Swagelok type connection. The Swagelok connection provides the necessary integrity for handling high pressure while the PEEK material provides insulation of the nail against the metallic body of the reactor. A 5V supply is given on regular in-

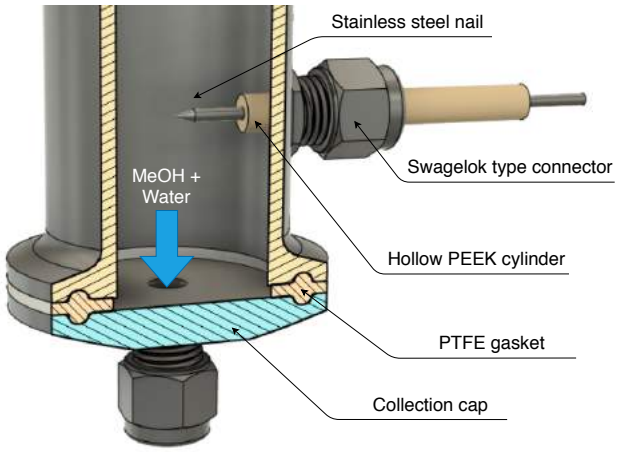

Figure 3.9: Section view of the level sensor assembly used in the reactor.

tervals to the nail from the micro-controller while the reactor body is grounded (see figure-3.10a). When there is not enough product condensate in the pipe, the circuit is incomplete. All the voltage drop occurs across the resistors and is measured by the analog output signal. As the condensate touches the pin, the circuit gets complete and the voltage drop gets divided between resistors and reactor body. A signal is created (sharp dip) which is logged against time by the controller (red line). Since, the controller only sets the supply high to 5 V while measuring for a fraction of second, and later turns it to low, there is very little risk of water electrolysis. Moreover, when the contact between the liquid phase and pin is established, the resistors bear a higher percentage voltage drop than the pin. In earlier experiments on the reactor, it was reported that 5-10 Bar pressure drop occurs due to liquid extraction. Figure-3.10a shows the level sensor in operation. It can be seen that the same pressure drop due to extraction was reduced to 0.4 Bar.

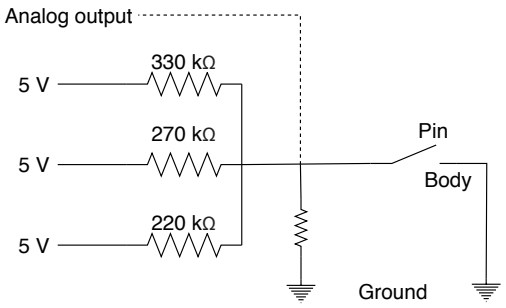

(a) *Electronic circuit for level sensor*

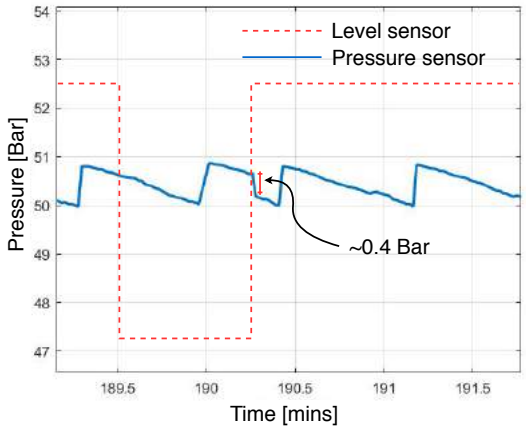

(b) *Pressure response of the reactor to methanol extraction.*

Figure 3.10: Circuit diagram and effectiveness of the level sensor assembly

3.7.2. Temperature Sensors

"Materials with Negative Temperature Coefficient show a decrease in resistance with rise of temperature. The voltage drop across such variable resistance can be calibrated against a known resistance and applied voltage to determine the temperature to which it is exposed."

A total of 24 temperature sensors were installed to monitor the reactor. Their location and number

is depicted in figure-3.12. Most of the NTCs are attached to the wall using PTFE tape. But, in order to measure the temperature of the gas flow closely, two thermal wells were constructed at the inlet and outlet of the bed.

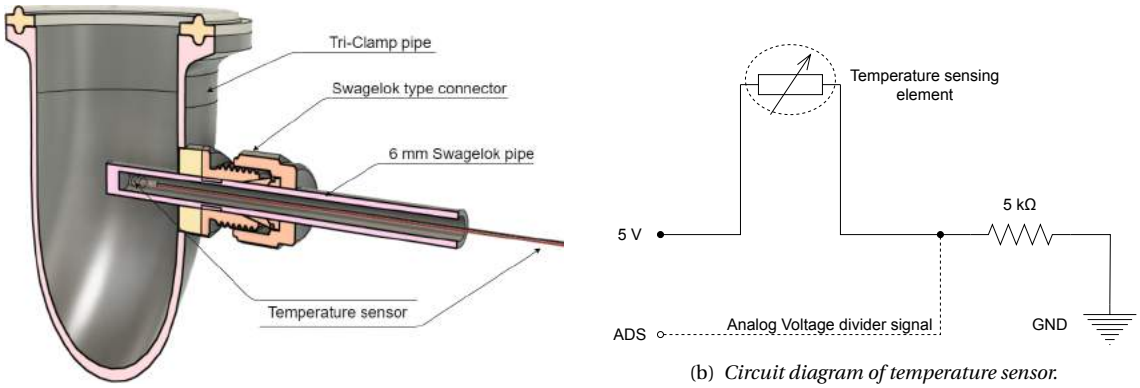

(a) design of thermal well used to measure gas temperatures.

(b) *Circuit diagram of temperature sensor.*

Figure 3.11: Design and Circuit diagram of temperature sensor assembly

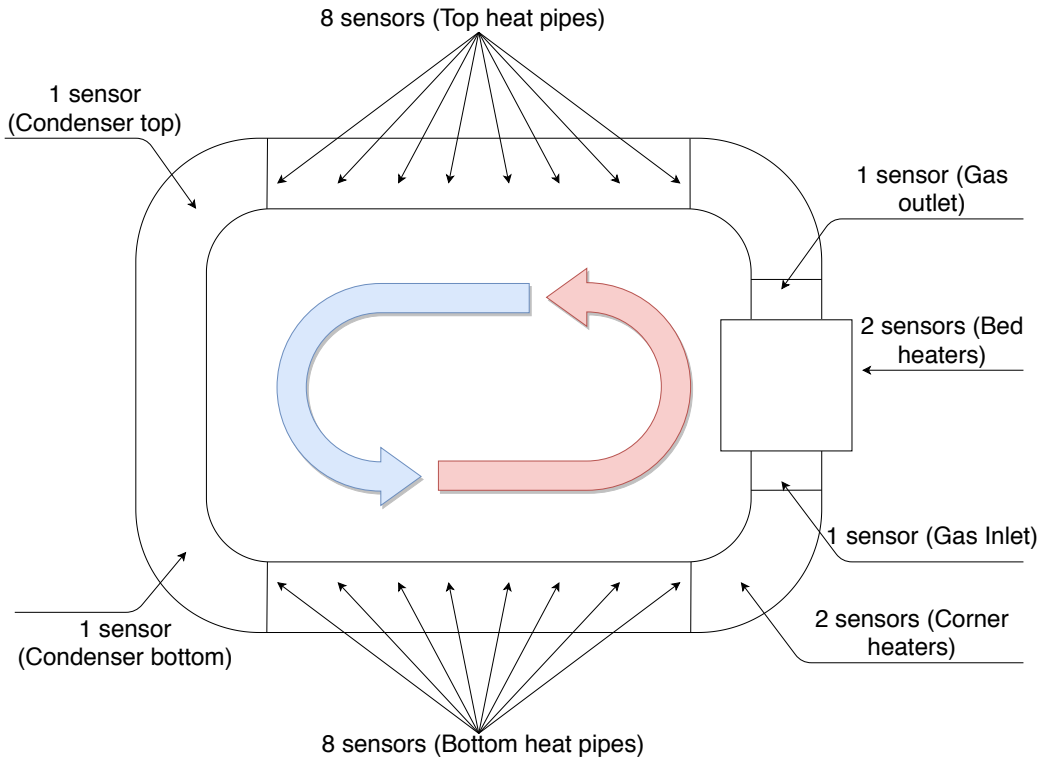

Figure 3.12: Schematic depicting the location and number of temperature sensors.

The design of the thermal well can be seen in figure-3.11a. A Swagelok pipe with outer diameter of 6 mm was inserted in the Tri-clamp pipe with one end open and other welded shut. The inner diameter of the pipe was drilled to 4 mm, leaving 1 mm wall thickness. A temperature sensor was inserted from the open end touching the closed end creating a thermal well. Once the outer surface was properly insulated using PTFE tape (Polytetrafluoroethylene), the sensor was able to measure the exact gas flow temperature. A very interesting validation of the gas flow temperature sensor accuracy is presented in Appendix-C. Prior to this design, two other techniques were also attempted

but were unsuccessful. They can be seen in Appendix-B. Picking up from the flaws of the previous designs, the current method was used.

3.7.3. Pressure sensor & reactor safety

A pressure sensor (ADZ-SML-37.0) with an operating range of -1 to 50 Bar and accuracy of ± 0.01 Bar was used to continuously monitor the pressure inside the reactor. The pressure feedback from the sensor is necessary for the control system to actuate the valves and replenish the feed gas. A validation of pressure sensor data accuracy can be seen in Appendix-C.

3.7.4. Printed Circuit Boards (PCBs)

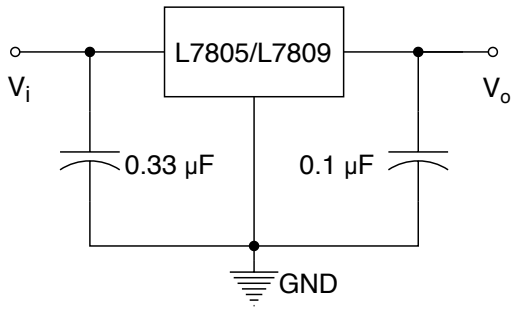

Figure 3.13: Circuit diagram for the Voltage regulator and low pass filter circuit.

If the connection of the above mentioned array of sensors is done via breadboard, it may lead to situations, which are hard to troubleshoot with so many wires. Each heater draws around 5 A current while in operation. Loops of wires drawing high currents in short period of time also causes interference with the sensor signals. It was observed with the help of an oscilloscope that heater operation affects the temperature reading by $\pm 5°C$, making the signal extremely noisy. Minor perturbations in the grid frequency also causes instability in the sensor signal. To avoid any hassles further down the line, two separate circuit boards were designed for the purpose of this thesis. These circuit boards

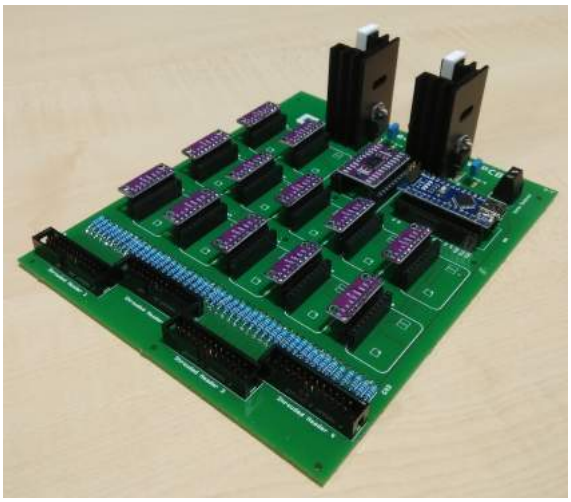

(a) *Fabricated Data PCB.*

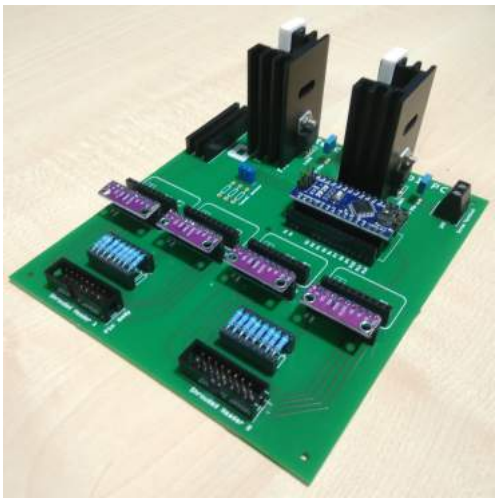

(b) *Fabricated Control PCB*

Figure 3.14: The control Board used in the methanol reactor

have upstream voltage regulator(L7809 & L7805) and low pass filters that prevent other components downstream from high frequency interference, while supplying stable power for sensor operation. They also have an on board Arduino Nano which is the controller for the PCB. The L7809 is used to

provide stable supply to the Arduino Nano (9 V), while the L7805 is used to power the sensor circuit (5 V). The circuit diagram for the same is given in figure-3.13.

The Control Board (figure-3.14b) houses all the important sensors that are pivotal to the control of reactor operation parameters. It reads the temperature sensors at the heater locations and regulates the heater power input by controlling the relays. Apart from that, it also reads the pressure sensor which provides the feedback that is necessary for pressure stabilization inside the reactor. All 4 solenoid valves are also connected to the control board. On the other hand all temperature sensors from the top and bottom heat pipes are connected to the Data Board (see figure-3.14a). A detailed circuit diagram can be seen in Appendix-D.

3.8. Final Process and Instrumentation Diagram

All the necessary schematics and design changes for the new reactor has already been discussed in the previous sections. The final process and instrumentation diagram for the entire experimental setup is presented in figure-3.15.

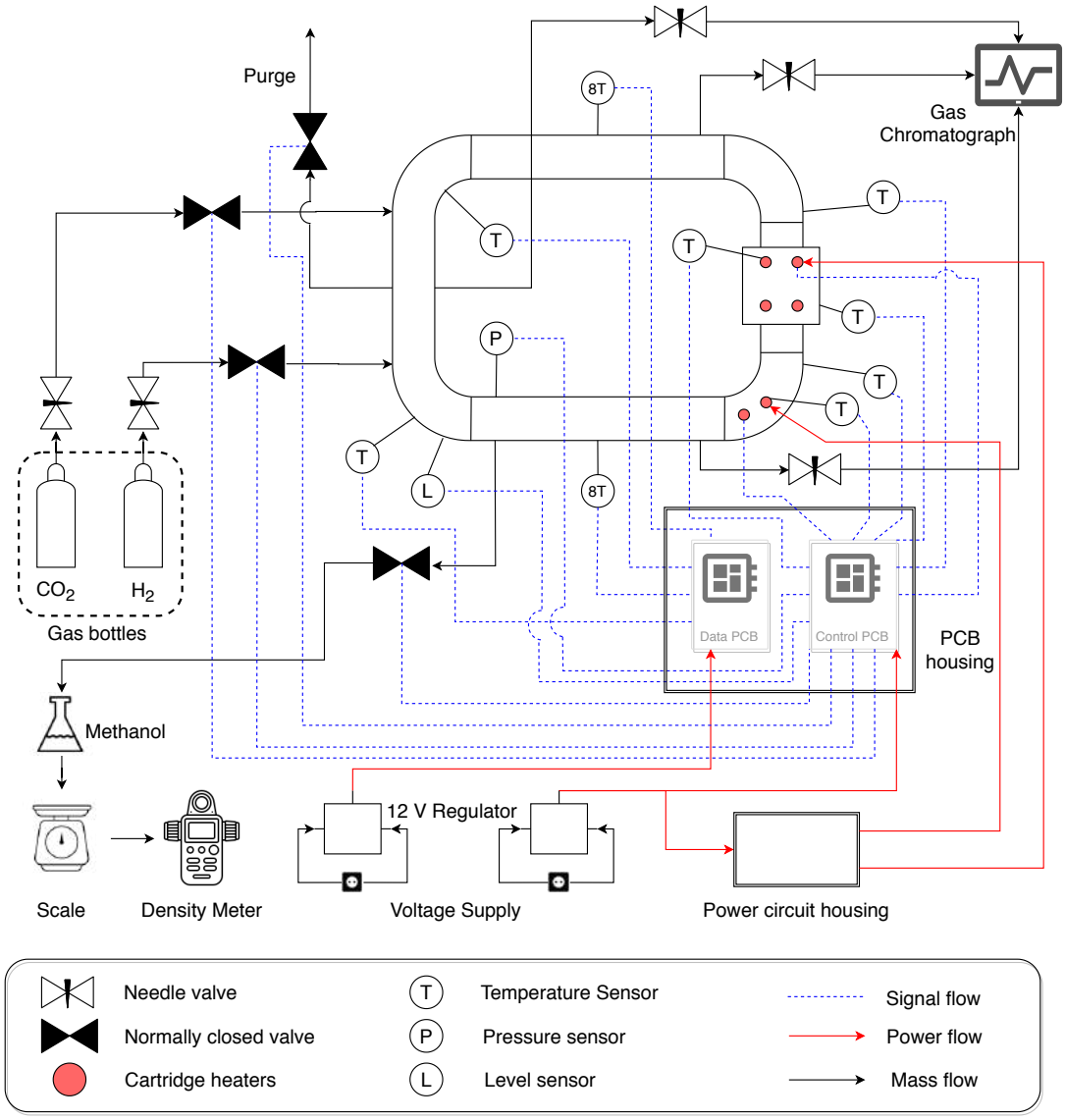

Figure 3.15: Process Diagram of the entire setup with all the equipments discussed so far.

Four types of gas cylinders were used for the reactor. Premixed cylinder containing feed gas (25 vol% of CO_2 in H_2), pure H_2 and CO_2 cylinders for making variable composition feed, and N_2 cylinder for pressure testing.

3.9. Experimental plan and Methodology

After all the planned modifications of all components in the reactor, and successful safety tests for leaks, the experiments were conducted. Figure-3.16, delineates graphically the path taken for conducting the experiments to answer the research questions posed for this thesis. The following sections discuss the methods used for calculations in results, analysis and discussion section.

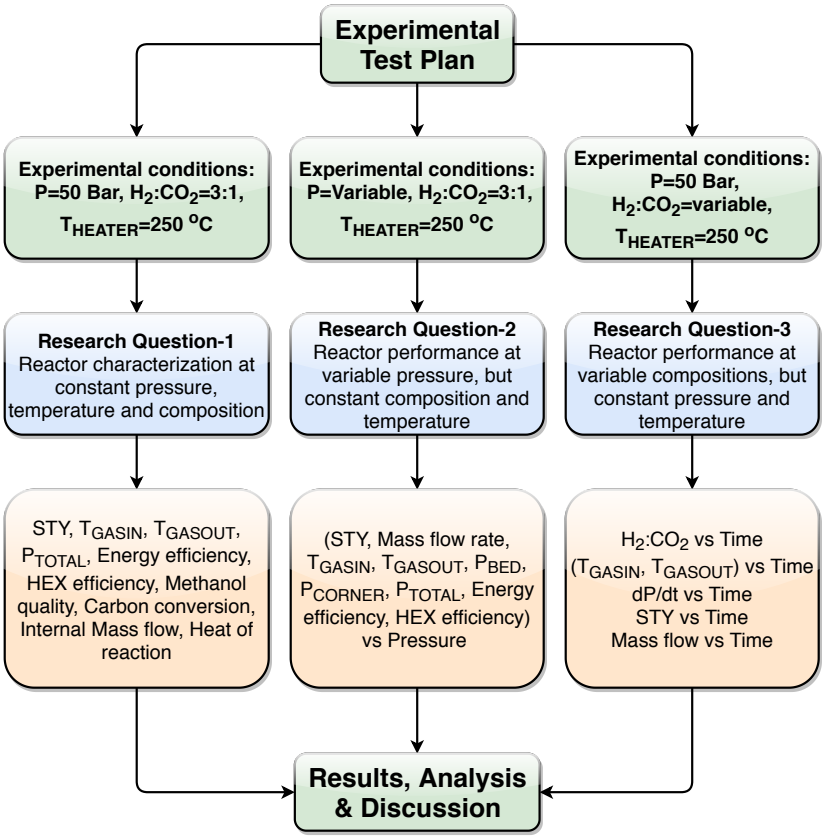

Figure 3.16: Experimental plan for this thesis.

3.9.1. Catalyst Activation Procedure

"Heating the catalyst in presence of a reducing environment like H_2 converts the Cupric Oxide (CuO) into metallic copper which is needed for methanol synthesis."

The catalyst was activated using pure H_2 at 50 Bar on a bed heater temperature of 250 °C. The process is described in figure-3.17 in detail. The Standard operating Procedure (SOP) regarding the currently used catalyst (HUL-98), provided by its manufacturer (Hutong Global), states that the catalyst must be reduced in $H_2 : N_2 = 5 : 95$ vol%. This composition is generally advised because large scale catalyst beds have very high volume and therefore, reducing the catalyst with pure hydrogen becomes hazardous. Since, the current methanol reactor is small scale, only pure hydrogen was used, which is better for reduction [36]. It also obviates the need for procuring N_2 for the overall ZEF plant. The catalyst weight was seen to reduce from 120 g to 96 g after activation due to water formation. The repeated purge operations mentioned in the procedure is used to dilute the air inside the reactor. After 3 purge operations the gas inside the reactor can be assumed to be the same as

the feeding cylinder. When the activation process starts, water is formed followed by phase change. This leads to pressure drop inside the reactor which needs to be replenished. When the pressure ceases the drop, it can be assumed that no more water is formed and the catalyst is activated. Water was sluiced out of the reactor after activation which was measured to be 22.8 g.

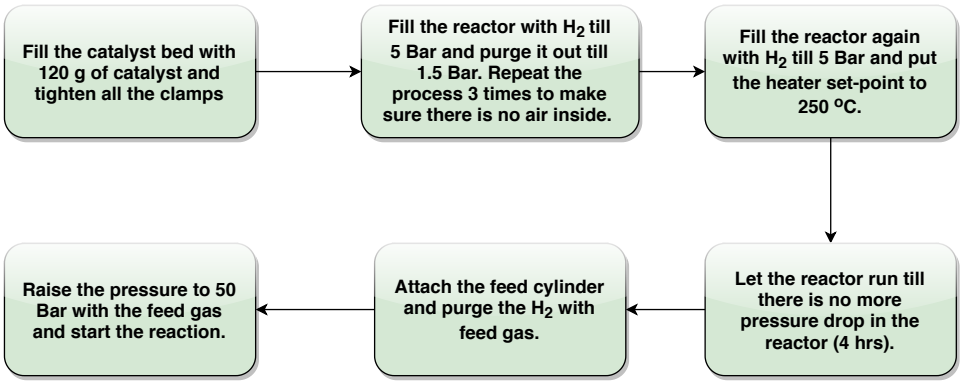

Figure 3.17: Catalyst activation procedure.

3.9.2. Mass Flow Rate Estimations

"If the temperature, heat flow and specific heat capacity of a fluid between two different locations is known, then the mass flow rate can be estimated by an energy balance. The following subsection identifies such locations in the reactor, which will be evaluated in the results"

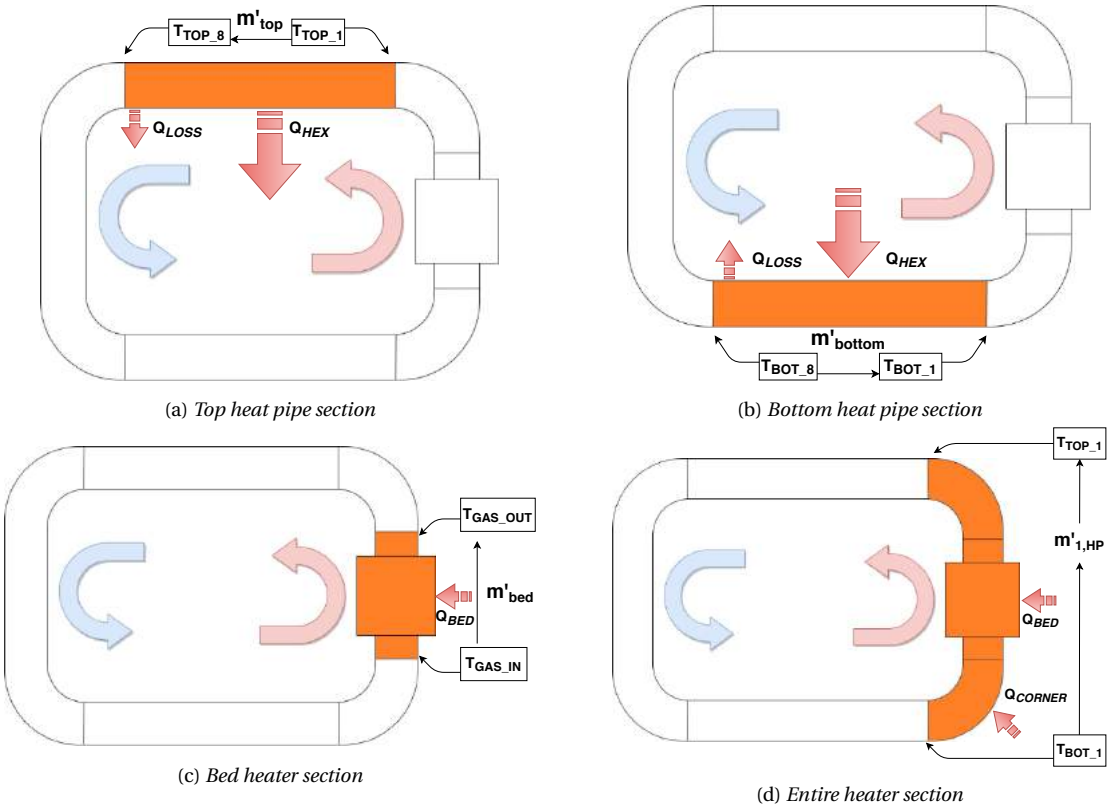

(a) *Top heat pipe section*

(b) *Bottom heat pipe section*

(c) *Bed heater section*

(d) *Entire heater section*

Figure 3.18: Illustration for different ways to estimate mass flow rate.

Mass flow estimation is an extremely important parameter for the current methanol reactor un-

der study because, unlike the conventional methanol plants, the flow inside is not forced. It is one of the key parameters, that defines the mass transfer to the catalyst surface. Systems that are driven by natural convection are very delicate and minor changes in parameters such as pressure, temperature and feed composition can throw them off balance leading to runaways. Pressure affects the density of gas which is important to the driving force for convection. Reaction temperature affects the gradient of temperature between the cold and hot side which also drives natural convection. While feed composition affects the density as well as the specific heat capacity of the gas. All these above mentioned parameters eventually trickle their effects on to the mass flow rate. Therefore, there is always an interplay between these parameters which are not mutually exclusive, and that makes a natural convection based system behave in an unpredictable manner. Due to these factors it is important to ascertain the mass flow rate inside the reactor in a **non-obstructive** way.

Figure-3.18 illustrates 4 different ways to estimate the mass flow rate which should ideally be the same. Equations-3.2, 3.3, 3.4, 3.5 express the same in mathematical form. The $\dot{Q}_{loss}$ mentioned in equations-3.2 and 3.3 is unknown and can be expected to be very low because the reactor was insulated well. Therefore, it can be safely ignored. The energy of the synthesis reaction can also be ignored since it is very small as compared to the heater duty.

$$\dot{m}_{Top} = \frac{\dot{Q}_{HEX} + \dot{Q}_{loss}}{c_p \, \Delta T_{topHEX}} \tag{3.2}$$

$$\dot{m}_{Bottom} = \frac{\dot{Q}_{HEX} - \dot{Q}_{loss}}{c_p \, \Delta T_{bottomHEX}} \tag{3.3}$$

$$\dot{m}_{Bed} = \frac{\dot{Q}_{Bed} + \dot{Q}_{Reaction}}{c_p \, \Delta T_{Gasflow}} \tag{3.4}$$

$$\dot{m}_{1,HP} = \frac{\dot{Q}_{Bed} + \dot{Q}_{Corner} + \dot{Q}_{Reaction}}{c_p \, \Delta T_{1,HP}} \tag{3.5}$$

In the above equations,

$\dot{m}_{Top}$	= Mass flow rate through the top heat integration section [g/s]
$\dot{m}_{Bottom}$	= Mass flow rate through the bottom heat integration section [g/s]
$\dot{m}_{Bed}$	= Estimated mass flow rate through the catalyst bed [g/s]
$\dot{m}_{1,HP}$	= Mass flow rate in the hot section using temperature gradient of heat pipe-1 [g/s]
$\dot{Q}_{HEX}$	= Combined heat pipe duty [W]
c_p	= Specific heat capacity of the flowing gas at respective temperatures [J/kg K]
ΔT_{topHEX}	= Temperature gradient along top heat pipe section ($T_{up,1}$-$T_{up,8}$) [K]
$\Delta T_{bottomHEX}$	= Temperature gradient along bottom heat pipe section ($T_{down,8}$-$T_{down,1}$) [K]
$\Delta T_{Gasflow}$	= Temperature difference between catalyst bed outlet and inlet [K]
$\Delta T_{1,HP}$	= Temperature difference between top and bottom of heat pipe-1 [K]
$\dot{Q}_{Bed}$	= Power input to catalyst bed [W]
$\dot{Q}_{Corner}$	= Power input to corner heaters [W]

3.9.3. Mole fraction estimation of extracted liquid

"If the density of the condensate product from the reactor is accurately known, then the mass fraction of methanol and water can be estimated by interpolating the experimental data."

The density (ρ) of the liquid effluent of the reactor was analysed using an Anton Parr DMA 5000 density meter with an accuracy of 10^{-5} kg/L. The density data was further used to ascertain the mass fraction of methanol (w_{MeOH}) and water. Figure-3.19a shows the variation of mass fraction of methanol with density of the solution at a temperature of 20 °C. The experimental data was taken

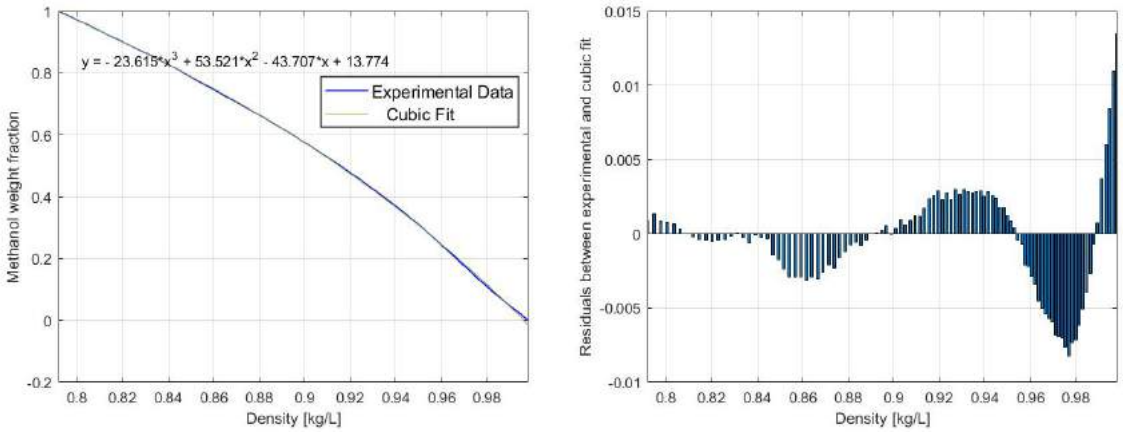

(a) *Experimental data for methanol and water mixture density with weight percent.*

(b) *Residuals between the experimental data and the Cubic curve fit.*

Figure 3.19: Method to determine methanol weight fraction from density measurements.

from handymath tool[3]. The cubic curve fit of the data reveals equation-3.6 as a way to interpolate the density data. Figure-3.19b shows the residuals between the predicted values and the known experimental values of methanol mass fraction against solution density. It can be seen that, equation-3.6 predicts the mass fraction of methanol within 0.005 for the range of densities applicable for the experiments.

$$w_{MeOH} = -23.615\rho^3 + 53.521\rho^2 - 43.707\rho + 13.774 \tag{3.6}$$

Where,

w_{MeOH} = Mole fraction of methanol in the reactor outlet
ρ = Density of the liquid sluiced from the reactor [kg/L].

Literature study has revealed that only trace amounts of byproducts of side reactions are present in the liquid with the current reaction conditions, choice of catalyst as well as feed gases. Hence, they were not analysed in the current study. Although, if necessary it can be done using High Performance Liquid Chromatography (HPLC), TCD, FID etc.

3.9.4. Heater duty calculations

"The heater pulses can be counted in an interval of steady state in the reactor and heat input be calculated by using the heater power rating."

The controller has been designed in such a way that it provides a boolean output (0 or 1) for the state of all heaters. When a time interval for the steady state is identified, it counts the number of pulses for both bed as well as corner heaters in that interval. Since, each pulse refers to 1 second of power supply to the heaters, the power supplied to the reactor was calculated using equations-3.7, 3.8, 3.9.

$$P_{bed} = \frac{C_{bed} \times P_{heater} \times N_{bed}}{(t_2 - t_1) \times 60} \tag{3.7}$$

$$P_{corner} = \frac{C_{corner} \times P_{heater} \times N_{corner}}{(t_2 - t_1) \times 60} \tag{3.8}$$

$$P_{total} = P_{bed} + P_{corner} \tag{3.9}$$

[3] https://handymath.com/cgi-bin/methanoltble3.cgi?submit=Entry

Where,

P_{bed} = Heater power duty of catalyst bed [W]
P_{corner} = Heater power duty of corner heaters [W]
P_{total} = Total reactor power duty [W]
C_{bed} = Pulse count for bed heaters in the interval t_1 to t_2
C_{corner} = Pulse count for corner heaters in the interval t_1 to t_2
$P_{heaters}$ = Power rating of a single heater [40 W]
N_{bed} = Number of heaters in catalyst bed [8]
N_{corner} = Number of heaters in corner section [4]

3.9.5. Heat pipe duty and performance calculations

"A well insulated stand alone heat pipe setup was given known heat inputs and temperature gradient data was taken. The obtained empirical results were then used to estimate heat transferred by using temperature gradient in reactor operation."

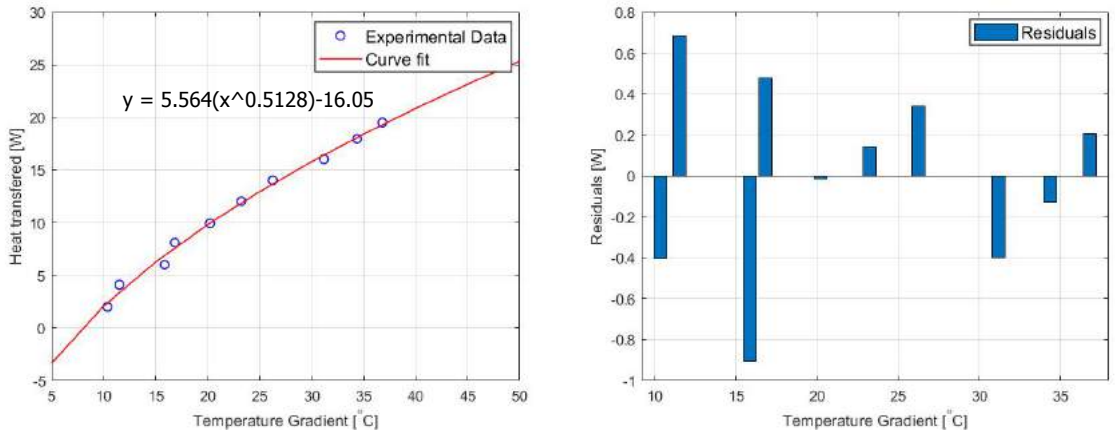

(a) *Experimental data and curve fit for heat transferred by heat pipes.* (b) *Plot of residuals between the empirical data and interpolated data.*

Figure 3.20: Interpolation of Heat transferred through heat pipes by using experimental data. [18]

Since, the heat pipes have been modified (300 mm heat pipes split into two heat pipes of 150 mm) in the current reactor before installation, the heat transferred by them can only be determined empirically. To this end, a stand alone heat pipe setup was made during the master's thesis of de Kruijf [18]. In this setup two heat pipes of 150 mm were joined using a copper cylinder as used in the reactor and kept at an angle of 20° from the vertical. The two ends were thoroughly insulated and one end was attached to the heater. Based on the heat supplied and steady state temperatures attained by the hot and cold ends of the compounded heat pipes, empirical data was obtained for heat transferred. Figure-3.20a shows the empirical data as well as the curve fit for the same. Equations-3.10 represents the equation used further for interpolation. Since, there are two such compounded heat pipes (front & back figure-3.5) in a single unit, the interpolated value needs to be doubled.

$$Q_{Heatpipe} = \left(5.564 \times \Delta T_{HP}^{0.5128} - 16.05\right) \times 2 \tag{3.10}$$

Where,

$Q_{Heatpipe}$ = Heat pipe duty of single heat pipe unit [W]
ΔT_{HP} = Temperature gradient between heat pipe hot section and cold section [K].

An important indicator for the heat exchanger performance is the heat transferred compared to the heat supplied to the flow, as shown below. It is a measure of how close the heat exchanger performance is to autothermal operation.

$$\xi_{HP} = \frac{\dot{Q}_{HP}}{\dot{Q}_{HP} + \dot{Q}_{heaters} + \dot{Q}_{reaction}} \tag{3.11}$$

3.9.6. Energy Efficiency Calculations

Energy efficiency is an important reactor performance indicator, which was calculated using equation-3.12.

$$\eta_{energy} = \frac{[LHV]MeOH}{[HHV]\mathrm{H_2} + P_{Total}} \tag{3.12}$$

In the above equation Lower Heating Value (LHV) of methanol has been used. By definition, it takes into account the latent heat of vaporization of water formed during the reaction. The energy required to make water vapor is not released. Moreover, HHV of H_2 has also been taken into account as it is also combustible and hence, a type of energy input. The HHV takes care of the fact that it is fed into the reactor at ambient temperature.

3.9.7. Heat of reaction calculations

The exothermicity of the methanol synthesis reaction is also taken into account as heat of formation. But the standard heat of formation is calculated at ambient temperature. At higher temperatures it is given by equation-3.13. The production rate of methanol [mol/hr] was used to determine the heat of reaction.

$$\mathrm{CO_2 + 3H_2} \rightleftharpoons \mathrm{CH_3OH + H_2O} \qquad \Delta \mathrm{H_{298K}} = -49.2\,\mathrm{kJ/mol}$$

$$\Delta H_{503\,\mathrm{K}} = \Delta H_{298\,\mathrm{K}} + \int_{298\,\mathrm{K}}^{503\,\mathrm{K}} c_p dT = -42.47 kJ/mol \tag{3.13}$$

3.9.8. Reactor Insulation

The reactor hot section needs to be insulated in order to save heater power. A good insulation also allows the heaters to attain the given set-point faster and higher. The condenser side of the reactor was left open to create the necessary temperature gradient between the hot and cold side. The

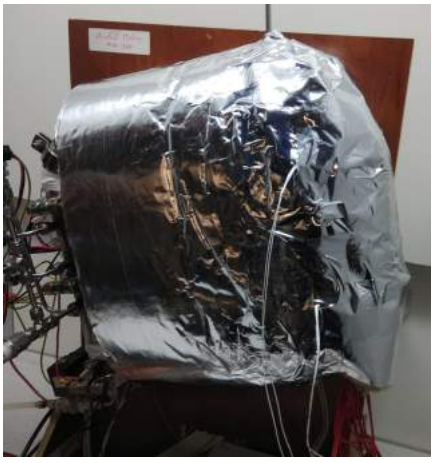

(a) *Outer Rockwool insulation in the reactor*

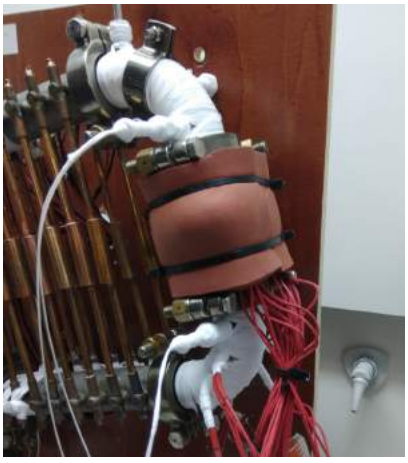

(b) *PTFE & silicone pad insulation in the reactor hot section.*

Figure 3.21: Insulation types used in the reactor.

reactor was insulated using Rockwool (k = 0.04 W/m/K) from the outside. On the other hand it was insulated using PTFE tape (Griffon, 0.076 mm thick) on the inside to cover the complex geometry of the reactor hot section. Moreover, silicone foam sheets with high fire safety ratings were also placed to increase insulation effectiveness.

4

Results, Analysis and Discussion

"If we knew what we were doing, It wouldn't be called research. Would it?"
-Albert Einstein-

4.1. Mass Flow Rate Validations

It is important to keep in mind the schematics discussed in section-3.9.2, figure-3.18 to understand the results obtained here. Table-4.1 shows the values of mass flow rates calculated from the the methodology described in that section, at different intervals of a steady state reactor run. Since, $\dot{Q}_{loss}$ has been neglected for calculations, the mass flow estimated by the top section is slightly underestimated and that from the bottom section is overestimated (using equation-3.2, 3.3). Therefore, it can be seen that they do not give the same value, and the real mass flow rate would lie between them if losses are also considered.

Table 4.1: Estimated mass flow rates by the methodology mentioned in section-3.9.2. The data for the calculations was taken from the reactor run mentioned in figure-4.4. Key parameters for the calculations for the interval 350-400 mins is also presented. P = 50 Bar, Heater set-point = 250 °C, feed composition $H_2 : CO_2$ = 3:1.

Interval [min]	$\dot{m}_{top}$ [g/s]	$\dot{m}_{bottom}$ [g/s]	$\dot{m}_{bed}$ [g/s]	$\dot{m}_{1,HP}$ [g/s]
200-250	0.911	1.013	1.141	2.173
250-300	0.917	1.018	1.132	2.188
300-350	0.912	1.016	1.124	2.164
350-400	0.917	1.023	1.153	2.222
Parameters for the interval 350-400 mins				
Heat flow rate [W]	155.96	155.96	58.88	153.6
ΔT [°C]	60.64	54.65	17.97	24.34
c_p [$Jkg^{-1}K^{-1}$]	2805.2	2790.7	2839.6	2839.6

It was seen that the mass flow rate estimated by the method presented in section-3.9.2, figure-3.18d ($\dot{m}_{1,HP}$) was very high as compared to the rest. It is because the temperature of the heat pipe in the top section is lower than the actual gas flow temperature for heat transfer to happen. While, the temperature of the heat pipes in the bottom section is higher than the actual gas flow temperature. Therefore, when ΔT is calculated only along the top or bottom section, the difference between the wall temperature of the heat pipe and gas, cancel each other to give the gradient in gas temperature which accurately predicts the mass flow rate. On the other hand when the difference between $T_{top,1}$ and $T_{bottom,1}$ is taken, they do not cancel out but rather add up. The resultant ΔT is therefore, the gradient of the heat pipe temperatures and not the gradient in the gas flow temperature which is

the reason for the observed anomaly in the mass flow rate. Using the mass flow rate predicted by the bed section, the $\Delta T_{1,HP}$ was back calculated, and was seen to be 46.91 °C. As seen in table-4.1, the observed $\Delta T_{1,HP}$ is rather 24.34 °C, which is 22.57 °C lower than it should be to predict the same mass flow rate as the bed section. Therefore, it can be concluded that the difference between the wall temperature measured by the sensors and the actual gas temperature is ±11.29 °C.

KEY INSIGHT-1

The heat pipe temperatures and heat input measurements from the heaters provide two different ways (temperature data, Heater data) to estimate the mass flow rate, which predict similar values (1.1 g/s). They also suggest a way to estimate the average difference between the wall temperature of the heat pipes and the real gas flow temperature. For the experiment mentioned above, it was found to be ±11.29 °C.

4.2. THERMAL GRADIENT ALONG HEAT PIPES

Figure-4.1 shows the temperature profile of the top (red) and bottom (blue) heat pipes during methanol production. It was seen that heat pipe number 2 and 5 showed peculiarly skewed thermal behaviour (dashed circles). This indicates that these heat pipes do not contribute to the heat integration. If they do not transmit any heat downwards then the temperature of the top section becomes higher and since, no heat is received at the bottom section its temperature is lower than expected (black dashed line). In other words the temperature showed by these heat pipes is more indicative of the gas flowing inside. In the previous section it was established that for heat transfer between the gas and heat pipe at steady state, there exists a temperature difference of approximately ±11.29 °C between the wall and gas. Indeed such a difference was seen during the reactor run as seen the figure-4.1. This problem was not observed in the previous works done on the reactor before this thesis. However, it becomes important to rectify it because, heat pipes 2 and 5 highly exaggerate the ΔT which gives an over prediction of the heat transmitted by them (equation-3.10). To avoid the overestimation of mass flow rate due to this observation, the contribution of heat pipe 2 and 5 was set to zero in further analysis.

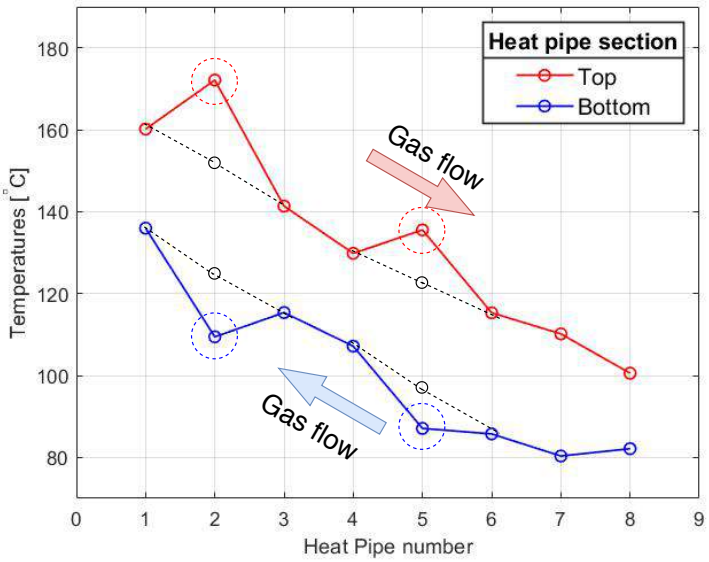

Figure 4.1: Gradient of temperatures along both top and bottom heat pipes. The black dashed lines represent the expected temperature of the heat pipe. The red dashed circle represents the actual measured temperature of the heat pipe.

KEY INSIGHT-2

Heat pipes 2 & 5 do not contribute to the heat integration of the system. This may have happened during installation or operation and points towards the overall unreliability of the heat pipes. The temperatures shown by them are more indicative of the gas flow temperature and therefore can be used to estimate the mass flow. In section-3.9.2, figure-3.18d, heat pipe-1 was suggested to estimate the mass flow which did not give good agreement in section-4.1. However, if heat pipe-2 is used instead, the results can be expected to be in better agreement if the above mentioned conclusions are accurate. Indeed, the said mass flow rate estimated from heat pipe-2 was found to be 0.88 g/s which matches the other estimations. Therefore, all 4 methods suggested, now provide similar mass flow rates.

4.3. EXPERIMENTS WITH PREMIXED FEED GAS COMPOSITION

The first set of experiments conducted on the reactor were concerned with using the premixed cylinder bottle (H_2 /CO_2 = 75/25 vol%). This composition is considered stochiometric for the methanol synthesis reaction from CO_2. The stochiometric number of the feed gas is 2 for this case, which is considered ideal. The aim of these experiments was to create a base case for comparison with previous works and also to observe any peculiar behaviour that wasn't looked at in the earlier experiments.

$$S = \frac{moles\,H_2 - moles\,CO_2}{moles\,CO_2 + moles\,CO} = \frac{75-25}{25+0} = 2$$

4.3.1. EXPERIMENTS WITH CONSTANT PRESSURE

Table-4.2 shows the values of the parameters obtained at steady state for two separate reactor runs under same conditions.

Table 4.2: Details about various parameters for premixed gas bottle. Experimental conditions: P = 50 Bar, Feed Gas = H_2:CO_2[3:1], Heater set-point = 250 °C.

Parameter	Run-1	Run-2	Unit
Space time yield	4.92	4.84	mmol/gcat/hr
Methanol mole fraction	0.492	0.495	-
Methanol output flow	18.92	18.61	g/hr
Water output flow	10.98	10.68	g/hr
Hydrogen input flow	3.61	3.54	g/hr
Carbon dioxide input flow	26.27	25.73	g/hr
Carbon conversion	98.9	99.3	%
Gas inlet Temperature	204.8	206.1	°C
Gas outlet Temperature	222.8	224.1	°C
Reactor internal mass flow rate	1.1	1.1	g/s
Heat of reaction ($\dot{Q}_{reaction}$)	6.97	6.85	W
Corner power duty (P_{corner})	94.72	97.8	W
Bed power duty (P_{bed})	58.88	58.5	W
Total Power duty (P_{total})	153.6	156.32	W
Heat pipe duty ($\dot{Q}_{HP}$)	154.4	155.3	W
Heat exchanger efficiency (ξ_{HP})	49.02	48.8	%
Energy Efficiency (η_{energy})	35.37	34.81	%
Average Extraction frequency	14.8	15	Min
Average Extraction Volume	5.8	5.8	mL

Reactor mass balance

A mass balance of the system was done after taking careful liquid output measurements (figure-4.2). Mass flow rates of methanol and water were determined by density measurements of the liquid output.Since, both water and methanol contain hydrogen, total hydrogen needed was estimated. The gas cylinder composition is fixed at 3:1, therefore, CO_2 intake was also estimated. The carbon conversion was seen to be 99.3%

Figure 4.2: Reactor mass balance for Run-2

Transient behaviours

Figure-4.3 shows the thermal behaviour of the top and bottom heat pipes during the experiment. It can be seen that when the pressure was around 25 Bar, there is almost linear rise in the temperatures as the heaters try to attain the set-point (250 °C). This is because there is conduction through the Tri-Clamp pipes, even though there is insignificant mass flow rate. As the pressure was increased higher than 40 bar, the heat pipes started to show convective behaviour indicating flow of gases inside the reactor. Moreover, heat pipes 2 & 5 are not operational. Therefore, it can be seen that when the flow is insignificant, they maintain the correct sequential order due to conduction being the only mode of heat transfer. However, when the flow starts to develop, heat pipes 2 & 5 deviate from the regular order. All the top heat pipes show smooth thermal patterns that are consistent

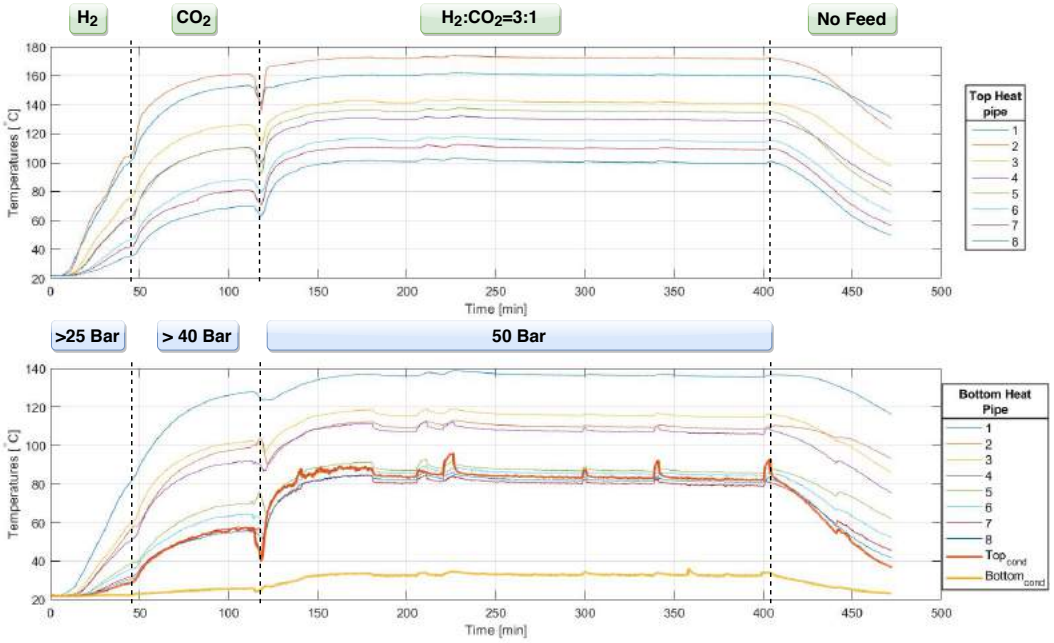

Figure 4.3: Thermal behaviour of top and bottom heat pipes throughout the experiment. Experimental conditions: P = 50 Bar, Feed Gas = H_2:CO_2 [3:1], Heater set-point = 250 °C.

with the log of events. However, the bottom heat pipes and the top condenser shows irregularities

in the pattern (spikes and dips). This is indicative of the two phase region in the reactor. As the condensate droplets clog the copper mesh, the mass flow rate is affected and the same pattern is seen in a lot of bottom heat pipes. The rise in temperatures is indicative of meshes getting clogged and vice versa. The unclogging of the meshes are all consistent with liquid sluicing operation, which creates a violent flow (50 Bar to ambient pressure) and flushes the droplets off the mesh.

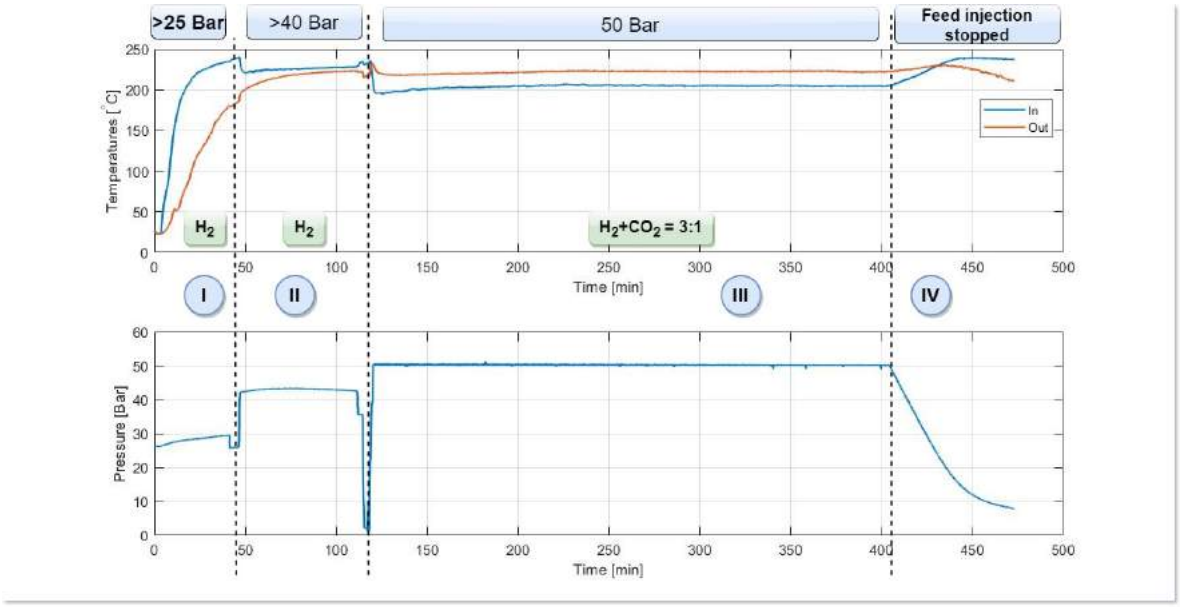

Figure 4.4: Inlet and outlet gas temperatures compared against pressure variations. Experimental conditions: P = 50 Bar, Feed Gas = H_2:CO_2 [3:1], Heater set-point = 250 °C.

Figure-4.4 depicts the changes in the inlet and the outlet gas temperatures against the corresponding pressures observed in the system. In region-I, the reactor was only filled with H_2 at >25 bar and heated. It can be seen that the gas temperatures rises in response to the temperature set-point of heaters. Also, the pressure rises slightly due to the rise in temperature. Although, since the inlet temperature is high compared to the outlet, it can be assumed that the mass flow is very less inside (partially choked). Therefore, in region-II the pressure was increased to >40 bar. Both the temperatures attemperate to a common temperature due to better circulation. In region-III, the H_2 is purged out and feed of H_2 /CO_2=3:1 is provided to the reactor. The control system keeps the pressure constantly maintained at 50 Bar. It can be seen that the inlet temperature drops below the outlet owing to more circulation and the exothermicity of the synthesis reaction. The STY is measured in the interval when both the temperatures reach steady state. In the region-IV, the feed was stopped while the temperature was still maintained at the set-point. Interestingly, it was seen that the pressure keeps dropping until 8 Bar which is characteristic of proceeding reaction. Due to the pressure drop, the gas temperatures also flip their order again denoting reduction in flow and eventually full or partial choking at the inlet.

KEY INSIGHT-3

It takes >40 Bar inside the reactor for the gases to circulate properly. The reactor exhibits two phase region in the bottom heat pipe section making droplets to condense and clog the pores of the copper mesh. These thermal patterns can only be affected externally by sluicing the condensate, which disturbs the system and unclogs the pores leading to better circulation and lowering of temperatures. The faulty heat pipes 2 and 5 as well as the gas flow temperatures are the only ways to determine whether or not there is proper circulation inside the reactor. The reaction seems to proceed unhampered by lowering the pressure to an extent.

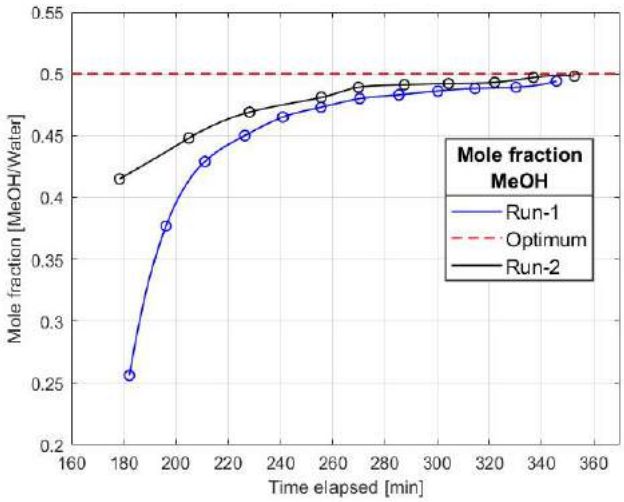

Figure 4.5: Variation of mole fraction with time for two different reactor runs. Experimental conditions for both runs: P = 50 Bar, Feed Gas = H_2:CO_2 [3:1], Heater set-point = 250 °C. Run-2 done after H_2 circulation for 30 mins.

Figure-4.5 shows the mole fraction of methanol sluiced from the reactor at different times for the same experiment (Run-1 marked blue). It can be seen that initially, the condensate was more water rich. As the reactor operation proceeds the quality of methanol improves and attains the optimum value. This is due to the partial catalyst deactivation at night after reactor shutdown. Equation-4.1 shows the primary synthesis reaction. But it has been seen in the literature that the reaction can be broken down crudely into equation-4.2 and 4.3, where a molecule of H_2 scavenges the dissociatively adsorbed O(s) from the methanol forming site, making it available for synthesis again. After reactor shutdown, such sites are scavenged by H_2 in the following day to give a higher water content in the condensate. To test this, another reactor run was carried out. But in this experiment, after methanol production the reactor was allowed to run with pure H_2 for 30 mins before shutdown while keeping heater supply the same as for production. It was seen that the quality of methanol on the following day was better (Run-2).

$$CO_2 + 3\,H_2 \rightleftharpoons CH_3OH + H_2O \tag{4.1}$$

$$CO_2 + 2\,H_2 \rightleftharpoons CH_3OH + O\,(s) \tag{4.2}$$

$$H_2 + O\,(s) \rightleftharpoons H_2O \tag{4.3}$$

KEY INSIGHT-4

The initial yield of the reactor is rich in water due to partial catalyst deactivation after shutdown in the previous run. It takes 1 hour and 46 minutes after the first methanol output, for the reactor to produce methanol which is within 10% of the optimal purity. Running the reactor with pure H_2 after stopping the methanol production, improves the methanol quality in the following day.

4.3.2. EXPERIMENTS WITH VARIABLE PRESSURE

Due to the findings stated in the previous section, experiments were conducted with lower pressures keeping the same premixed feed cylinder and temperature set-point of heaters to see if comparable methanol production can be achieved at reduced pressure. The reactor was operated at 50 bar till steady state was obtained. The pressure was then lowered in steps and measurements were taken at each steady state for different pressures. It can be seen in figure-4.6, that the yield at first increased after lowering the pressure from 50 bar and then decreased after lowering the pressure further. As the methanol synthesis reaction is favored by high pressures, this result is counter-intuitive and

suggests that reactor conditions are far from equilibrium, to the point that effect of pressure is less prominent. This behaviour can be understood by observing the mass flow rate inside the reactor at different pressures.

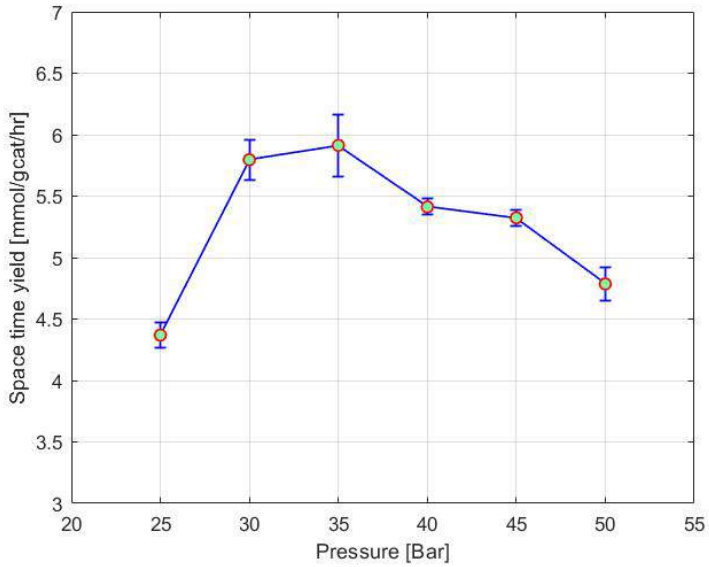

Figure 4.6: Variation of Space time yield with changing pressure. Experimental conditions: P = variable, Feed Gas = H_2:CO_2 [3:1], Heater set-point = 250 °C.

Figure-4.7a shows that the mass flow rate decreases with the decrease of pressure. As the pressure decreases, so does the gas density, which leads to less driving force for natural convection and reduces the mass flow. The mass flow reduction due to that, leads to higher residence time at the heating section leading to higher inlet temperatures (Figure-4.7b), even though the heater set-point is constant at all times. Higher inlet temperatures are conducive to better kinetics, which is observed as higher yield of methanol from the reactor.

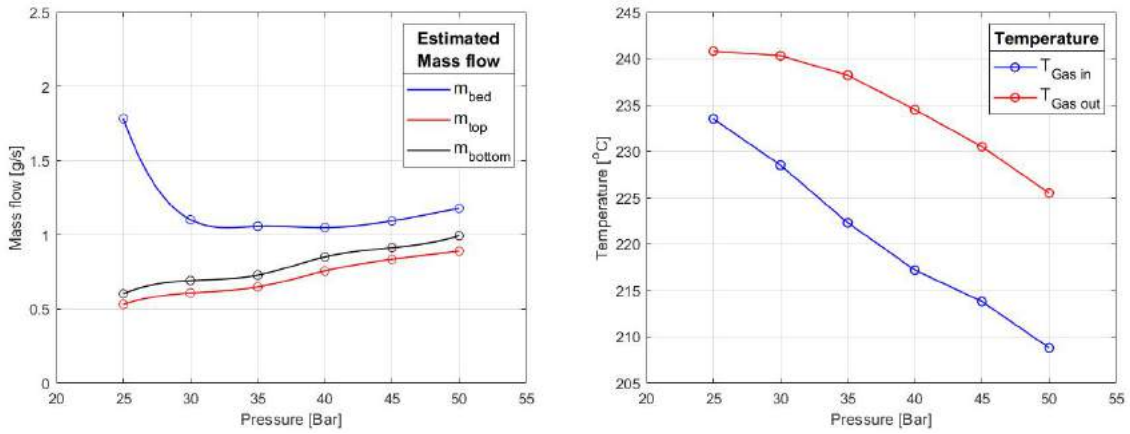

(a) *Estimated mass flow rate in different reactor section.*

(b) *Reactor inlet and outlet temperatures.*

Figure 4.7: Mass flow rate variations with pressure. Experimental conditions: P = variable, Feed Gas = H_2:CO_2 [3:1], Heater set-point = 250 °C.

The mass flow rate estimated by the top and bottom heat pipe section monotonically decreases with the pressure reduction. However, the mass flow rate estimated by the catalyst bed section de-

creases initially and then starts of increase rapidly due to pressure reduction. This anomaly occurs when considerable flow stagnation starts to occur at the bed inlet. The random catalyst packing in the bed is by far the most prominent factor that offers resistance to the flow inside the reactor. The pressure drop across the bed starts overwhelming the natural convective flow. Due to this, there is formation of local flow re-circulation region at the bed inlet (see figure-4.8a), and the flow becomes partially choked. Since the inlet temperature sensor is located in this region, it reads a relatively higher value. It can be seen in figure-4.7b that the gas inlet temperature monotonically increases as the pressure is lowered. Since, the flow appears to get partially choked below 35 bar (Figure-4.7a), the mass flow diffusion into the bed goes down drastically. It can be expected that the yield would go down as well as the gas outlet temperature, due to less reaction. It is indeed what was observed in the data. The gas outlet temperature also followed a similar trend till 35 Bar, after which the temperature increase was hindered. The temperature gradient can be seen decreasing with pressure reduction. Since, ΔT has an inverse relation with mass flow, the estimated mass flow rate is high.

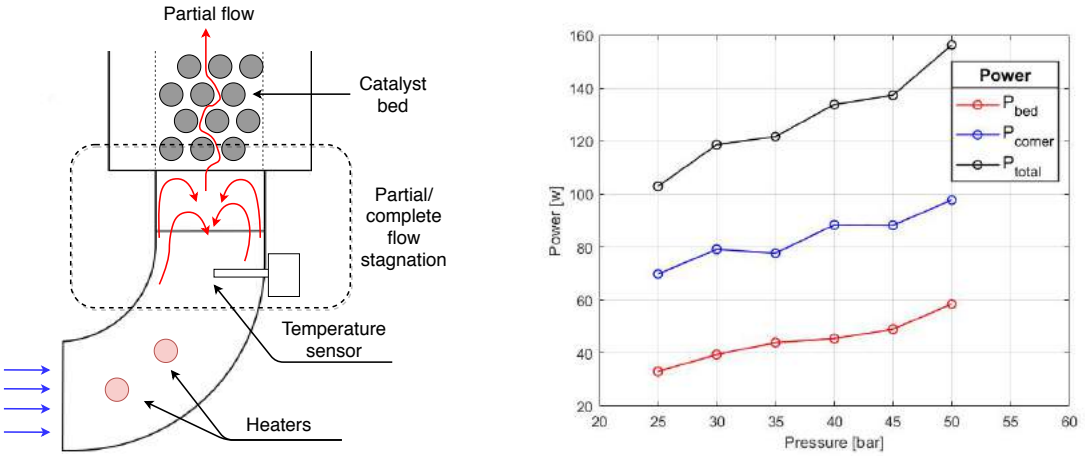

(a) *Illustration of the expected flow stagnation due to catalyst bed.*

(b) *Heater duty as a function of pressure.*

Figure 4.8: Mass flow rate and Heater duty variations with pressure. Experimental conditions: P = variable, Feed Gas = H_2:CO_2 [3:1], Heater set-point = 250 °C.

KEY INSIGHT-5

The methanol yield increases slightly with the reduction of pressure, although it should ideally decrease. This emphasizes the importance of mass flow rate in the current system. Due to pressure reduction the mass flow rate goes down, which increases the inlet temperature. This is an indication that the yield is kinetically limited in the reactor and not equilibrium limited. The flow starts to stagnate at the bed inlet below 35 Bar.

Another implication of this flow reduction due to the lowering of pressure, is the reduction in the heater duty. As the heaters are constantly maintained at the same set-point (250 ° C) throughout different pressures, it can be expected that the power requirement of reactor would go down due to low mass flow rate. This is because the mass flow rate has a cooling effect on the heaters. It can be seen in figure-4.8b that the heater duty goes down monotonically with pressure decline. It must also be noted that it has the same pattern as the mass flow rate of the top and bottom section (Figure-4.7a). This is an interesting observation due to two factors. Firstly, the data used for these calculations was collected by separate PCBs; heat pipes (Data PCB), heaters (Control PCB). Therefore, they are decoupled against any interference. Secondly, mass flow rate was estimated using temperatures of heat pipes, while power was calculated by counting the heater pulses. The fact that both exhibit the same pattern indicates the accuracy of the inference. Moreover, since the bed heaters are attached to aluminium blocks, while the corner heaters are attached to copper meshes, it can be expected

that bed heaters would have more thermal inertia. Indeed, figure-4.8b shows that the power curve for bed is much more smooth than the corner.

Energy efficiency Calculations

The energy efficiency of the reactor at every pressure and corresponding methanol output was estimated using the method suggested earlier in section-3.9.6. It can be seen in figure-4.9a that the reactor operates at much higher efficiency at lower pressures. This is an immediate result of two complementary phenomenons. It was shown earlier that the methanol output is higher as the pressure goes down. Moreover, the heater power duty also goes down due to lower internal mass flow rate inside the reactor. Therefore, the efficiency is also higher. As the flow starts to stagnate below 35 Bar, the power duty keeps going down but at the same time, the methanol production is also hampered. As a result of this trade off the efficiency stops rising after 35 Bar till 30 Bar, and then starts declining upon further pressure reduction. The heat exchanger efficiency has also been plotted in figure-4.9b which can be seen increasing. As the heater power goes down with pressure decline, the heat pipe duty increasingly becomes a larger fraction of total heat supplied to the flow. This also gives evidence for increased residence times because of which the heat pipes are able to transmit more heat.

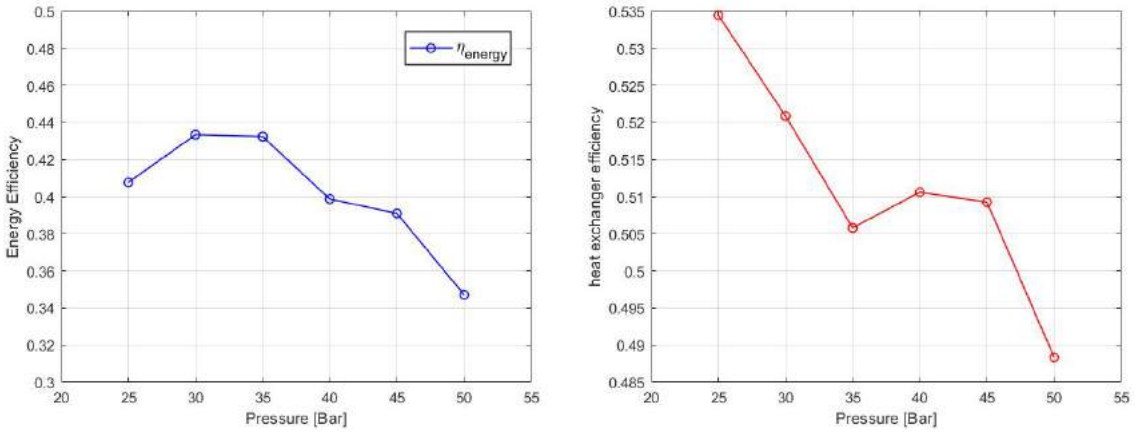

(a) *The variation of energy efficiency with pressure.* (b) *Heat exchanger efficiency with reducing pressure.*

Figure 4.9: Reactor performance efficiency variation with pressure. Experimental conditions: P = variable, Feed Gas = H_2:CO_2[3:1], Heater set-point = 250 °C.

Key Insight-6

The efficiency of the reactor is higher at lower pressures due to higher methanol production and lower power requirement. At 35 Bar it is 43.2% as compared to 34.7% at 50 Bar. Similarly the heat exchanger performance also increases with pressure decline due to decreasing power input, as well as low mass flow, promoting heat transfer.

4.4. Experiments with pure hydrogen

All previous experiments showed the importance of mass flow rate as an important parameter for methanol yield. To understand this behaviour better, experiments were conducted with pure hydrogen at different pressures and the same temperature set-point (250 °C). The use of pure hydrogen as the working gas removes the exothermicity of the synthesis reaction from the picture. When there is no reaction going on in the reactor, dynamics can be closely observed and there are no condensed products. It is also important to know the flow behaviour in the reactor with pure hydrogen because it is used to activate the fresh catalyst and also before every startup operation. The reactor was

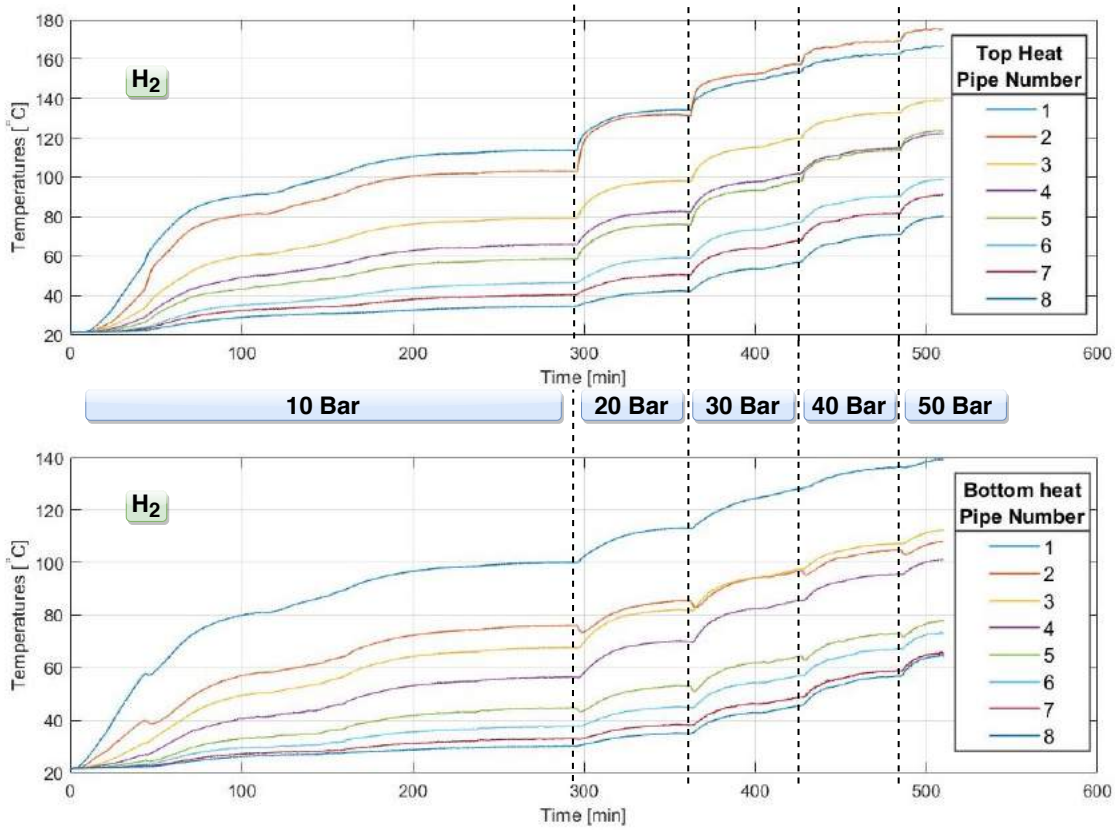

Figure 4.10: Top and bottom heat pipe temperature variations with pressure with H_2 as working gas. Experimental conditions: P = variable, Feed Gas = H_2, Heater set-point = 250 °C.

filled up with H_2 up to 10 Bar and was allowed to attemperate to steady state keeping the heaters at 250 °C. Hereafter, the pressure was raised in steps of 10 Bar and temperature measurements were conducted.

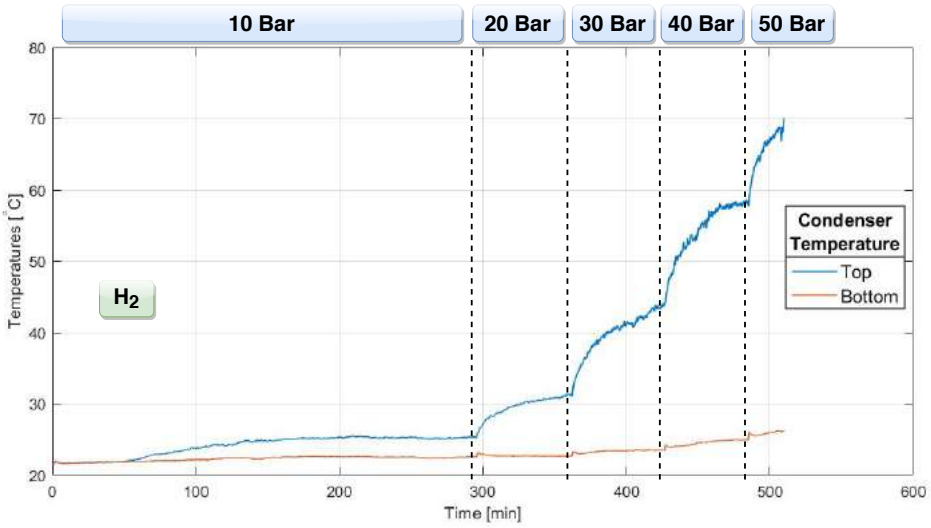

Figure 4.11: Top and bottom condenser temperature variations with pressure with H_2 as working gas. Experimental conditions: P = variable, Feed Gas = H_2, Heater set-point = 250 °C.

Figure-4.10 shows the observed behaviour. It was observed that at different pressures the heat

pipes attained different states indicating a different flow behaviour at every pressure. In the initial stages, the reactor tries to attain the heater set-point and the temperature rise of the heat pipes is mostly due to conduction through the Tri-Clamp pipes. It is evident by the linear nature of the temperature rise as well as the bottom heat pipe temperatures being higher than their top counterparts because they are closer to the heaters. After 50 minutes some non linear rise in the temperature was

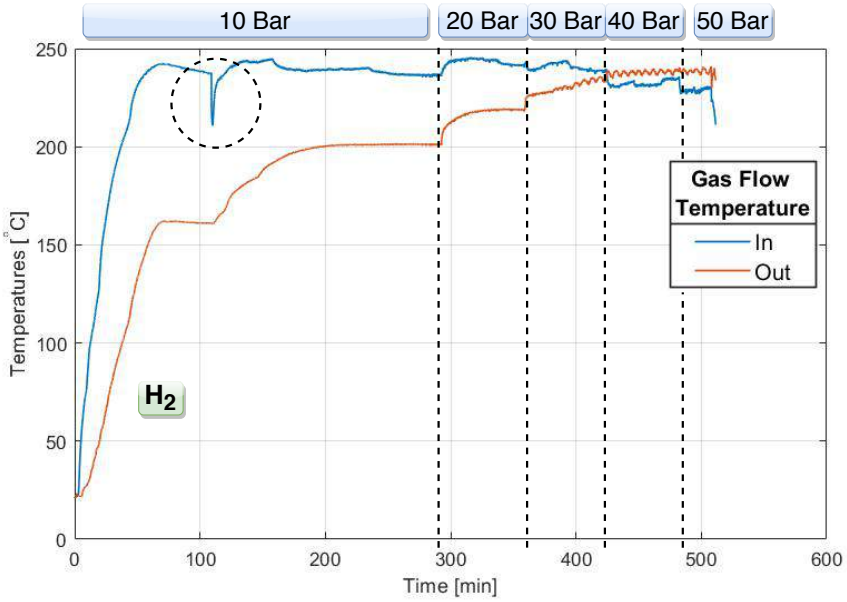

Figure 4.12: Gas inlet and outlet temperature variations with pressure with H_2 as working gas. The circle in the graph is the point where the heater set-point was accidentally set to 0 °C. Experimental conditions: P = variable, Feed Gas = H_2, Heater set-point = 250 °C.

seen indicating some convective flow inside the reactor. It is the same time when the top condenser temperature also starts to rise, as seen in figure-4.11. Both the condenser temperatures were earlier at room temperature, since no gas flow from the hot section was received till this point. Even though there was a temperature rise it was still quite low, indicating very less amount of H_2 reaching the condenser. Figure-4.12 shows that the gas inlet temperature at this point was 240 °C. At this point it must be brought to mind that the initial procedure suggested for catalyst activation was to run the reactor at 5 Bar and 250 °C heater set-point. As a result of this experiment it can be seen that those conditions would lead to a very low and non-homogeneous mass flow of H_2 over the catalyst bed. Therefore, the bed will be rendered partially inactive and will get activated later on when feed gas is injected at 50 Bar. Higher pressures are required to create a homogeneous mass flow of H_2 through the bed so that the entire bed can be used for methanol production later.

As the pressure was increased further, the rise in mass flow rate caused the heat pipes and condenser to attain higher temperatures. This operation had a negative impact on the gas inlet temperature as more H_2 flow was able to pass through the bed leading to less stagnation at the inlet. Consequently, it can be seen in figure-4.12 that the gas outlet temperatures constantly increase with pressure rise. When the pressure was raised to 40 Bar, the gas inlet temperature dropped below the gas outlet, indicating a proper H_2 flow build up inside the reactor with no stagnation at the inlet. This is in agreement with the previous observations using the premixed gas bottle and variable pressure, where it was seen that the stagnation starts to happen at around 35 Bar. Since, this experiment was conducted with a pressure increment of 10 Bar, it was expected that this point would lie between 30-40 Bar.

The mass flow rate and power consumption as a function of pressure for this experiment is presented in figure-4.13a and 4.13b. As discussed above the mass flow rate can be seen increasing

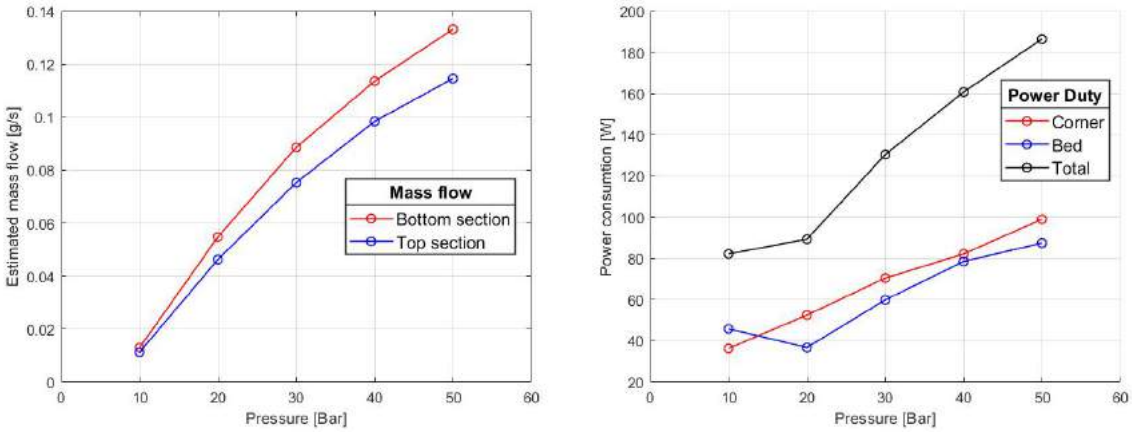

(a) *Mass flow rate of the top and bottom heat pipe section.*

(b) *Corner and Bed Duty*

Figure 4.13: Variation of mass flow and power consumption as a function of pressure. Experimental conditions: P = variable, Feed Gas = H_2, Heater set-point = 250 °C.

monotonically with increase in pressure. When the pressure is as low as 10 Bar, it was observed that both the estimated mass flows are identical. This can be understood by considering that when the mass flow is extremely low, the gas circulation is not enough to raise the temperature of the cold section. The temperatures of the cold section are so less that there is negligible heat loss to the environment. As discussed earlier, there is always heat loss from the top and bottom section which can be assumed to be equal. As such, the top section loses some heat due to heat pipes and losses to environment. On the other hand the bottom section gets heat from the top section and loses some heat to the environment. For mass flow rate estimation only heat pipe duty is considered. Therefore, the top section always underestimates the flow, while the bottom section always overestimates the flow. When the losses to the environment are negligible they estimate the same value. As their temperatures increase due to better circulation, their mass flow estimation start to diverge, which is seen in figure-4.13a. In figure-4.13b it can be seen that the power consumption rises due to more power required to heat the increased flow. Although, at 20 Bar it is seen that bed power requirement goes down. This is because hot pocket of some gas at the inlet gets displaced into the bed section, as also seen in figure-4.12 in the 20 Bar range.

KEY INSIGHT-7

5 Bar H_2 was seen to be insufficient to cause enough circulation inside the reactor, as opposed to the procedure suggested by the catalyst manufacturer. Instead atleast 35 Bar pressure is needed for H_2 to circulate properly and achieve catalyst activation.

4.5. EXPERIMENTS WITH VARIABLE FEED GAS COMPOSITION

After examining the behavior of reactor at constant compositions, experiments were conducted with different compositions, keeping the pressure and temperature set-point constant. The composition was varied by changing the opening times of H_2 and CO_2 valves during feed injection. As discussed earlier, every liquid sluicing operation carried out at 50 Bar after level sensor actuation, gives 5.6 mL of condensate output. Therefore, the frequency of sluicing, apart from methanol quality is the major deciding factor for determining the STY. After some time the methanol quality approaches stable values around the optimum (0.5 mol%) and the frequency becomes the only deciding factor. It was seen during the preliminary experiments that at different compositions, the time difference between each sluicing operation was stretched from 15 mins, which is optimum, to 90 mins. Such high intervals made it difficult to get STY data for steady states at every composition.

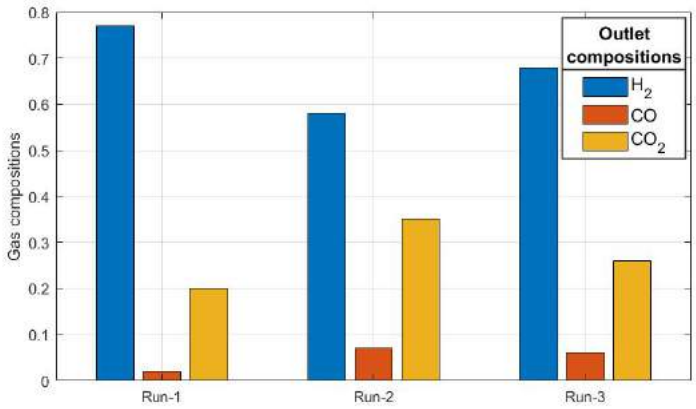

Figure 4.14: Initial composition measurements at the reactor outlet for different runs. Reactor was filled using separate cylinders using same valve opening time ratio of H_2 : CO_2=100 : 110 ms.

Another problem with such an experiment was the runaway of any reactant. By adjusting the valve opening times, an offset in the composition of H_2 and CO_2 can be created but since, the reactants are consumed at only stochiometric ratio (3:1), it always leads to excess buildup of one of the reactants. Therefore, for constant operation it is required that the reactor be injected with offset composition initially, but thereafter be given stochiometric feed to keep the composition stable. Even after several attempts to establish a constant composition, it could not be achieved and the reactor always showed excess reactant buildup after some time. This can be due to two reasons. Firstly, since the control system operated the valves in a small range of 50-100 ms, it may not have been able to do so accurately for every operation. Secondly, since the CO_2 cylinder can only be obtained for 54 Bar at ambient temperature, it may not be able to provide stable gas flow for every valve operation.

Figure-4.14 shows this behaviour. The reactor was filled multiple times with H_2 and CO_2 from separate cylinders using the same valve opening ratio of H_2 : CO_2=100 : 110 ms. A gas sample was taken after waiting for 10 mins and analysed using the Gas Chromatograph. It can be seen from figure-4.14 that the initial composition is different in every experiment even though the procedure for gas injection was the same. Improper mixing of the gases can be ruled out, because the reactor exhibited internal circulation behaviour, and the gases should mix properly after passing through several copper meshes in the heat integration section.

KEY INSIGHT-8

The flow through the valves could not be estimated theoretically but rather needs to be determined empirically. High valve opening times (>1000 ms) lead to violent gas injection that may unsettle the catalyst bed. Low valve opening times (<1000 ms) makes it difficult for the controller to operate consistently. The gas flow through the valve needs to be reduced, so that the opening times can be increased for the controller to handle it properly

4.5.1. dP/dt AS A PROXY FOR METHANOL YIELD

To circumvent the problems mentioned above, a different approach was tried. Figure-4.15 shows the pressure response of the system for a reactor run. In this experiment the reactor was heated till 250 °C, so that it produced methanol at steady state, and thereafter, the heaters were turned off while still feeding the reactor. It can be expected that as the bed cannot maintain the reaction temperature for long, the reaction rate goes down. As seen in the figure-4.15, the reduction in reaction rate is apparent by the decrease in the pressure derivative (dP/dt). As time progresses, it takes longer for

the pressure to drop by the same amount and eventually the curve becomes flat.

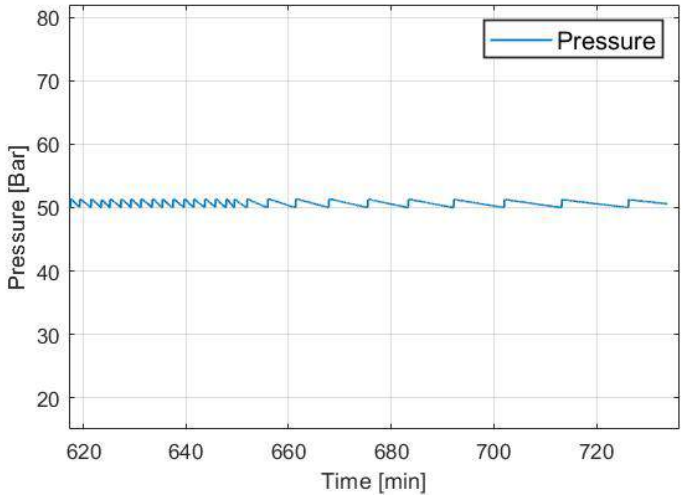

Figure 4.15: Variation of pressure gradients with reaction rate. Feed: H_2:CO_2=3:1, Heater set-point=250 °C.

Figure-4.16 shows the Space Time Yield as a function of pressure for premixed gas cylinder experiments (also discussed earlier in figure-4.6). Apart from that, dP/dt values at the respective pressures have also been plotted. The two graphs show remarkable resemblance and the dP/dt follows the trend of STY graph.

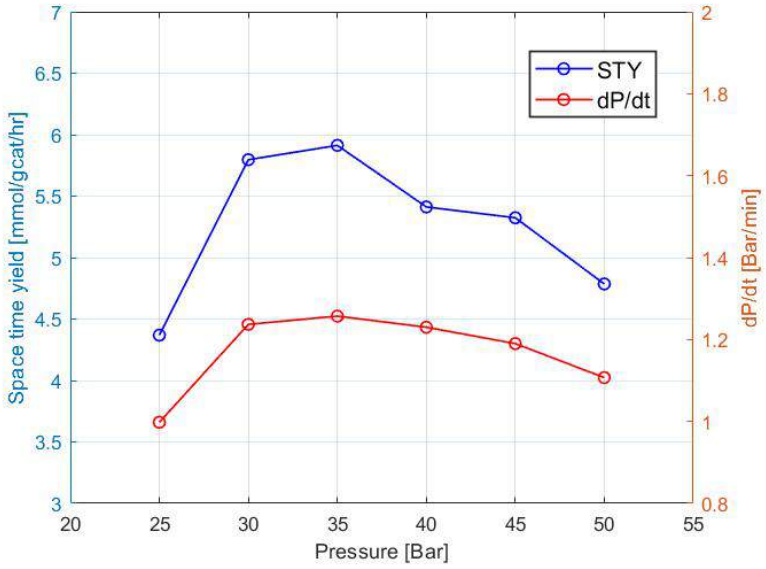

Figure 4.16: Comparison of variation in STY and dP/dt of reactor operation with different pressure. Feed- H_2 : CO_2=3 : 1, heater set-point=250 °C.

KEY INSIGHT-9

dP/dt can be used as a proxy for determining trends in Space Time Yield, for cases where getting a yield is time consuming and impractical. One cycle of pressure response is enough to comment on the instantaneous methanol production and be used as a monitoring criteria for performance.

4.5.2. Estimation of methanol yield through dP/dt data

Since, it was established that the dP/dt trends follow closely the Space time yield trend, the correlation between them was worked out. The reactor volume is always fixed. The observed reduction in pressure is due to the reduction in number of moles of gas inside the reactor. As 1 mole of CO_2 reacts with 3 moles of H_2, 1 mole of methanol and water each are formed in vapor phase. The reaction products quickly undergo phase change to liquid, due to the temperature gradient in the reactor and therefore, can no longer exert pressure. As a result the effect of one reaction is to remove 4 moles of gas from the reactor. The data regarding rate of pressure decline is effectively stored in the dP/dt curve. Since, both cylinders were maintained at constant pressures and feed valve opening times were fixed, every valve operation at same pressure set-point, led to the same final pressure inside the reactor (P_1). The pressure P_2, after one second was calculated using the dP/dt data as shown in equation-4.4.

$$P_2 = P_1 - \left[P_1 \times \frac{dP}{dt} \times \frac{10^5}{60} \right] \tag{4.4}$$

$$n_1 = \frac{P_1 \times V_{reactor}}{Z \times R \times T_{Avg}} \tag{4.5}$$

$$n_2 = \frac{P_2 \times V_{reactor}}{Z \times R \times T_{Avg}} \tag{4.6}$$

$$n_{MeOH} = \frac{\Delta n}{4} \tag{4.7}$$

$$STY_{predicted} = \frac{n_{MeOH}}{g_{cat}} \times 3600 * 1000 \tag{4.8}$$

Where,

P_1	= Pressure inside reactor after each valve operation [Pa],
P_2	= Pressure inside the reactor after 1 second [Pa],
dP/dt	= Pressure derivative at that instant [Bar/min],
n_1	= Number of moles of gas inside the reactor at P_1 [mol],
n_2	= Number of moles of gas inside the reactor at P_2 [mol],
$V_{reactor}$	= Volume of reactor [1.42×10^{-3} m^3],
Z	= Compressibility factor of gas mixture [by COCO, REFPROP],
R	= Gas constant [8.314 J/mol/k],
T_{avg}	= Average gas temperature in the reactor [K],
n_{MeOH}	= Number of moles each of methanol and water formed [mol],
g_{cat}	= Catalyst weight used in the reactor [120 g],
$STY_{predicted}$	= Estimated space time yield through dP/dt [mmol/g_{cat}/hr]

Using equation-4.5 and 4.6, the number of moles of gas mixture inside the reactor was calculated. Since, every 4 mole reduction in the pressure corresponds to 1 mole of CO_2 hydrogenation, The number of moles of methanol production, and thereafter, space time yield was estimated using equations-4.7 and 4.8. Figure-4.17, shows the comparison between the predicted STY and the experimentally determined STY of the same experiment shown in figue-4.16,4.6. It can be seen that the predicted values are very close the experimental. The same method was used to predict the experimentally unknown STY of the experiment mentioned in figure-4.15. The reactor gas composition was measured ($H_2 : CO_2$=55 : 45 vol%), and the heater power supply was completely turned OFF. It can be seen in figure-4.18 that the predicted STY was around 3 before the heaters went OFF. As the reactor fails to maintain the temperature of the bed, the predicted STY drops quickly.

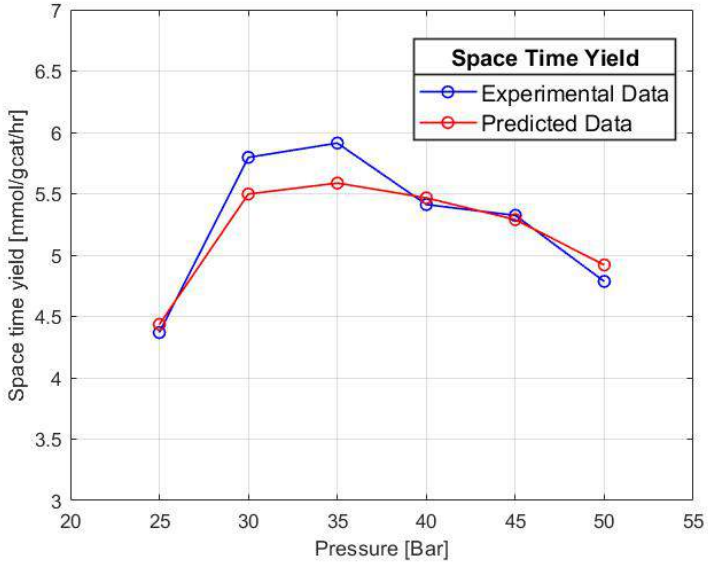

Figure 4.17: Comparison of experimentally and theoretically determined space time yield for methanol. Heater set-point = 250 °C.

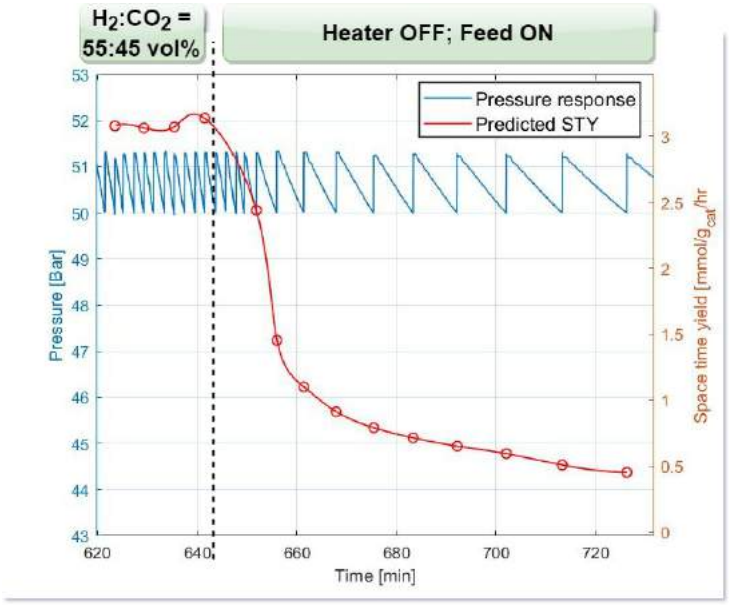

Figure 4.18: Comparison of experimentally and theoretically determined space time yield for methanol.

KEY INSIGHT-10

dP/dt can be used to predicted the methanol production using the gas law for cases where experimental data is unknown. The match between experimental and predicted data also provides evidence for the accuracy of data acquisition system. It was also seen that for the above experiment, the STY dropped by 80% within 120 mins of power supply cut off.

4.5.3. Experiments with continuously varying compositions

Since, a way to estimate the STY is established, experiments were conducted with continuously varying compositions where continuous STY measurements were not possible. The reactor was

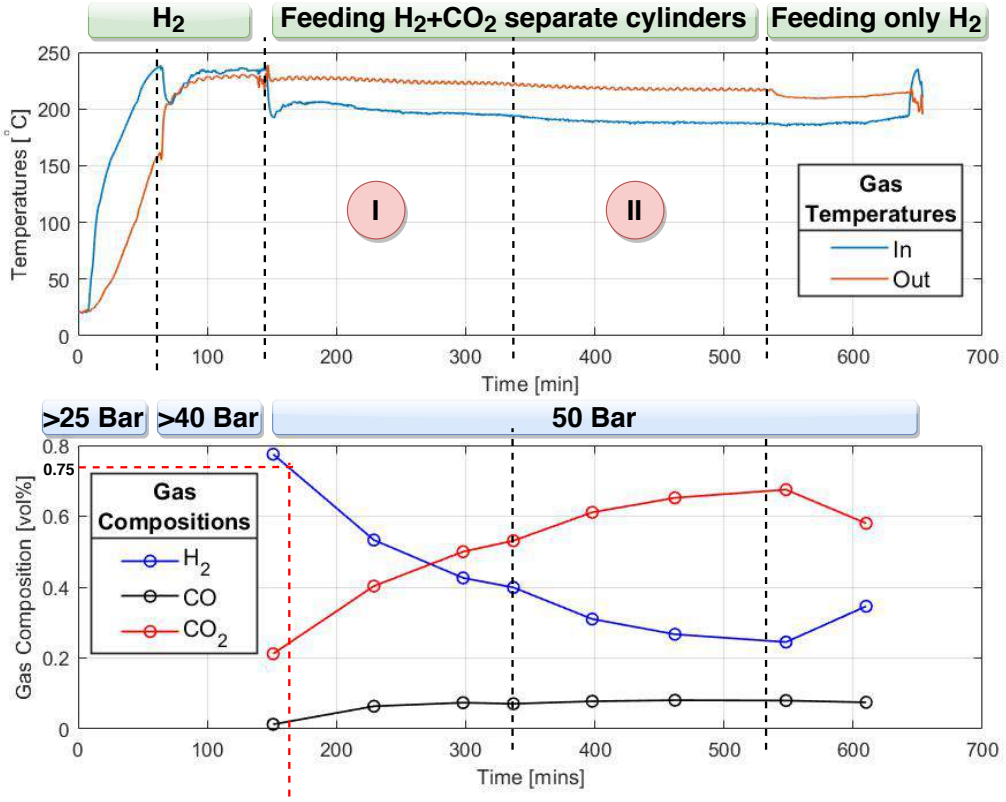

(a) *Variations in Gas inlet and outlet temperatures with time compared against gas inlet composition.*

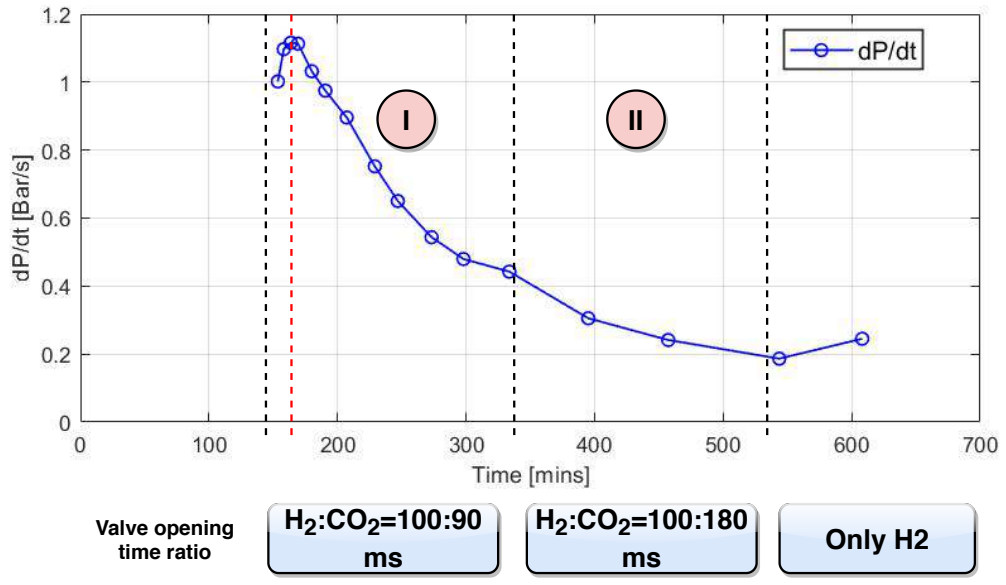

(b) *variation in pressure derivative with time.*

Figure 4.19: Plot for gas inlet and outlet temperatures compared against the pressure derivative and composition of gas at the inlet. Experimental conditions: P=50 Bar, Feed Gas = H_2 : CO_2=variable, Heater set-point = 250 °C.

heated with heater set-point of 250 °C, after which H_2 and CO_2 were fed at 50 Bar by two separate gas cylinders. Figure-4.19a shows the gas inlet and outlet temperatures compared against the gas inlet compositions at different times during the experiment. The ratio of valve timings in region-I was $H_2 : CO_2$ = 100 : 90 ms. It can be seen that the initial composition was $H_2 : CO_2 : CO$ = 77 : 22 : 1 vol% which is very close to the stochiometric composition. Moreover, it shows trace amount of CO formation due to the RWGS reaction. As time progresses the composition of H_2 goes down against CO_2 because of CO_2 overfeeding. In region-II the valve timings were changed again to $H_2 : CO_2$ = 100 : 180 ms which is immediately seen in the gas composition measurements. The CO_2 cylinder was closed shut after 537 mins, because of which the H_2 composition starts rising again.

Figure-4.19b shows the pressure derivative plotted against time for the same experiment. The dP/dt values follow the same trend as the H_2 composition for most of the reactor run except, when the H_2 composition crosses 75 vol%. The dP/dt values reach a maximum at $H_2 : CO_2 : CO$ composition of 75 : 23 : 2. It must also be noted that dP/dt value at 75 vol% H_2 is the same as shown earlier in figure-4.16, when premixed gas at stochiometric composition ($H_2 : CO_2$=75 : 25 vol%) was supplied from a premixed cylinder at 50 Bar. Similar works in literature, done by Ipatieff & Monroe [62] suggests that the decrease in yield in not due to another product being favored other than methanol, but rather due to H_2 being the limiting reactant.

Figure-4.20 shows the predicted STY for the experiment using the dP/dt values of figure-4.19b. It can be seen that the STY at stochiometric composition of $H_2 : CO_2$ = 75 : 25 vol% (red dashed line) is 4.98 which is close to the experimental value (4.84) observed earlier. Moreover, it can also be seen that the predicted STY at a composition of $H_2 : CO_2$ = 55 : 45 vol% (dashed circle) is 3.1, which is again close to the value predicted in figure-4.18. Even though both values are predicted STYs and not experimentally determined, the experiments are different, and yet the dP/dt data is consistent.

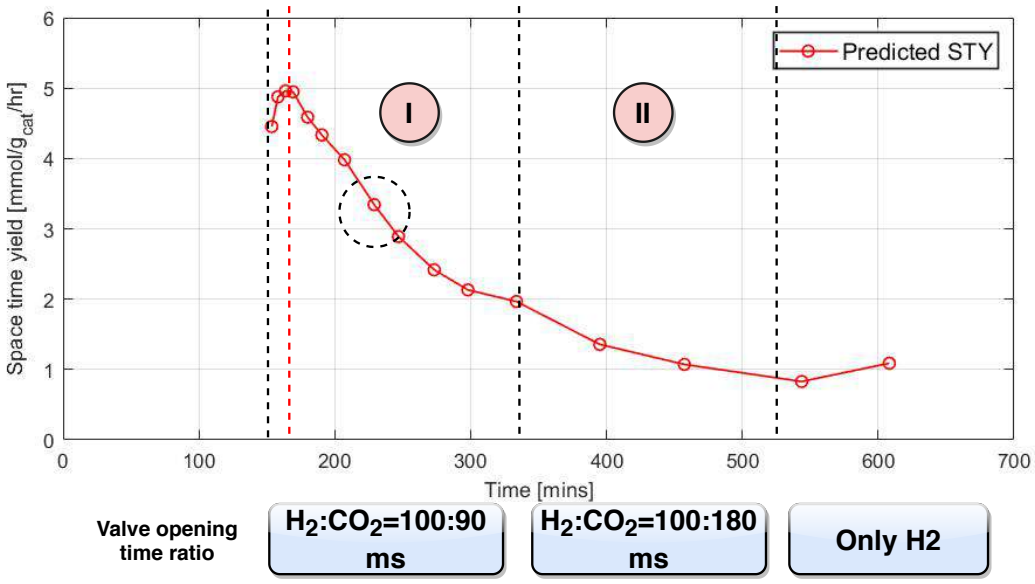

Figure 4.20: Estimated STY of the reactor through dP/dt values. Experimental conditions: P=50 Bar, Feed Gas = $H_2 : CO_2$=variable, Heater set-point = 250 °C.

Figure-4.19a also shows that even though the reactor control parameters are constant (Pressure=50 Bar, Heater set-point=250 °C), the gas inlet and outlet temperatures go down continuously. This can be explained by observing the internal mass flow rates, which should increase to cause such an effect. The reduction in methanol production also promotes lower temperature due to lesser heat of reaction, but that can only affect outlet temperatures. It can be seen in figure-4.21, that the estimated mass flow rate goes up as the compositions changes towards a CO_2 rich mixture,

which puts more work on heaters and reduces the temperature. This points towards the fact that a constant heater set-point can not sustain a constant gas inlet temperature at varying compositions. The mass flow rates that use heater duties ($\dot{m}_{bed}$, $\dot{m}_{2,HP}$) for calculations, exhibit fluctuations in the

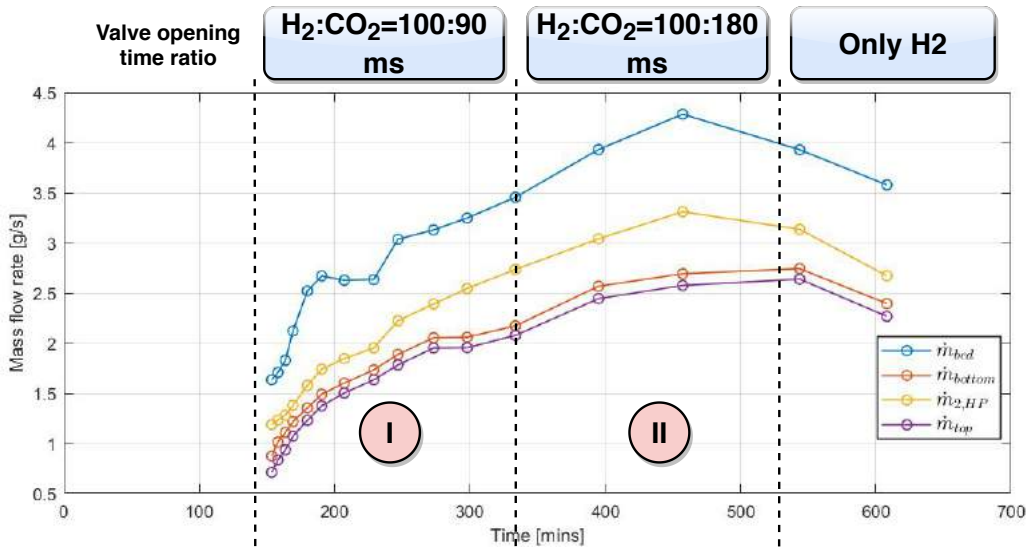

Figure 4.21: variation of estimated mass flow rates in the reactor with time. Experimental conditions: P=50 Bar, Feed Gas = H_2 : CO_2=variable, Heater set-point = 250 °C.

beginning. This is because, the gas was fresh inside the reactor after pressurizing to 50 Bar, so the heater duty was high. Ideally this should be estimated at steady states, but it was not possible as the gas composition was rapidly changing.

KEY INSIGHT-11

The dependence of mass flow rate on pressure was already observed with premixed cylinder experiments. But the composition also has a huge impact on the mass flow rate even though the pressure is same. The control system was unable to maintain constant gas inlet temperatures with changing compositions.

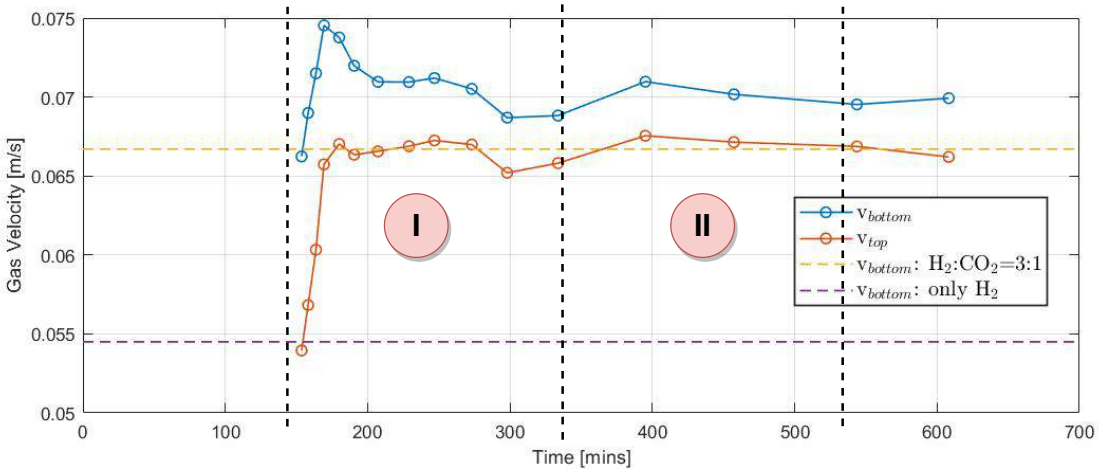

Figure 4.22: Variations in estimated gas velocities inside the reactor with time. P=50 Bar; $T_{heaters}$=250°C for all plots.

The specific heat capacity of the gas mixture in this experiment also goes down as the mixture becomes more CO_2 rich. This is the reason for the observed mass flow rise, as c_p has an inverse rela-

tionship with it. Unlike the constant gas mixture experiments discussed earlier, in this experiment, even though the mass flow rate is increasing, it is not an indicator for gas velocity inside the reactor. Because for the constant mixture experiments shown in figure-4.13a and 4.7a, the specific heat capacity of the gas mixture was always constant. Therefore, the mass flow was an indicator for gas flow velocity and hence, residence time at heaters (equation-4.9). Lower the mass flow rate became, higher was the residence time and hence, gas flow temperatures increased. Figure-4.22 shows the estimated gas velocities for the varying composition experiment. For clarity, only the mass flow rate estimated by the bottom heat pipe section was used. Counterparts of gas velocities from the pure H_2 experiment and premixed cylinder experiments at 50 Bar are also shown for reference. It was observed that the velocities show very less variation throughout the experiment. Therefore, it can be concluded that the reduction in gas inlet and outlet temperatures has very limited dependence on residence time. It also gives an indication for the highest possible velocities in the reactor. The velocity for pure H_2 was low because it is less dense, and therefore, has the least driving force for natural convection at comparable temperature gradients.

$$v_{gasflow} = \frac{\dot{m}_{reactor}}{A_{cross} \times \rho_{gas}} \tag{4.9}$$

Where,

$v_{gasflow}$ = Estimated gas flow velocity in the condenser section [m/s]
$\dot{m}_{reactor}$ = Estimated mass flow rate inside the reactor by bottom heat pipe section [Kg/s].
ρ_{gas} = Density of the gas mixture [Kg/m^3].
A_{cross} = cross sectional area of the condenser where there are no meshes [m^2].

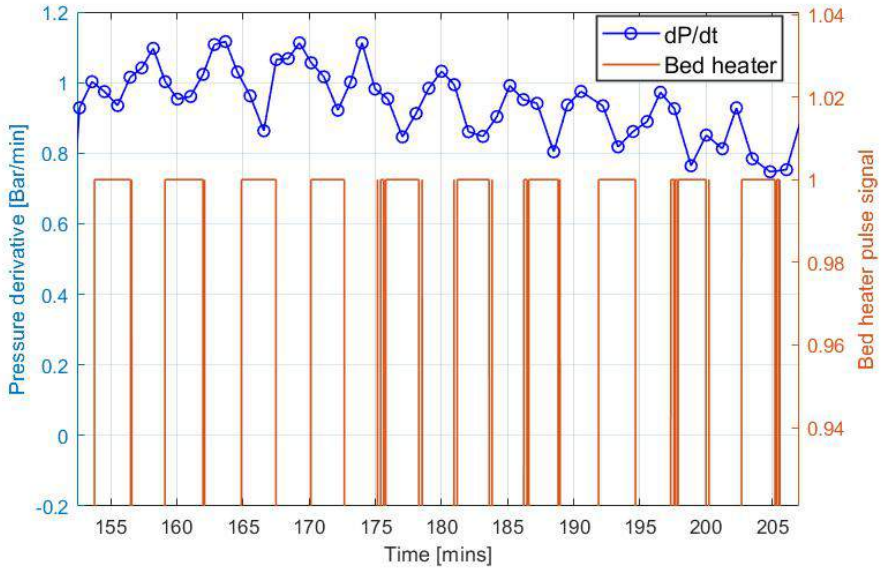

Figure 4.23: A section of continuous plot of dP/dt values compared against heater pulses. Experimental conditions: P=50 Bar, Feed Gas = H_2 : CO_2=variable, Heater set-point = 250 °C.

The dP/dt variation against time as shown in figure-4.19b only shows values against specific times that the gas composition measurements were also done. Figure-4.23 shows a section of continuous changes in dP/dt values against time and bed heater power supply signal (1 meaning heater ON) as obtained from MATLAB. It was seen that the actual dP/dt response of the reactor had periodic rise and falls. When compared to the bed heater power supply signal, it showed complete

agreement. As the PID controller (Proportional Integral Derivative) tries to attain the bed heater set-point (250 °C), it repeatedly controls the heater relays in a periodic manner based on the feedback provided by the temperature sensors. It can be seen that dP/dt signal starts to rise every time after the heaters are turned ON and vice versa with a slight delay that is due to thermal inertia. The number of data points in the dP/dt signal between subsequent rise and fall also indicates that it is not just a noise in the data acquisition circuit. This plot emphasizes the instantaneous correlation between the bed temperature and reaction kinetics which affects the instantaneous yield.

KEY INSIGHT-12

The reduction in gas inlet and outlet temperatures is not limited by residence time as in case of the premixed cylinder experiments at varying pressures. A characteristic gas velocity value inside the reactor is around 0.07 m/s in a naturally convecting flow for future model requirements. The STY values predicted by dP/dt measurements, shows fluctuations consistent with heater operation, when looked at more closely.

5

Conclusions and Recommendations

"No matter how many instances of white swans we may have observed, this does not justify the conclusion that all swans are white. To conclude is to not mix the truth with falsehood or conceal the truth while you know it. "
-Karl Popper-

5.1. Conclusions of Experiments

The objective of this thesis was to observe the reactor behaviour in transient conditions. The transient scenarios along with key performance criterias have already been formulated and discussed earlier.

1. **What is the reactor characterization with the current enhancements in the design?**

   Experimental conditions: Pressure = 50 Bar; Gas used: $H_2 : CO_2$ = 75 : 25 vol%; Heater set point = 250 °C; Catalyst: $Cu/ZnO/Al_2O_3$.

   The methanol output of the reactor at the above mentioned experimental conditions was **4.8 mmol/g_{cat}/hr** or **18.61 g/hr**. This is slightly higher than van Laake[17], which was at 4.1 mmol/g_{cat}/hr, due to better heating of reactants before they enter the catalyst bed. The mass flow rate of CO_2 and H_2 required to achieve this production was **25.73 g/hr** and **3.54 g/hr** respectively. These flow rates point towards a carbon conversion efficiency of **99.3%**. Some amount of CO_2 is always lost as dissolved CO_2 in water due to high pressures and also to by-product formations. The reactor produces first methanol after **182 mins** of start up with a low quality of **0.256 mol%** due to partial catalyst deactivation at night. The quality improves with time and after 2.5 hrs was seen to peak at **0.495 mol%**. The quality of first methanol was seen to increase (0.415 mol%) if the reactor was operated with pure H_2 feed, 30 mins before shutdown in the previous run.

   The characteristic inlet and outlet gas temperatures were seen to be 206.1 °C and 224.1 °C, respectively with the help of new gas flow sensors, which are lower than the reactor wall temperature (250°C). The reactor mass flow rate was **1.1 g/s** at experimental conditions. The total power duty was **156.3 W**, which is higher than van Laake[17] (125 W). But this is due to the addition of corner heaters, as the bed heater duty was seen to be lower at **58.5 W**. This shows that **62.5%** of the power was used to heat the reactant gases at inlet. The heat of reaction (**6.85 W**) was low compared to heater input.

   The heat pipe duty with the new heat integration system was **155.3 W**, which gives a heat exchanger efficiency of **48.76%**. This is higher compared to the single heat pipe system of van Laake[17] (32.3%).

2. **What is the effect of lowering the pressure on reactor performance with premixed gas cylinder?**

   Experimental conditions: Pressure = 50 Bar to 25 Bar; Gas used: $H_2 : CO_2$ = 75 : 25 vol%; Heater set point = 250 °C; Catalyst: $Cu/ZnO/Al_2O_3$.

   The reactor methanol production slightly increased from **4.8 mmol/g_{cat}/hr** at 50 Bar to **5.96 mmol/g_{cat}/hr** at 35 Bar. Upon further decreasing the pressure it dropped again from 5.96 mmol/g_{cat}/hr at 35 Bar to **4.36 mmol/g_{cat}/hr** at 25 Bar (figure-4.6). This is in direct conflict with the existing understanding of the methanol synthesis process. At thermodynamic equilibrium, methanol yield should be lowered upon decreasing the pressure.

   A key assumption in the above reasoning, which is often overlooked is that it assumes thermodynamic equilibrium in the reactor. In reality, methanol reactors are not at perfect thermodynamic equilibrium. In these cases, it often falls under the analysis of whether the yield is thermodynamically, kinetically, or stochiometrically limited. Since the reactor was given a feed from a premixed cylinder, which provided the exact molar ratio of reactants as they were needed, it can be ruled out that the yield is not stochiometrically limited at these conditions.

   Further analysis of the mass flow rate estimations suggested that the internal mass flow rate of the reactor dropped from **1.1 g/s** at 50 Bar to around **0.72 g/s** at 25 Bar. This observation has 2 implications:

   (a) Reduced mass flow rate at a constant composition (which means almost constant c_p), leads to reduced load on the heaters. This helps to regulate the temperature set-point quicker.

   (b) Reduced mass flow also means higher residence time at the heaters due to which heat transfer is enhanced.

   Because of the above two reasons it was observed that the the reactor inlet temperatures increased from 208 °C at 50 Bar to 234 °C at 25 Bar. The increase in temperature of gas at the reactor inlet indicated better kinetics of the synthesis reaction. As a result the methanol production was observed higher. In response to this, the gas outlet temperature of the reactor also raised from 225.5 °C at 50 Bar to 237.5 °C at 35 Bar, and further to 241 °C at 25 Bar (figure-4.7b).

   Below, 35 Bar the reactor yield decreased again. Since the reaction is exothermic, the rate of gas outlet temperature rise was slowed down below 35 Bar (see figure-4.7b). This indication is supported by the lowering of methanol production below 35 Bar. Although, at the same time the gas inlet temperature kept rising at the same rate. It was concluded that the reaction was limited by the mass flow into the catalyst bed below 35 Bar. As the pressure decreases, it affects the density of the gas. A less dense gas reduces the driving force for natural convection by buoyancy. The pressure drop across the bed and the copper meshes in the reactor pipe is still unknown due to its complex geometry and random nature. But, with that said, it was observed that below a pressure of 35 Bar, the driving force for natural convection was not able to overcome the pressure drop inside the reactor. This led to partial choking at the reactor inlet, which explains the reduced mass flow into the bed and gas outlet rate of temperature rise.

   Due to reduced mass flow it was observed that heater power requirement was reduced from 156.3 W at 50 Bar to 102.9 W at 25 Bar (figure-4.8b), which also validates the above assumptions about mass flow rate. As a result of the decrease in power requirement and increase in production, the energy efficiency was seen to increase from 34.7 % at 50 Bar to 43.2 % at

35 Bar (figure-4.9a). Due to decrease in production below this point, it was again seen to drop to 40.7 % at 25 Bar.

Based on the above mentioned evidences it was concluded that, at these experimental conditions, the reactor yield is kinetically limited. After the mass flow and gas inlet temperature limitations have been optimized in future, thermodynamic equilibrium can be expected to exert its effect prominently after lowering the pressure. The RWGS reaction is not dependent on pressure, thus it was seen that the CO composition remained the same throughout the experiment at 4 vol% (5 tested samples) and can be concluded to have reached equilibrium. Even though it is an endothermic reaction, it is a stronger function of CO_2 concentration in the feed, which stays constant throughout the experiment.

3. **What is the reactor performance with continuously changing feed gas compositions?**

   Experimental conditions: Pressure = 50 Bar; Gas used: $H_2 : CO_2$ = 80 : 20 vol% to $H_2 : CO_2$ = 20 : 80 vol%; Heater set point = 250 °C; Catalyst: $Cu/ZnO/Al_2O_3$.

   The methanol yield from the reactor became kinetically as well as stochiometrically limited on both sides of the ideal composition of $H_2 : CO_2$ = 75 : 25 vol%. The rate of pressure decline in the reactor (dP/dt) was correlated with the space time yield and a detailed plot for it was obtained at every composition (Figure-4.20).

   The methanol yield at $H_2 : CO_2$ = 75 : 25 vol% when mixed manually by separate cylinders (**4.92 mmol/g_{cat}/hr**) was seen to match the experimental observations from the premixed cylinder earlier (**4.84 mmol/g_{cat}/hr**). Additionally, the methanol yield from a different experiment at a measured gas composition of $H_2 : CO_2$ = 55 : 45 vol% (**3.02 mmol/g_{cat}/hr**, figure-4.18) also matched with the value obtained for this experiment (**3.1 mmol/g_{cat}/hr**). Therefore, **a method to determine the space time yield of methanol by just observing one cycle of rate of pressure decline (which takes on an average 45 s) was deduced and validated through experiments**.

   Apart from affecting the methanol yield, the change in gas composition had an effect on the mass flow rate. As the gas became increasingly CO_2 rich, the estimated mass flow rate in the reactor was seen increasing (figure-4.21). The increasing mass flow had an impact on the heater load, and the gas inlet and outlet temperatures were both seen decreasing (figure-4.19a) as the gas became CO_2 rich. It was concluded that the mass flow inside the reactor gets affected by both pressure (Research question-2) as well as gas composition, and thereafter, it affects the gas inlet temperatures.

   Moreover, instantaneous effects of bed temperature on the methanol yield were also detected and reported. The frequency with which the PID controller turns the heaters ON and OFF in order to maintain the set-point, was seen to be same as the frequency with which the dP/dt and hence, the methanol production rate fluctuates (figure-4.23).

OTHER CONCLUSIONS:
Some other conclusions from the reactor that were observed, but not pursued thoroughly due to being out of scope of the test plan are:

1. **Experimental Conditions:** Pressure = 50 Bar; Gas used: $H_2 : CO_2$ = 75 : 25 vol%; Heater set point = 250 °C; Catalyst: $Cu/ZnO/Al_2O_3$; Reactor tilt = 30°.
   When the reactor tilt was set to 30°, the driving force for convection was reduced to such an extent that, sometimes no mass flow was seen even after pressurizing to 50 Bar. On the other hand, for normal reactor tilt (20°) used for all other experiments, circulation was seen

immediately after raising the pressure above 35 Bar. This was in line with the findings of van Laake[17] who showed that higher reactor tilt was conducive to less circulation.

2. **Experimental Conditions:** Pressure = 50 Bar; Gas used: $H_2 : CO_2$ = 75 : 25 vol%; Heater set point = 250 °C; Insulation: Rockwool/PTFE+Rockwool.
The reactor was tested with 2 different types of insulation material. It was seen that the average heat up time of the reactor with only Rockwool insulation was 28 mins. However, when the Rockwool insulation was augmented by PTFE tape in the hot section, the same startup time was reduced to 13 mins. This was possible due to better insulation coverage possible with the PTFE tape for the complex geometry of the hot section. It is theorized that a very thin layer of air gets trapped between the reactor pipe and the PTFE tape, which provided the improvement in the insulation. Due to this the reactor was also able to retain the bed temperature above 200 °C for 25 mins, after the power supply was completely cut off.

3. **Experimental Conditions:** Pressure = 10 Bar-50 Bar; Gas used: H_2; Heater set point = 250 °C.
It was observed that 5 Bar hydrogen was not sufficient to cause enough circulation inside the reactor, that could provide homogeneous catalyst activation. Instead it was observed that at least 35 Bar pressure was needed to see the characteristic convective flow behavior in the reactor.

5.2. Recommendations for future experiments

The following recommendations are suggested for future experiments and improvements on the methanol reactor at ZEF:

1. **Experiments with current setup:**
A method of predicting the space time yield from dP/dt calculations has been suggested in the results. But due to temperature safety limitations, the experiment could not be conducted above the heater set-point of 250 °C. The activity of the catalyst is affected by the gas composition, and therefore, the temperature of maximum methanol production may change with composition. The current reactor needs to be operated at different temperatures to obtain their relation for optimization later on. The process to follow is:

   (a) Heat the reactor to the chosen temperature and fill it with 95% H_2 and 5% CO_2. Initially this can be done by filling the reactor in steps with the ratio of partial pressures required.

   (b) As the reactor starts making methanol, set the valve timing ratio to $H_2 : CO_2$ = 100 : 110 ms, which corresponds to CO_2 overfeeding. The composition of CO_2 will eventually rise in the reactor due to this.

   (c) Monitor the gas composition frequently, and obtain the dP/dt data, which can give the space time yield.

2. **Solenoid valve experiments:**
Theoretical calculations of gas flow rates through the valve orifice were not sufficient to predict the output composition. This may be due to problems with gas non ideality, fluctuations due to pipe friction, or controller malfunction. Empirical measurements of the discharge volume from valves can solve the problems with theoretical inaccuracy. Moreover, valve opening times of more than 1000 ms lead to violent gas injections, while lesser than 500 ms may cause controller problems (**Key Insight-8**). Therefore, the valve opening times need to increase, while at the same time flow rates be lowered. This can be done by using an augmented orifice in the Swagelok pipe connection. This may reduce the mass flow enough, so that the valves can be opened for 2 seconds without unsettling the catalyst bed. Such high operation times can be handled easily by the controller.

3. **HEAT INTEGRATION NETWORK :**
   Although, heat pipe as a medium of heat transfer is effective, it is not very reliable and robust (**Key Insight-2**). Heat pipes 2 and 5 were damaged during installation or operation and could not contribute to heat integration. Therefore, if considerable machining operation is needed, then heat pipes should be avoided in future designs. It should also be noted that if the heat pipes get knocked by a heavy tool while working on the reactor, the sintered wick lining may get damaged and block the liquid flow, rendering it useless. Dents were seen on both heat pipe 2 and 5 which may have been caused during assembly. Moreover, adding additional complexity to the reactor design creates problems with proper insulation.

   The method used by power plants for air preheating can be utilized and evaluated for the future designs. Such a design features the flow of outgoing hot and incoming cold gases over opposite surfaces of a conducting sheet of material. There are three benefits of this design:

   (a) It reduces the distance by which heat energy has to be transferred. If the distance is high, it only opens room for more heat losses to environment or higher cost of insulation, like in the case of current heat pipes.

   (b) It greatly reduces the complexity of the outer geometry. The outer geometry needs to be as simple as possible to facilitate easier insulation. It was extremely challenging to insulate the reactor with the current heat integration network. Proper insulation may even make up for slightly low heat transfer effectiveness in the reactor long run.

   (c) Such a design will also make use of counter current flow between gases that maximizes heat transfer.

4. **MASS FLOW RATE ESTIMATION:**
   The mass flow rate of the reactor is extremely delicate and is prone to fluctuations due to pressure, temperature gradient and feed gas composition variations. Effects of both pressure and composition variations on mass flow rate has been demonstrated earlier (**Key Insight-5, 11**). Therefore, the mass flow rate needs to be continuously monitored, in order to control the reactor operating parameters.

   The best way to non obstructively measure the mass flow rate inside the reactor is by selecting two points for which the gas flow temperature and heat flow between them is known accurately. The gas flow temperature sensors should also be distant from the heaters (**Key Insight-5**), so that they do not affect measurements. For the current reactor, heat pipe duty and catalyst bed insulation losses are not known with high accuracy, which comes forward as an area of improvements in reactor design.

   A solution may be obtained by building up on the idea presented above in the heat integration section, and the problem of not knowing the heat flow between the 2 temperature points. If the heat integration section is built by the above concept, then it just needs to be well insulated from the outside. That way, the heat transferred by the hot gas to the cold gas will still be unknown, but equal due to energy conservation. Four Gas flow temperature sensors instead to two, carefully placed at the inlets and the outlets of both these streams can be used to estimate the mass flow rate by an energy balance. Since the heat integration section will be away from the heaters, it will not affect the measurements, as is the case with the current reactor.

5. **MASS FLOW RATE REGULATION:**
   The adjustment of the reactor conditions (Temperature, Pressure, Composition) to achieve a certain mass flow rate is impractical. Therefore, an external mass flow control valve needs to be designed and implemented. An example is the butterfly valve shown in figure-5.1(Source[1]).

[1] https://valvesolutions.com/product/replaceable-seat-butterfly-valve-series-2200/

Such valves are available for the current Tri-Clamp pipe setup, but the pressure rating may not be suitable. Such valves can even be designed indigeneously by ZEF for implementation. In this way, the reactor can be designed for maximum driving force for convection, and when the flow is too much as sensed by the mass flow control system, it can be lowered according to the needs.

Figure 5.1: A simple design of Butterfly Valve.(Source in footnote)

6. **REACTOR CONTROL SYSTEM:**
The current control system of the reactor is designed in such a way that it can achieve any set-point of the heater temperature as long as it is below the safety limit (300 °C) of the sensors. While this is still good for the reactor bed to avoid catalyst sintering, it is not suitable for the corner heaters. The corner heater control system should be redesigned such that it regulates its heater set-point to achieve the desired gas inlet temperature. In the current system the heater set-point stays constant (250 °C) and the gas inlet temperatures can freely vary according to the internal mass flow rate in the reactor. Implementing the new design will make the reactor control system smarter, and lead to better experimental data.

7. **COMPOSITION FEEDBACK SYSTEM:**
It has been shown by experiments that, even if the reactor is to be operated at constant compositions, there is a need for frequent feedback from a compositions measuring system. Over time the reactor can show variations in gas compositions due to many reasons that account for carbon losses. For instance, if the reactor is fed with a constant ratio of H_2 and CO_2, then for every carbon lost by the system due to solubility in water, by products etc, it always gets supplied by excess H_2, which can eventually buildup inside the reactor.

A

VALVE BLOCK ITERATION

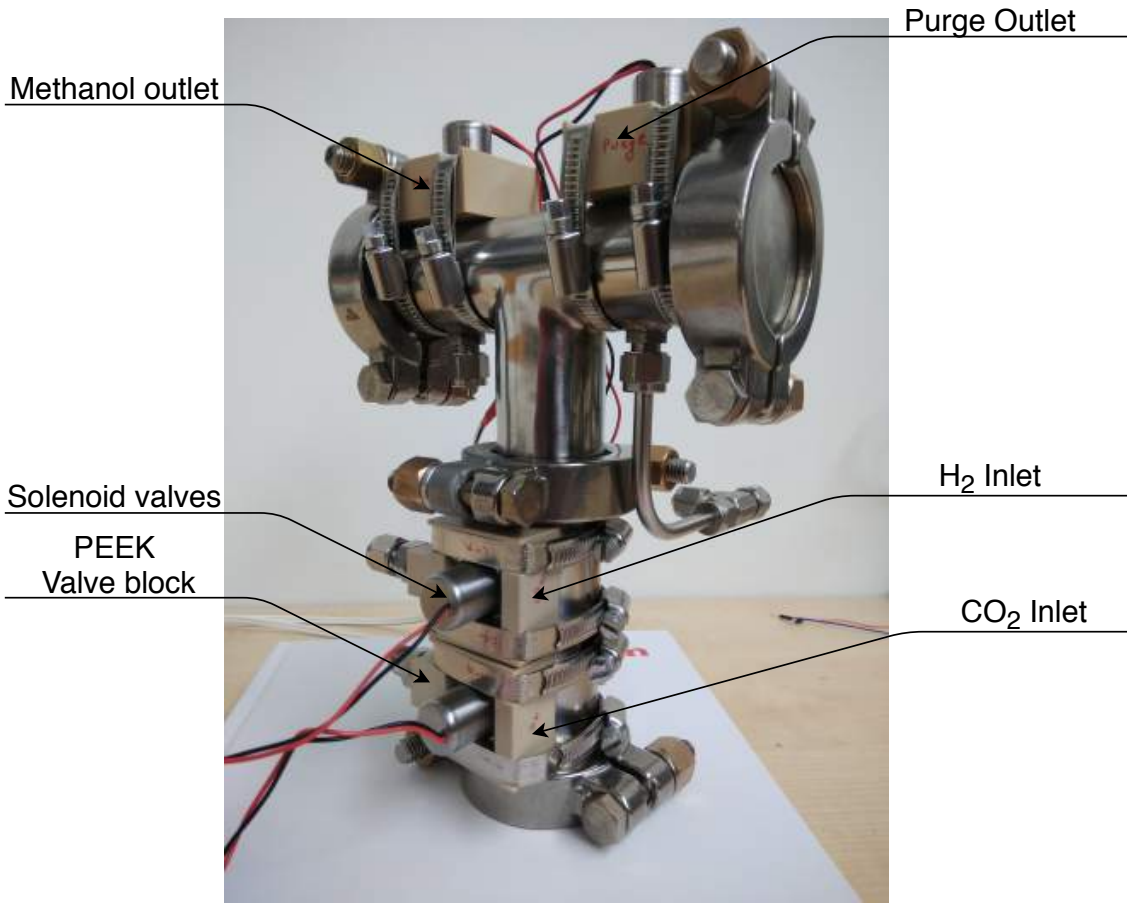

Figure A.1: Valve block design with PEEK blocks.

In the initial valve block design for condenser section, PEEK blocks were CNC machined to create valve seats for the Bi-stable solenoid valves (figure-A.1). The in-house manufacturing of the valve seats was implemented to provide compactness to the condenser and reduce the flow area of the valves. However, when these valve designs were tested, they were not found to be suitable for reliable reactor operation. As the reactor holds high pressures upto 55 Bar, the valve springs were not able to work against the gas force and close the valve every time. Due to the unreliability of

the valves, they were discontinued in favor of normally closed valves which had springs with higher spring constant and powerful solenoid coil to retract the plunger. The internal designs of the inlet and outlet valve seats are shown in figure-A.2.

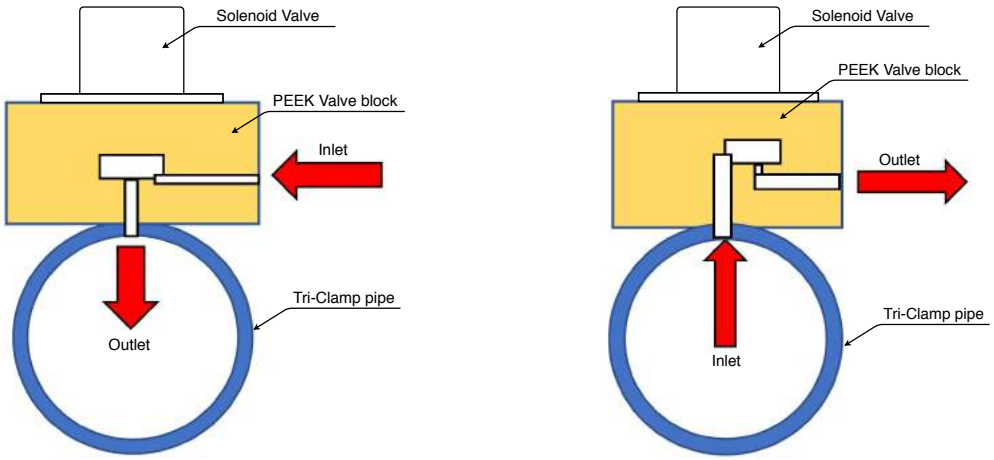

(a) *The design of the inlet valve seat.* (b) *The design of the outlet valve seat.*

Figure A.2: Schematic of the PEEk valve seats employed for initial valve system design.

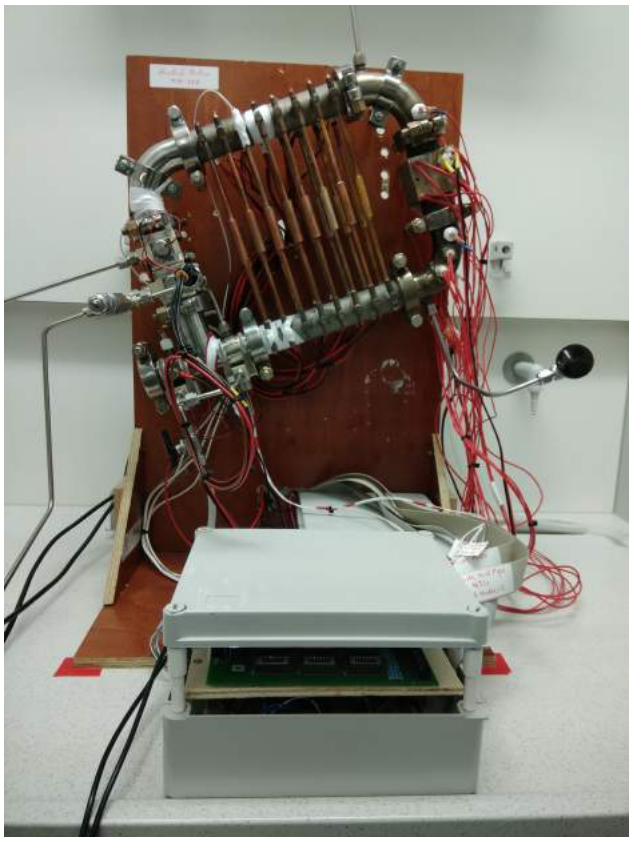

Figure A.3: The methanol reactor assembly with the old valve block design.

B

GAS FLOW TEMPERATURE SENSOR ITERATIONS

A major problem with installing the temperature sensing elements for the gas flow temperature inside the reactor is that the fabrication must be able to withstand 50 Bar and also be electrically isolated from the metallic body of the reactor. The developmental process for such a sensor is discussed below.

B.1. PEEK-NAIL PASS THROUGH

PEEK is a semi crystalline thermoplastic that has excellent chemical and mechanical resistance. Since, it is a plastic material it is also an insulator. Several electrical pass-through connections were fabricated using the PEEK for both level as well as temperature sensing. Two holes (10 mm) were drilled on the Tri-Clamp pipe opposite to each other and Swagelok connectors were welded on to them. The inside diameter of the Swagelok connector was made uniform using a 6 mm drill. PEEK round tubes with outside diameter of 6 mm were turned using a Lathe machine. A 9 cm long galvanized steel nail was jammed into the PEEK tube after using a 3 mm drill. The fabrication was then inserted into the Swagelok connector and fastened using the ferrule. Once fastened, the ferrules attach to their position and the interference fit between the connector and PEEK tube provides the necessary mechanical integrity (figure-B.1a. The PEEK tube also insulates the metallic nail from touching the reactor body. The temperature sensor was attached to the opposite nails of two of

(a) *PEEk and nail pass through fabrication.*

(b) *Peek and nail pass through in the reactor Tri-Clamp pipe.*

Figure B.1: PEEK-Nail electrical pass-through connection.

these pass-throughs using copper crocodile clamps inside the reactor pipe. They were electrically

connected outside too with the power supply using the same crocodile clamps (figure-B.2a). The above mentioned fabrication was seen to easily withstand 65 Bar pressure at cold reactor conditions. However, when the reactor was heated and allowed to cool down, these pass-throughs started leaking after several reactor runs (figure-B.2b). This was due to the the play between the Swagelok connector and the peek tube created by the thermal expansion and consequently contraction when cold again. Even though PEEK is a hard thermoplastic, it was not able to withstand the thermal hysteresis.

(a) *The outside connection of the PEEK-Nail electrical pass-through.*

(b) *The leak in the PEEK-Nail electrical pass-through after getting subjected to high temperature.*

Figure B.2: PEEK-Nail electrical pass-through outside connection.

B.2. GLOW PLUG PASS THROUGH

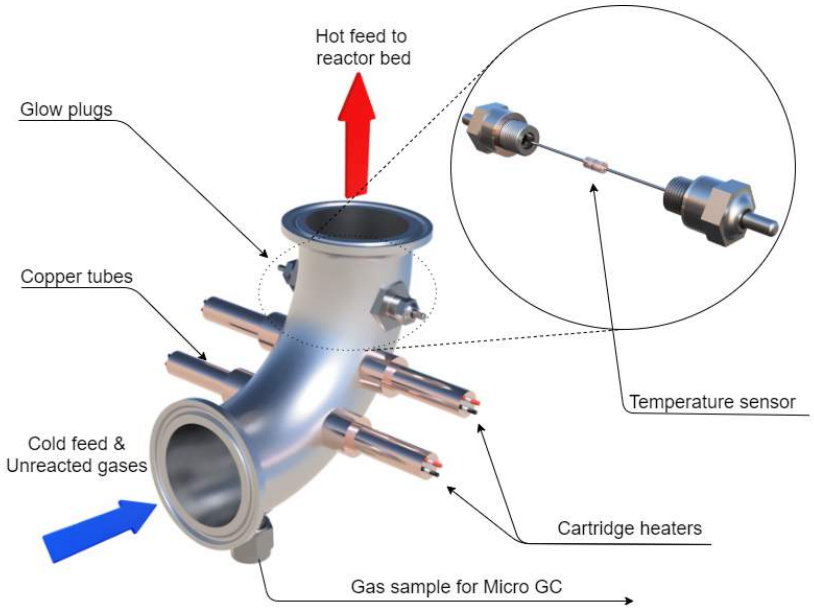

Figure B.3: Setup schematic of the corner piece with the Glow plug pass through.

Due to the problems faced with the leaks in the PEEK-Nail pass-throughs, a different approach was used. Glow plugs are readily available for use in the internal combustion engines to supply voltage

inside the pressurized cylinder, while keeping it leak proof and isolated from the body. Therefore, two glow plugs were installed inside-out facing opposite to each other in the reactor Tri-Clamp pipe. The voltage supply wire of these glow plugs was connected the two ends of the temperature sensor. Thereby, leaving the sensor hanging between these glow plugs, at the center of the reactor Tri-Clamp pipe. The outer pin of both these glow plugs was then electrically connected to the power supply using the copper crocodile clamps.

It was observed that the fabricated assembly was able to easily withstand high pressures upto 60 Bar. It was also able to withstand the thermal stresses which ensue due to frequent reactor heat up and cool down. Unfortunately, in this seemingly working fabrication, the temperature sensors started loosing their characteristics after several reactor runs. This was due to the temperature sensor getting exposed to the gas environment inside the reactor, while in operation. It was concluded that the sensor must be shielded from the reactor environment, for it to perform satisfactorily. This laid the foundation of the shielded thermal well assembly that was finally used and worked properly.

(a) *The glow plug attachment to the temperature sensor.*

(b) *The glow plug temperature sensor connection with reactor Tri-clamp pipe.*

Figure B.4: The design of Glow plug temperature sensor

C

GAS FLOW TEMPERATURE SENSOR ACCURACY VALIDATION

The volume of the reactor is always fixed. Therefore, any change in the pressure inside the system, affects the temperature of gas;Increase in pressure increases temperature and vice versa. In figure-C.1 a small interval of pressure response and one of the gas flow temperature sensors (Bed Outlet) during reactor preparation before start up with H_2 is shown. It can be seen that as the pressure rises it creates a rise in the temperature signal too and vice versa. The temperature slowly comes back to normal within a few seconds. Therefore, qualitatively speaking, the temperature sensors seem to obey the laws of thermodynamics.

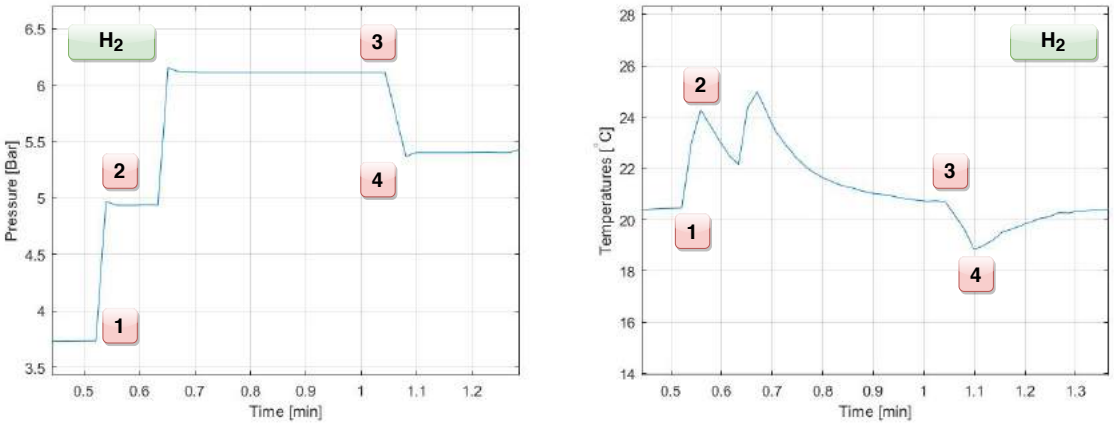

(a) *The pressure response of the reactor.*

(b) *The temperature response of the gas outlet temperature sensor*

Figure C.1: Validation of gas flow temperature sensors.

To validate it quantitatively, ideal gas law was used to predict the rise and fall of temperatures. The compressibility factor (Z) for the gas is assumed to be 1 due to very low pressure range. The number of mole of H_2 occupying the reactor at both pressures can be calculated using equation given below. The details of calculations are given in Table-C.1.

$$n_{mol} = \frac{V_{reactor} \times \rho_{P,T}}{M_{H_2}} \tag{C.1}$$

$$T = \frac{P \times V_{reactor}}{R \times n_{mol}} \tag{C.2}$$

It can be seen that the correlation between the sensed pressure and gas temperature data matches very well with the predictions of the gas law. Therefore, these calculations are a testament to the accuracy of the pressure and temperature sensor data acquired for this thesis.

Table C.1: Details about temperature calculations

Parameter	**Value**	**Unit**
Reactor volume (V)	1.42×10^{-3}	m^3
Gas constant (R)	8.314	J/mol/K
ρ_1	0.30766	Kg/m^3
ρ_2	0.40371	Kg/m^3
n_1	0.2167	mol
n_2	0.2844	mol
P_1	3.734	Bar
P_2	4.967	Bar
Calculated T_1	21.14	$^\circ C$
Calculated T_2	25.18	$^\circ C$
Calculated ΔT_{rise}	**4.04**	$^\circ C$
sensor ΔT_{rise}	**3.82**	$^\circ C$
ρ_3	0.0.5026	Kg/m^3
ρ_4	0.0.4445	Kg/m^3
n_3	0.0.3540	mol
n_4	0.0.3131	mol
P_3	6.113	Bar
P_4	5.37	Bar
Calculated T_3	21.77	$^\circ C$
Calculated T_4	19.80	$^\circ C$
Calculated ΔT_{fall}	**1.97**	$^\circ C$
sensor ΔT_{fall}	**1.84**	$^\circ C$

D

CIRCUIT BOARD DESIGNS

The design of the Data and Control board is shown in figure-D.1 and D.2. The circuit diagram was made in the Fritzing software[1]. The PCB was then printed by AISLER[2]. Individual components of the board were ordered separately and soldered onto the board. Both the PCBs are double layered. Therefore, the yellow lines indicate the top layer and the orange lines indicate the bottom layer and thus, they do not intersect.

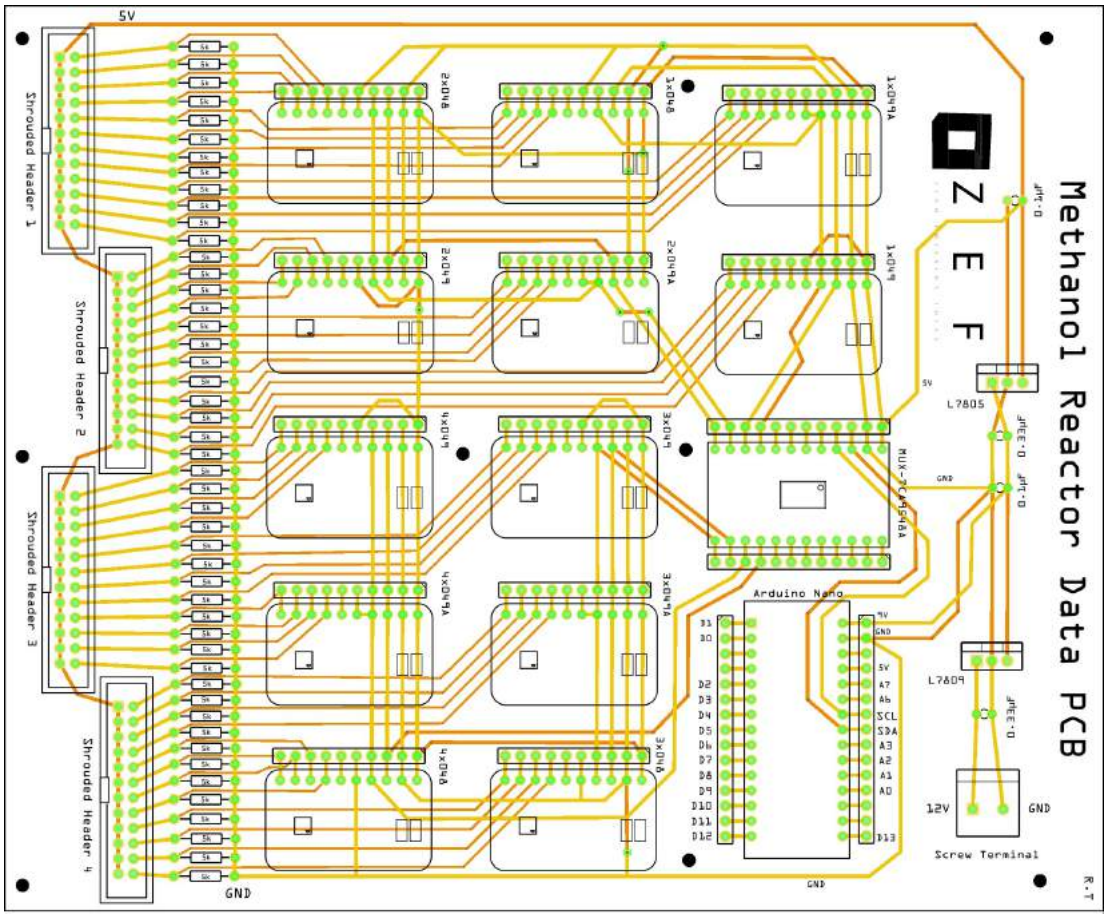

Figure D.1: Circuit diagram for the data PCB.

[1] https://fritzing.org/download/
[2] https://aisler.net/

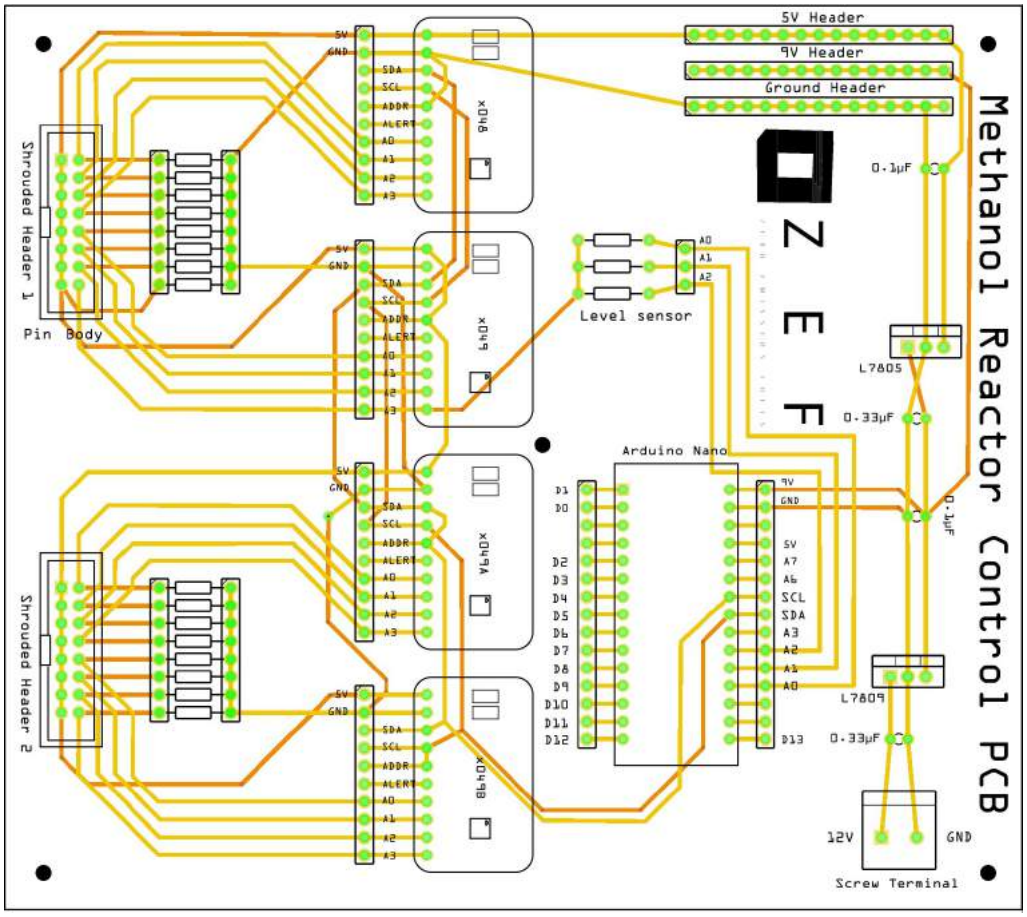

Figure D.2: Circuit diagram for the Control PCB.

Table D.1: Details about the components used in the Data and Control Circuit Board

Component	Control Board	Data Board
Adafruit ADS1115	4	12
Arduino Nano	1	1
Multiplexer	-	1
L7805 Voltage regulator	1	1
L7809 Voltage regulator	1	1
Thin film resistor 5.1 kΩ±1%	16	48

E

Real Setup Pictures

This chapter contains some images of the real setup. In the report only 3D models have been used for description due to better clarity.

(a) *The basket used for catalyst pellet support.*

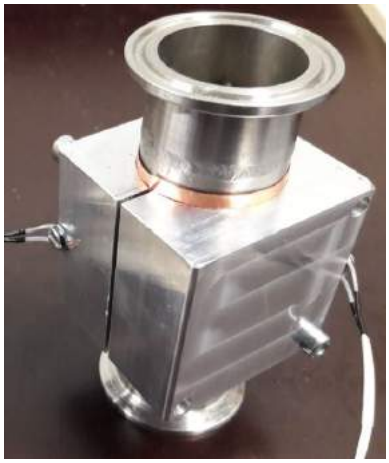

(b) *The assembly of catalyst reactor bed pipe and heater blocks.*

Figure E.1: Images from catalyst bed section.

(a) *The copper mesh inside the reactor pipe at heat pipe locations.*

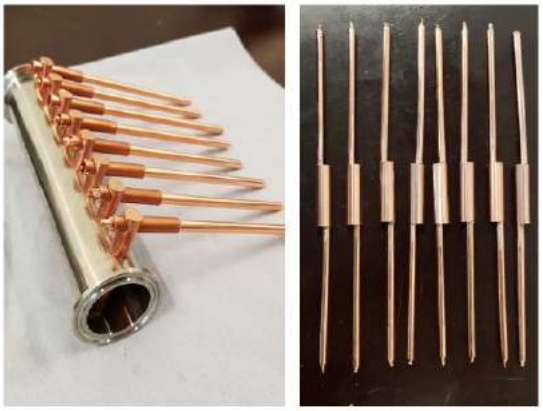

(b) *The assembly of the heat pipe with the reactor pipe.*

Figure E.2: Images from heat integration section.

(a) *The temperature sensor wiring behind the reactor.* (b) *The inner silicone sheet insulation for the reactor*

Figure E.3: Insulation and wiring of heat integration section.

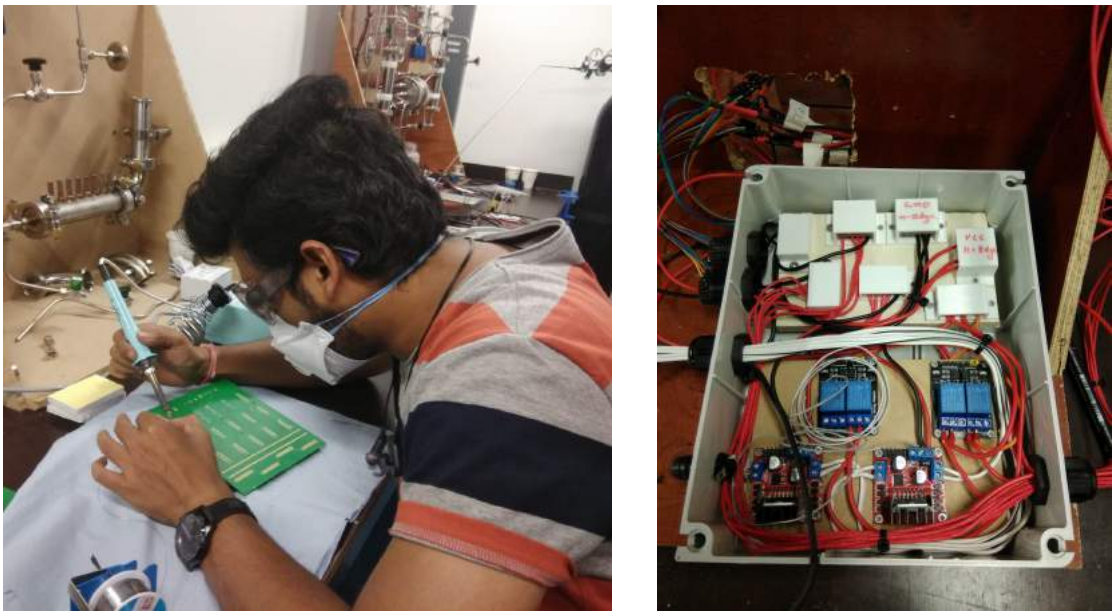

(a) *PCb fabrication.* (b) *TThe wiring of the power circuit housing.*

Figure E.4: Images from Sensors and electronics section.

Figure E.5: The design of the thermowell well for gas flow temperature measurements.

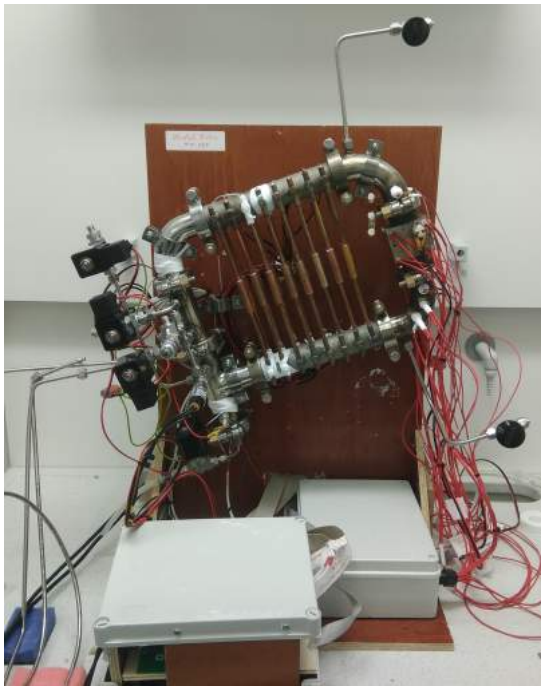

(a) *The methanol reactor without insulation.*

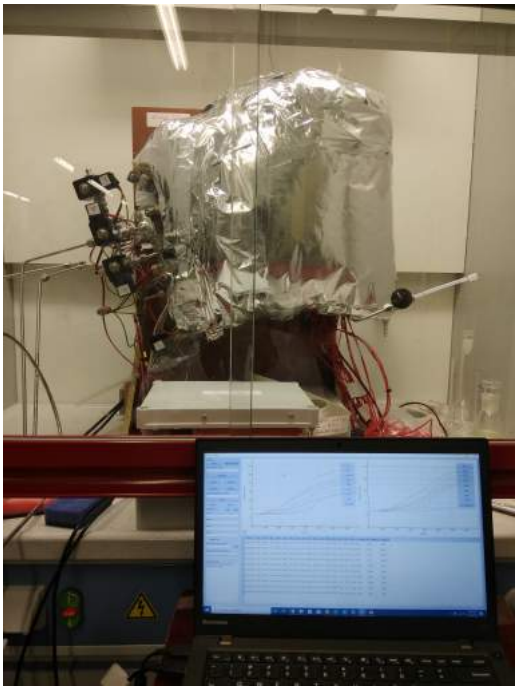

(b) *The methanol reactor after insulation inside fumehood.*

Figure E.6: Images of reactor.

Bibliography

[1] H. Ritchie and M. Roser, "Fossil fuels", *Our World in Data*, 2020. https://ourworldindata.org/fossil-fuels.

[2] H. Ritchie and M. Roser, "Renewable energy", *Our World in Data*, 2020. https://ourworldindata.org/renewable-energy.

[3] G. Olah, A. Goeppert, and G. Prakash, "Chemical recycling of carbon dioxide to methanol and dimethyl ether: From greenhouse gas to renewable, environmentally carbon neutral fuels and synthetic hydrocarbons", *Journal of Organic Chemistry*, 74(2):487–498, 2009. doi:10.1021/jo801260f.

[4] M. Saito, T. Fujitani, M. Takeuchi, and T. Watanabe, "Development of copper/zinc oxide-based multicomponent catalysts for methanol synthesis from carbon dioxide and hydrogen", *Applied Catalysis A: General*, 138(2):311–318, 1996. doi:10.1016/0926-860X(95)00305-3.

[5] J. Skrzypek, M. Lachowska, and D. Serafin, "Methanol synthesis from CO2 and H2: dependence of equilibrium conversions and exit equilibrium concentrations of components on the main process variables.", *Chemical Engineering Science*, 45(1):89–96, 1990. doi:10.1016/0009-2509(90)87083-5.

[6] G. Bozzano and F. Manenti, "Efficient methanol synthesis: Perspectives, technologies and optimization strategies", *Progress in Energy and Combustion Science*, 56:71 – 105, 2016. doi:https://doi.org/10.1016/j.pecs.2016.06.001.

[7] D. Sheldon, "Methanol production - a technical history", *Johnson Matthey Technology Review*, 61:172–182, 07 2017. doi:10.1595/205651317X695622.

[8] C. T. Herbschleb, "ReactorSTM : imaging catalysts under realistic conditions", Doctoral thesis, Leiden University, 2011. URL http://hdl.handle.net/1887/17620.

[9] K. Vanden Bussche and G. Froment, "A steady-state kinetic model for methanol synthesis and the water gas shift reaction on a commercial Cu/ZnO/Al2O3 catalyst", *Journal of Catalysis*, 161 (1):1–10, 1996.

[10] M. Bos and D. Brilman, "A novel condensation reactor for efficient CO2 to methanol conversion for storage of renewable electric energy", *Chemical Engineering Journal*, 278:527 – 532, 2015. ISSN 1385-8947. doi:https://doi.org/10.1016/j.cej.2014.10.059.

[11] J.-D. Grunwaldt, A. Molenbroek, N.-Y. Topsøe, H. Topsøe, and B. Clausen, "In Situ Investigations of Structural Changes in Cu/ZnO Catalysts", *Journal of Catalysis*, 194(2):452 – 460, 2000. ISSN 0021-9517. doi:https://doi.org/10.1006/jcat.2000.2930.

[12] P. C. Vesborg, I. Chorkendorff, I. Knudsen, O. Balmes, J. Nerlov, A. M. Molenbroek, B. S. Clausen, and S. Helveg, "Transient behavior of Cu/ZnO-based methanol synthesis catalysts", *Journal of Catalysis*, 262(1):65 – 72, 2009. ISSN 0021-9517. doi:https://doi.org/10.1016/j.jcat.2008.11.028.

[13] M. Shahrokhi and G. Baghmisheh, "Modeling, simulation and control of a methanol synthesis fixed-bed reactor", *Chemical Engineering Science*, 60(15):4275 – 4286, 2005. ISSN 0009-2509. doi:https://doi.org/10.1016/j.ces.2004.12.051.

[14] S. S. Iyer, T. Renganathan, S. Pushpavanam, M. V. Kumar, and N. Kaisare, "Generalized thermodynamic analysis of methanol synthesis: Effect of feed composition", *Journal of CO2 Utilization*, 10:95 – 104, 2015. ISSN 2212-9820. doi:https://doi.org/10.1016/j.jcou.2015.01.006.

[15] M. Bukhtiyarova, T. Lunkenbein, K. Kähler, and R. Schlögl, "Methanol synthesis from industrial co2 sources: A contribution to chemical energy conversion", *Catalysis Letters*, 147(2):416–427, 2017. doi:10.1007/s10562-016-1960-x.

[16] P. Basarkar, "Experimental characterization of a novel small scale natural circulation loop Methanol Synthesis Reactor", Master's thesis, Delft University of Technology, 2018. URL http://resolver.tudelft.nl/uuid:3f5c1c51-d04f-4026-88a5-0bb4c800cf2b.

[17] D. Van Laake, "Development And Characterization Of A Small Scale Methanol Synthesis Reactor Based On Natural Convection", Master's thesis, Delft University of Technology, 2019. URL http://resolver.tudelft.nl/uuid:4d6d1637-9c56-4069-9d7b-323eeeea84b9.

[18] T. de Kruijf, "Optimalisatie van warmteoverdracht binnen een kleinschalige methanolreactor", Master's thesis, Delft University of Technology, 2019.

[19] G. Olah, "After oil and gas: Methanol economy", *Catalysis Letters*, 93(1-2):1–2, 2004.

[20] G. A. Olah, "Beyond oil and gas: The methanol economy", *Angewandte Chemie International Edition*, 44(18):2636–2639, 2005. doi:10.1002/anie.200462121.

[21] S. Lewis and M. Maslin, "Defining the anthropocene", *Nature*, 519:171–80, 03 2015. doi:10.1038/nature14258.

[22] C. A. Horowitz, "Paris agreement", *International Legal Materials*, 55(4):740–755, 2016. doi:10.1017/S0020782900004253.

[23] P. Lemke, J. Ren, R. Alley, I. Allison, J. Carrasco, G. Flato, Y. Fujii, G. Kaser, P. Mote, R. Thomas, and T. Zhang. *IPCC, 2007. Climate Change 2007. Synthesis Report. Contribution of Working Groups I, II and III to the Fourth Assessment Report of the Intergovernmental Panel on Climate Change. Geneva.* 01 2007. doi:10.1017/CBO9780511546013.

[24] H. Ritchie and M. Roser, "Energy", *Our World in Data*, 2020. https://ourworldindata.org/energy.

[25] D. Mignard and C. Pritchard, "Processes for the synthesis of liquid fuels from CO2 and marine energy", *Chemical Engineering Research and Design*, 84(9 A):828–836, 2006. doi:10.1205/cherd.05204.

[26] A. B. Stiles, "Methanol, past, present, and speculation on the future", *AIChE Journal*, 23(3):362–375, 1977. doi:10.1002/aic.690230321.

[27] F. Keil, "Methanol-to-hydrocarbons: Process technology", *Microporous and Mesoporous Materials*, 29(1-2):49–66, 1999. doi:10.1016/S1387-1811(98)00320-5.

[28] T. Weimer, K. Schaber, M. Specht, and A. Bandi, "Methanol from atmospheric carbon dioxide: A liquid zero emission fuel for the future", *Energy Conversion and Management*, 37(6):1351 – 1356, 1996. ISSN 0196-8904. doi:https://doi.org/10.1016/0196-8904(95)00345-2. Proceedings of the International Energy Agency Greenhouse Gases: Mitigation Options Conference.

[29] X. Xiaoding and J. Moulijn, "Mitigation of CO2 by chemical conversion: Plausible chemical reactions and promising products", *Energy and Fuels*, 10(2):305–325, 1996. doi:10.1021/ef9501511.

[30] C. Arcoumanis, C. Bae, R. Crookes, and E. Kinoshita, "The potential of di-methyl ether (DME) as an alternative fuel for compression-ignition engines: A review", *Fuel*, 87(7):1014–1030, 2008. doi:10.1016/j.fuel.2007.06.007.

[31] S. Surampudi, S. Narayanan, E. Vamos, H. Frank, G. Halpert, A. LaConti, J. Kosek, G. Prakash, and G. Olah, "Advances in direct oxidation methanol fuel cells", *Journal of Power Sources*, 47 (3):377–385, 1994. doi:10.1016/0378-7753(94)87016-0.

[32] O. Deutschmann, H. Knözinger, K. Kochloefl, and T. Turek. *Heterogeneous Catalysis and Solid Catalysts, 1. Fundamentals*. 2011. ISBN 9783527306732. doi:10.1002/14356007.a05_313.pub3.

[33] M. Spencer, "Stable and metastable metal surfaces in heterogeneous catalysis", *Nature*, 323: 685–687, 09 1986. doi:10.1038/323685a0.

[34] M. Twigg and M. Spencer, "Deactivation of copper metal catalysts for methanol decomposition, methanol steam reforming and methanol synthesis", *Topics in Catalysis*, 22(3-4):191–203, 2003. doi:10.1023/A:1023567718303.

[35] J. R. Rostrup-Nielsen, "Catalytic steam reforming.", *Catalysis: Science and Technology*, 5:1–117, 1984.

[36] J. Bart and R. Sneeden, "Copper-zinc oxide-alumina methanol catalysts revisited", *Catalysis Today*, 2(1):1–124, 1987. doi:10.1016/0920-5861(87)80001-9.

[37] J. van Bennekom, R. Venderbosch, J. Winkelman, E. Wilbers, D. Assink, K. Lemmens, and H. Heeres, "Methanol synthesis beyond chemical equilibrium", *Chemical Engineering Science*, 87:204–208, 2013. doi:10.1016/j.ces.2012.10.013.

[38] B. Canete, C. Gigola, and N. Brignole, "Synthesis gas processes for methanol production via ch4 reforming with co2, h2o, and o2", *Industrial and Engineering Chemistry Research*, 53(17): 7103–7112, 2014. doi:10.1021/ie404425e.

[39] K. Omata, M. Hashimoto, Y. Watanabe, T. Umegaki, S. Wagatsuma, G. Ishiguro, and M. Yamada, "Optimization of cu oxide catalyst for methanol synthesis under high co 2 partial pressure using combinatorial tools", *Applied Catalysis A: General*, 262(2):207–214, 2004. doi:10.1016/j.apcata.2003.11.028.

[40] B. Tabiś, "Methanol synthesis in a fluidized-bed reactor coupled with an external heat exchanger: The effect of feedback deformation", *Chemical Engineering Journal*, 83(3):191 – 200, 2001. doi:https://doi.org/10.1016/S1385-8947(00)00254-0.

[41] X. Cui and S. K. Kær, "A comparative study on three reactor types for methanol synthesis from syngas and co2", *Chemical Engineering Journal*, 393:124632, 2020. doi:https://doi.org/10.1016/j.cej.2020.124632.

[42] B. Redondo, M. Shah, V. Pareek, R. Utikar, P. Webley, J. Patel, W. Lee, and T. Bhatelia, "Intensified isothermal reactor for methanol synthesis", *Chemical Engineering and Processing - Process Intensification*, 143, 2019. doi:10.1016/j.cep.2019.107606.

[43] G. Graaf, E. Stamhuis, and A. Beenackers, "Kinetics of low-pressure methanol synthesis", *Chemical Engineering Science*, 43(12):3185–3195, 1988. doi:10.1016/0009-2509(88)85127-3.

[44] E. Boomer and H. Morris, "The hydrogen-carbon dioxide reaction", *Journal of the American Chemical Society*, 54(1):407, 1932. doi:10.1021/ja01340a509.

[45] R. Herman, K. Klier, G. Simmons, B. Finn, J. Bulko, and T. Kobylinski, "Catalytic synthesis of methanol from CO H2. I. Phase composition, electronic properties, and activities of the Cu/ZnO/M2O3 catalysts", *Journal of Catalysis*, 56(3):407–429, 1979. doi:10.1016/0021-9517(79)90132-5.

[46] K. Klier, "Methanol synthesis", *Advances in Catalysis*, 31(C):243–313, 1982. doi:10.1016/S0360-0564(08)60455-1.

[47] A. Rozovskii, "Modern problems in the synthesis of methanol", *Russian Chemical Reviews*, 58 (1):41–56, 1989. doi:10.1070/RC1989v058n01ABEH003425.

[48] G. Chinchen, K. Waugh, and D. Whan, "The activity and state of the copper surface in methanol synthesis catalysts", *Applied Catalysis*, 25(1-2 C):101–107, 1986. doi:10.1016/S0166-9834(00)81226-9.

[49] T. Lunkenbein, F. Girgsdies, T. Kandemir, N. Thomas, M. Behrens, R. Schlögl, and E. Frei, "Bridging the time gap: A copper/zinc oxide/aluminum oxide catalyst for methanol synthesis studied under industrially relevant conditions and time scales", *Angewandte Chemie - International Edition*, 55(41):12708–12712, 2016. doi:10.1002/anie.201603368.

[50] G. Chinchen, P. Denny, D. Parker, M. Spencer, and D. Whan, "Mechanism of methanol synthesis from CO2/CO/H2 mixtures over copper/zinc oxide/alumina catalysts: use of14C-labelled reactants", *Applied Catalysis*, 30(2):333 – 338, 1987. ISSN 0166-9834. doi:https://doi.org/10.1016/S0166-9834(00)84123-8.

[51] T. Tagawab, G. Pleizier, and Y. Amenomiya, "Methanol synthesis from co2+h2 i. characterization of catalysts by tpd", *Applied Catalysis*, 18(2):285–293, 1985. doi:10.1016/S0166-9834(00)84007-5.

[52] Y. Zhang, Q. Sun, J. Deng, D. Wu, and S. Chen, "A high activity cu/zno/al2o3 catalyst for methanol synthesis: Preparation and catalytic properties", *Applied Catalysis A: General*, 158 (1-2):105–120, 1997. doi:10.1016/S0926-860X(96)00362-6.

[53] E. Supp. *How to Produce Methanol from Coal*, Volume 1. 1990. doi:10.1007/978-3-662-00895-9.

[54] E. Ramaroson, R. Kieffer, and A. Kiennemenn, "Reaction of CO-H2 and CO2-H2 on copper-zinc catalysts promoted by metal oxides of groups III and IV", *Applied Catalysis*, 4(3):281–286, 1982. doi:10.1016/0166-9834(82)80111-5.

[55] M. Hirano, T. Akano, T. Imai, and K. Kuroda, "Methanol synthesis from carbon dioxide on cuo-zno-al2o3 catalysts", *Energy Conversion and Management*, 36(6-9):585–588, 1995.

[56] B. Denise and R. Sneeden, "Oxide-supported copper catalysts prepared from copper formate: Differences in behavior in methanol synthesis from co/h2 and co2/h2 mixtures", *Applied Catalysis*, 28(C):235–239, 1986. doi:10.1016/S0166-9834(00)82507-5.

[57] P. Villa, P. Forzattl, G. Buzzl-Ferrarls, G. Garone, and I. Pasquon, "Synthesis of alcohols from carbon oxides and hydrogen. 1. kinetics of the low-pressure methanol synthesis", *Industrial and Engineering Chemistry Process Design and Development*, 24(1):12–19, 1985. doi:10.1021/i200028a003.

[58] K. Bussche and G. Froment, "A Steady-State Kinetic Model for Methanol Synthesis and the Water Gas Shift Reaction on a Commercial Cu/ZnO/Al2O3Catalyst", *Journal of Catalysis*, 161 (1):1 – 10, 1996. ISSN 0021-9517. doi:https://doi.org/10.1006/jcat.1996.0156.

[59] Graaf, G.H. and Sijtsema, P.J.J.M. and Stamhuis, E.J. and Joosten, G.E.H., "Chemical equilibria in methanol synthesis", *Chemical Engineering Science*, 41(11):2883–2890, 1986. doi:10.1016/0009-2509(86)80019-7.

[60] J. Lee, K. Lee, S. Lee, and Y. Kim, "A comparative study of methanol synthesis from CO2/H2 and CO/H2 over a Cu/ZnO/Al2O3 catalyst", *Journal of Catalysis*, 144(2):414–424, 1993. doi:10.1006/jcat.1993.1342.

[61] M. Sahibzada, I. Metcalfe, and D. Chadwick, "Methanol synthesis from co/co2/h2 over cu/zno/al2o3 at differential and finite conversions", *Journal of Catalysis*, 174(2):111–118, 1998. doi:10.1006/jcat.1998.1964.

[62] V. Ipatieff and G. Monroe, "Synthesis of methanol from carbon dioxide and hydrogen over copper-alumina catalysts. mechanism of reaction", *Journal of the American Chemical Society*, 67(12):2168–2171, 1945. doi:10.1021/ja01228a032.

[63] J. Ott, V. Gronemann, F. Pontzen, E. Fiedler, G. Grossmann, D. B. Kersebohm, G. Weiss, and C. Witte. *Methanol*. American Cancer Society, 2012. ISBN 9783527306732. doi:10.1002/14356007.a16_465.pub3.

[64] M. Kuczynski, M. Oyevaar, R. Pieters, and K. Westerterp, "Methanol synthesis in a countercurrent gas-solid-solid trickle flow reactor. an experimental study", *Chemical Engineering Science*, 42(8):1887–1898, 1987. doi:10.1016/0009-2509(87)80135-5.

[65] K. Westerterp, M. Kuczynski, and C. Kamphuis, "Synthesis of methanol in a reactor system with interstage product removal", *Industrial and Engineering Chemistry Research*, 28(6):763–771, 1989. doi:10.1021/ie00090a018.

[66] P. Reubroycharoen, T. Vitidsant, K. Asami, Y. Yoneyama, and N. Tsubaki, "Accelerated methanol synthesis in catalytically active supercritical fluid", *Catalysis Communications*, 4(9):461–464, 2003. doi:10.1016/S1566-7367(03)00113-4.

[67] B. Haut, V. Halloin, and H. Ben Amor, "Development and analysis of a multifunctional reactor for equilibrium reactions: Benzene hydrogenation and methanol synthesis", *Chemical Engineering and Processing: Process Intensification*, 43(8):979–986, 2004. doi:10.1016/j.cep.2003.09.006.

[68] K. Ushikoshi, K. Mori, T. Kubota, T. Watanabe, and M. Saito, "Methanol synthesis from CO2 and H2 in a bench-scale test plant", *Applied Organometallic Chemistry*, 14(12):819–825, 2000. doi:10.1002/1099-0739(200012)14:12<819::AID-AOC90>3.0.CO;2-\#.

[69] N. Rezaie, A. Jahanmiri, B. Moghtaderi, and M. Rahimpour, "A comparison of homogeneous and heterogeneous dynamic models for industrial methanol reactors in the presence of catalyst deactivation", *Chemical Engineering and Processing: Process Intensification*, 44(8):911–921, 2005. doi:10.1016/j.cep.2004.10.004.

[70] M. Bowker, H. Houghton, and K. Waugh, "Mechanism and kinetics of methanol synthesis on zinc oxide", *Journal of the Chemical Society, Faraday Transactions 1: Physical Chemistry in Condensed Phases*, 77(12):3023–3036, 1981. doi:10.1039/F19817703023.

[71] J. Nerlov, S. Sckerl, J. Wambach, and I. Chorkendorff, "Methanol synthesis from CO2, CO and H2 over Cu(100) and Cu(100) modified by Ni and Co", *Applied Catalysis A: General*, 191(1):97 – 109, 2000. ISSN 0926-860X. doi:https://doi.org/10.1016/S0926-860X(99)00311-7.

[72] M. Günter, T. Ressler, R. Jentoft, and B. Bems, "Redox Behavior of Copper Oxide/Zinc Oxide Catalysts in the Steam Reforming of Methanol Studied by in Situ X-Ray Diffraction and Absorption Spectroscopy", *Journal of Catalysis*, 203(1):133 – 149, 2001. ISSN 0021-9517. doi:https://doi.org/10.1006/jcat.2001.3322.

[73] T. Fujitani, I. Nakamura, T. Uchijima, and J. Nakamura, "The kinetics and mechanism of methanol synthesis by hydrogenation of co2 over a zn-deposited cu(111) surface", *Surface Science*, 383(2-3):285–298, 1997. doi:10.1016/S0039-6028(97)00192-1.

[74] J. M. Smith. *Introduction to chemical engineering thermodynamics*, Volume 27. 1950. doi:10.1021/ed027p584.3.

[75] J. S. Lee, S.-H. Han, H. Kim, K. Lee, and Y. Kim, "Effects of space velocity on methanol synthesis from CO2/CO/H-2 over Cu/ZnO/Al2O3 catalyst", *Korean Journal of Chemical Engineering*, 17: 332–336, 04 2012. doi:10.1007/BF02699049.

[76] G. Liu, D. Willcox, M. Garland, and H. Kung, "The rate of methanol production on a copper-zinc oxide catalyst: The dependence on the feed composition", *Journal of Catalysis*, 90(1):139–146, 1984. doi:10.1016/0021-9517(84)90094-0.

[77] A. Bansode, B. Tidona, P. Von Rohr, and A. Urakawa, "Impact of k and ba promoters on co2 hydrogenation over cu/al2o3 catalysts at high pressure", *Catalysis Science and Technology*, 3 (3):767–778, 2013. doi:10.1039/c2cy20604h.

[78] B. Doss, C. Ramose, and S. Atkins, "Optimization of methanol synthesis from carbon dioxide and hydrogen: Demonstration of a pilot-scale carbon-neutral synthetic fuels process", *Energy and Fuels*, 23(9):4647–4650, 2009. doi:10.1021/ef900466u.

[79] I.-C. Lo and H.-S. Wu, "Methanol formation from carbon dioxide hydrogenation using $Cu/ZnO/Al_2O_3$ catalyst", *Journal of the Taiwan Institute of Chemical Engineers*, 98:124–131, 2019. doi:10.1016/j.jtice.2018.06.020.

[80] J. Wu, M. Saito, M. Takeuchi, and T. Watanabe, "The stability of cu/zno-based catalysts in methanol synthesis from a co2-rich feed and from a co-rich feed", *Applied Catalysis A: General*, 218(1-2):235–240, 2001. doi:10.1016/S0926-860X(01)00650-0.

[81] R. Lammerink, "Mathematical characterization and simulation of natural convective flow in a condensing CO_2 to methanol reactor", Master's thesis, University of Twente, 2015.

[82] G. Gutierrez Neri, "Modeling of a natural circulation flow reactor for methanol synthesis from renewable sources", Master's thesis, Delft University of Technology, 2018. URL http://resolver.tudelft.nl/uuid:c1c40d2c-ee55-4e42-bec2-17a525579337.

[83] D. R. Simbeck, E. Chang, D. R. Simbeck, and E. Chang. "Hydrogen supply: Cost estimate for hydrogen pathways – scoping analysis". national renewable energy laboratory". Technical report, National Renewable Energy laboratory, 2002.

[84] J. Gorman, E. Sparrow, and J. Abraham, "Differences between measured pipe wall surface temperatures and internal fluid temperatures", *Case Studies in Thermal Engineering*, 1(1):13 – 16, 2013. ISSN 2214-157X. doi:https://doi.org/10.1016/j.csite.2013.08.002.

[85] E. M. Moghaddam, E. A. Foumeny, A. I. Stankiewicz, and J. T. Padding, "Rigid Body Dynamics Algorithm for Modeling Random Packing Structures of Nonspherical and Non-convex Pellets", *Industrial & Engineering Chemistry Research*, 57(44):14988–15007, 2018. doi:10.1021/acs.iecr.8b03915.

[86] S. Afandizadeh and E. Foumeny, "Design of packed bed reactors: guides to catalyst shape, size, and loading selection", *Applied Thermal Engineering*, 21(6):669 – 682, 2001. ISSN 1359-4311. doi:https://doi.org/10.1016/S1359-4311(00)00072-7.

[87] B. Zohuri. *Heat Pipe Design and Technology*. Springer, 2016. ISBN 9783319298412. doi:10.1007/978-3-319-29841-2.

[88] "Heat Pipes and Vapor Chambers". Technical report, Radian thermal products, 2014. URL https://www.radianheatsinks.com/.

Shashish Mishra

Department: Process and Energy, Faculty 3mE
Section: Large Scale Energy Storage

Graduation Committee:

Prof. dr. ir. W. de Jong (TU Delft)
Prof. dr. ir. E. Goetheer (TU Delft)
Dr. ir. H. B. Eral (TU Delft)

Ir. J. van Kranendonk (ZEF BV)

May, 2020

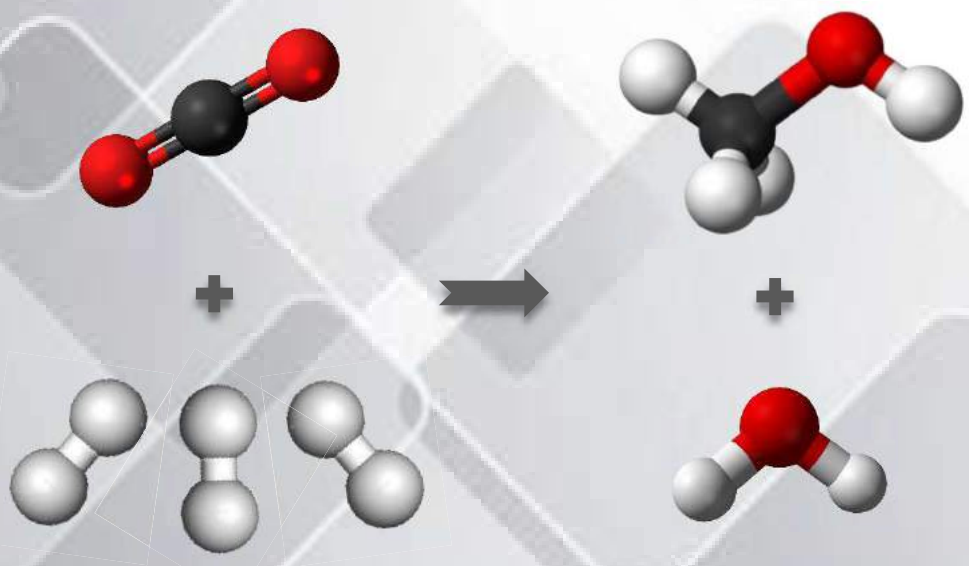

TU Delft Delft University of Technology

ZEF

Challenge the future